

NASA Contractor Report 180810

LEWIS GRANT  
IN- CAT. 26

94201

2-20-87

## Ductility and Fracture in B2 FeAl Alloys

(NASA-CR-180810) DUCTILITY AND FRACTURE IN  
B2 FeAl ALLOYS Ph.D. Thesis Final Report  
(Case Western Reserve Univ.) 220 p Avail:  
NTIS EC A10/MF A01 CSCL 11P

N87-27771

G3/26 Unclass  
0094201

Martin A. Crimp  
*Case Western Reserve University*  
*Cleveland, Ohio*

August 1987

Prepared for  
Lewis Research Center  
Under Grant NAG3-563



National Aeronautics and  
Space Administration

#### ACKNOWLEDGEMENTS

I would like to express my appreciation to a number of people for their assistance in completing this work. The assistance and guidance of my advisor, Dr. Krishna M. Vedula is gratefully acknowledged. I would also like to thank Dr. Gary M. Michal, Dr. John J. Lewandowski, and Dr. Terence E. Mitchell for their helpful discussions and advice during this study. The financial support of NASA-Lewis Research Center is gratefully acknowledged. I would also like to thank Dr. J. R. Stephens, Dr. M. V. Nathai and R. H. Titran for permitting the use of various research facilities at NASA-Lewis Research Center. The technical assistance of D. J. Gaydosh and T. J. Kahoe at NASA-LRC and R. W. Howe at CWRU is also acknowledged.



# TABLE OF CONTENTS

	<u>page</u>
I. INTRODUCTION	1
FeAl Alloys	2
Mechanical Behavior of FeAl Alloys	7
Fe <sub>3</sub> Al Fracture, Ductility, and Yielding	9
Fe <sub>3</sub> Al Substructures and Dislocations	12
FeAl Fracture, Ductility, and Yielding	13
FeAl Substructures and Dislocations	15
Effect of Boron on Ni <sub>3</sub> Al	19
Boron Effects in Other Materials	22
The Present Study	23
II. EXPERIMENTAL PROCEDURE	25
Material	25
Powder Extrusions	25
Cast Extrusions	30
Single Crystals	31
Heat Treatments	32
Optical Microscopy	33
Transmission Electron Microscopy	36
Texture Determination	37
III. EXPERIMENTAL RESULTS	38
Optical Microstructures	38
Powder Extrusions	38
Cast Extrusions	43
Grain Growth	50
Texture Observation	53
Mechanical Behavior	56
Tensile Tests	56
Tensile Fracture Surfaces	71
Compression Tests	85
Single Crystal Compression Tests	89
Transmission Electron Microscopy	101
Burgers Vector Analysis	101
Dislocation Loop Observations	122
Precipitates	122
IV. DISCUSSION	135
Materials/Processing	135
Mechanical Behavior/Stoichiometry Effects	139
Mechanical Behavior/Boron Effects	152
Fe-50Al Alloys	152
Fe-40Al Alloys	156
Mechanical Behavior/Cooling Rate Effects	163
Yield Behavior/Grain Size Effects	167
V. CONCLUSIONS	172
VI. SUGGESTIONS FOR FUTURE WORK	175
VII. REFERENCES	177
VIII. APPENDIX A - extrusion sheets	182
IX. APPENDIX B - APB energy as a function of stoichiometry	212

## INTRODUCTION

Ordered intermetallic aluminides are currently receiving considerable research interest as potential materials for moderate to high temperature structural applications [1]. These materials have a number of advantages over the alloys currently being used in these applications. These advantages include lack of strategic additions such as Co and Cr [2] and relatively low material costs. Additionally, because of their large aluminum contents, ordered aluminides display significant density advantages and promise excellent oxidation resistance.

Unfortunately, most of the intermetallic aluminides are limited by their lack of ductility and low toughness [1]. Although some progress has recently been made in overcoming these problems [3,4] in some materials, most aluminides are still hampered by these problems. Because of this, continued work is necessary to understand the mechanical behavior of these alloys.

The B2 aluminides (FeAl, NiAl, CoAl) are typical of these ordered alloys, displaying many of these same advantages [2]. However, because of their very high Al contents (50% at stoichiometry), the density and oxidation advantages are maximized in the B2 alloys.

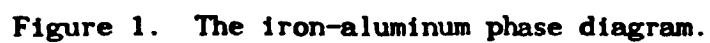
In this investigation, one of these B2 alloys, FeAl, was studied to gain a better understanding of the mechanical behavior of ordered alloys. As an introduction to this investigation, the

critical literature concerning Fe-Al alloys will be reviewed. To begin, the Fe-Al phase diagram will be discussed and the relationship of the various ordered alloys based on the  $\alpha$ -bcc phase. Following this, the available literature on the mechanical behavior of these alloys will be presented. This will cover both macroscopic behavior and the related substructural aspects. Next, the role of boron in the ductilization of  $\text{Ni}_3\text{Al}$  will be introduced, along with the effect of boron in other materials. Finally, the objectives of this work will be presented based on the literature survey.

### Fe-Al Alloys

Figure 1 displays the iron-aluminum phase diagram. Starting with the 100% iron side, and extending to approximately 51 at% Al, the phases present are all based on the bcc structure (except for the small  $\gamma$ -fcc loop near pure iron). This composition range is bounded at high temperatures by a solidus line, which decreases with increasing Al content. However, a number of ordering transformations occur across this composition range.

Beginning with the terminal solid solution, the bcc  $\alpha$  phase exists up to 21 at% Al at room temperature. At this composition, a two phase field begins containing  $\alpha$  and  $\text{Fe}_3\text{Al}$ . The single phase  $\text{Fe}_3\text{Al}$  phase begins at 24.5 at% Al and exists to approximately 33 at% Al. This  $\text{Fe}_3\text{Al}$  phase is an ordered form of the bcc alloy known as the  $\text{DO}_3$  structure. The basic  $\text{DO}_3$  unit cell is made up of



8 bcc unit cells and can be thought of as 4 interpenetrating fcc cells. This fcc lattice has 3 Fe and 1 Al atom per lattice site, with the iron atoms at  $(0,0,0)$ ,  $(\frac{1}{2},0,0)$ ,  $(0,\frac{1}{2},0)$ , and the aluminum atoms at  $(\frac{1}{4},\frac{1}{4},\frac{1}{4})$ . This phase is stable over the composition range described above, and exists up to  $540^{\circ}\text{C}$  where this  $\text{DO}_3$  phase undergoes a transformation to the B2 phase. Recent work [5] has shown that alloying additions of Mo, Si, and Ti can increase this stability to as much as  $250^{\circ}\text{C}$  above the binary transformation temperature.

At compositions above 33 at% Al, the B2 structure becomes the stable phase up to aluminum contents of 51%. This B2 phase, which will be the focus of this study, is also based on the  $\alpha$ -bcc terminal structure. Figure 2 shows the B2 crystal structure which is also known as the CsCl structure. This structure is made up of 2 interpenetrating simple cubic lattices with Fe atoms on one lattice and Al atoms on the other. Unlike the  $\text{DO}_3$  structure, the B2 structure in Fe-Al does not go through any transformations, and remains ordered to its melting point [6].

While the B2 phase exists over a wide range of compositions, 33 at% to 51 at% Al, it should be remembered that the perfect B2 structure will only exist at 50 at% Al and deviations from this composition requires a breakdown of the structure. It has been shown [7] that iron rich deviations from stoichiometry result in the excess iron atoms substituting on aluminum sites. These types of defects are known as antistructure defects. Deviations from

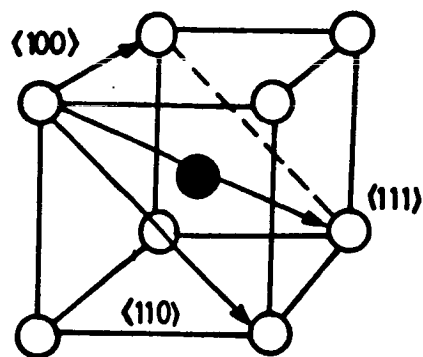


Figure 2. Schematic representation of the B2 FeAl unit cell.

stoichiometry on the aluminum rich side are not as well understood. Originally, Bradley and Jay [7] concluded that antistructure defects also occurred with excess aluminum. In contrast, Newmann, Chang, and Lee [8] have suggested the possibility of a mixture of antistructure defects and vacancies, known as triple defects. These defects consist of a pair of vacancies on Al sites and one Al atom on a Fe site, hence the name triple defect. Further theoretical calculations based on the enthalpy of formation [9,10] of these defects support this conclusion.

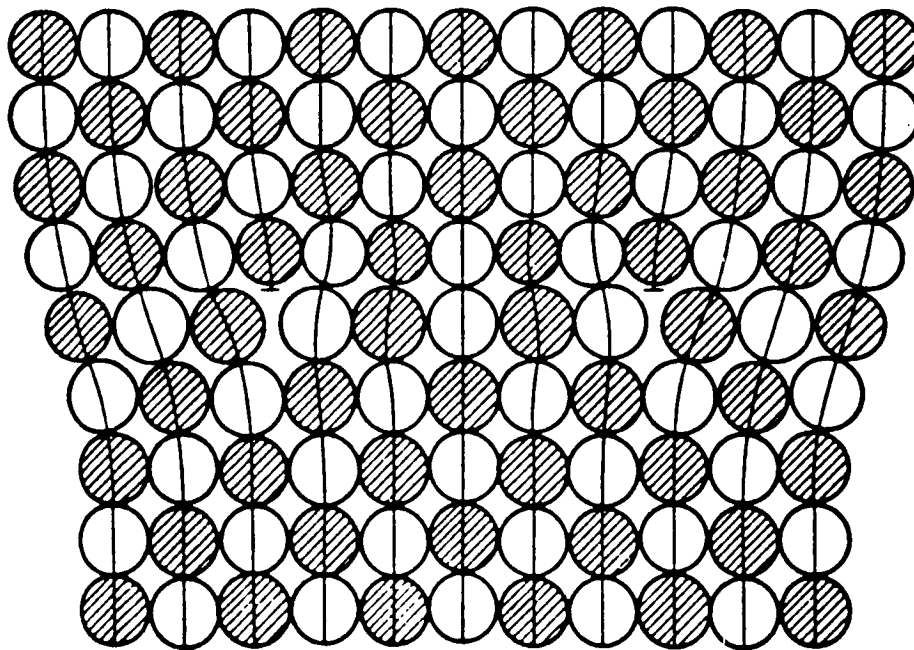
As has been noted, above 37 at% Al, the B2 phase remains ordered to its melting point [6]. Although the order does not change significantly with temperature, the concentration of thermal vacancies increases dramatically. Using Simmons-Balluffi analysis [11], Ho and Dodd [12] have shown thermal vacancy concentrations up to  $9.21 \times 10^{-3}$  at  $900^{\circ}\text{C}$  in Fe-50Al. In a more complete series of studies using dilatometry and field ion microscopy, Paris and co-workers [13,14] found vacancy concentrations as a function of composition and temperature. These studies found that at a given temperature, the vacancy concentration increased with Al composition (as expected, because  $T_m$  decreases with Al concentration), and the concentrations reached a maximum at approximately  $1050^{\circ}\text{C}$ . The vacancy maxima are  $1.4 \times 10^{-2}$  for Fe-46Al and  $2.2 \times 10^{-2}$  for Fe-51Al. These vacancy concentrations are very high when compared with

conventional metals which normally have concentrations on the order of  $10^{-4}$  near their melting point [15]. More importantly, these studies have shown that large numbers of these vacancies can be quenched in at room temperature. For example, a Fe-49.5Al alloy quenched from 1000 °C displays a room temperature vacancy concentration of  $1.85 \times 10^{-2}$  [13]. A number of studies [16,17] have examined the annealing out of these quenched in vacancies using electron microscopy. Fourdeux and Lesbats [16] observed no loops or dots in the as quenched state. However, Junqua et al. [17] observed a limited number of loops in the as quenched state. Both of these studies found complex loop and helical formation during annealing.

#### Mechanical Behavior of FeAl Alloys

Before discussing the mechanical behavior of Fe-Al alloys, it is important to briefly review the consequences an ordered lattice has on dislocation motion. Because of the ordered lattice, the passage of a dislocation on certain planes causes a disordering of the lattice behind the dislocation known as an antiphase boundary (APB). Another dislocation passing on the slip plane is required to reorder the structure. This process is schematically shown in fig. 3. This phenomenon has a number of different consequences on dislocation motion, depending on crystal structure and slip plane. In its simplest form, a pair of dislocations moves through the lattice as a coupled unit with an antiphase boundary between them.





**Figure 3.** Schematic illustration of a superdislocation pair and associated antiphase boundary.

This type of configuration is known as a superdislocation. The separation between the dislocations is a balance between the energy associated with the formation of the APB and the repulsive force of the dislocations. If the APB energy is low enough, dislocations may move separately, leaving behind trails of APB.

In the case of  $\text{Fe}_3\text{Al}$  with the  $\text{DO}_3$  crystal structure, the simple cases above are further complicated. Because of the more complex crystal structure, the passage of a second dislocation reorders the nearest neighbor bonds, but disorders the next nearest neighbor bonds. This results in a situation where four dislocations are required to maintain perfect order in the crystal. Thus, there are nearest neighbor antiphase boundaries (NNAPB) and next nearest neighbor antiphase boundaries (NNNAPB).

To further complicate matters, the individual dislocations in a super dislocation configuration may dissociate into stacking faults bounded by partial dislocations. Thus, a large number of dislocation configurations may occur in ordered alloys. Figure 4 displays schematically a number of these dislocation configurations which may occur in B2 and  $\text{DO}_3$  alloys.

#### $\text{Fe}_3\text{Al}$ Fracture, Ductility and Yielding

Very early studies have indicated that even at low concentrations (13.5 at%), aluminum has an embrittling effect on iron [18]. This brittle nature has in general been attributed to all alloys in the  $\alpha$ -bcc based composition range. However, close

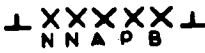



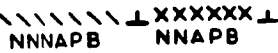



	<u>Burgers Vector</u>	<u>Dislocation type</u>
<b>B2</b> 	$2 \times \frac{a}{2} \langle 111 \rangle$	Super dislocation
	$\frac{a}{2} \langle 111 \rangle$	Ordinary with APB
	$a \langle 100 \rangle$	Ordinary
<b>DO<sub>3</sub></b> 	$4 \times \frac{a}{4} \langle 111 \rangle$	Super dislocation
	$2 \times \frac{a}{4} \langle 111 \rangle$	Imperfect super dislocation
	$\frac{a}{4} \langle 111 \rangle$	Ordinary with APB
	$2 \times \frac{a}{2} \langle 100 \rangle$	Super dislocation
	$\frac{a}{2} \langle 100 \rangle$	Ordinary with APB

Figure 4. Illustration of the types of dislocation configurations possible in Fe-Al alloys.

examination of the literature reveals that the degree of brittleness, along with other mechanical properties, vary among the alloys.

As with the random solid solution alloys, the  $\text{Fe}_3\text{Al}$  alloys were originally reported as displaying brittle behavior when tested in tension at room temperature [19,20]. These alloys, which exhibited brittle, intergranular failure, were manufactured by casting techniques. However, a recent study [21] has shown that significant tensile ductility can be realized in  $\text{Fe}_3\text{Al}$ . These alloys of Fe-25 and Fe-31 at% Al have been produced by extrusion of rapidly solidified powder, and display ductilities of up to 8%. Additionally, Kerr [22] has recently reprocessed the material used in reference [19] to decrease the carbon content. This decarburized material was found to have greater than 4% ductility in four point bending. In both cases where  $\text{Fe}_3\text{Al}$  has displayed significant ductility, transgranular cleavage was the predominant fracture mode. Therefore, it appears that the brittleness displayed in  $\text{Fe}_3\text{Al}$  may be related to impurities weakening the grain boundaries.

The yield behavior of  $\text{Fe}_3\text{Al}$  has been studied in tension [21,23] and compression [24], and these results are in good agreement. It has been found that the yield strength decreases somewhat with increasing aluminum content, especially above 25 at%. Leamy and Kayser [24] have attributed this behavior to difficulty in nucleating superdislocations at low aluminum

concentrations. This results in deformation by motion of ordinary dislocations and associated NN and NNNAPB trails. At higher aluminum contents, nucleation of super dislocations can take place more easily, this resulting in lower yield strengths.

These yield studies have also found an anomalous increase in yield strength near the  $DO_3$ -B2 order-disorder transformation [21,23]. Marcinkowski and Brown [25] have attributed this to a breakdown in short-range order, resulting in disordered pairs of atoms causing stress fields that oppose dislocation motion.

#### $Fe_3Al$ Substructures and Dislocations

A number of studies have explored the substructures of  $Fe_3Al$  alloys [25-30]. Marcinkowski and Brown [26] carried out the first of these studies and found substructures containing thermal APB domains. It was found that in order to reveal these antiphase domain boundaries using transmission electron microscopy, the foil must be oriented for strong diffraction by a superlattice reflection [26]. In the deformed state [26], this group observed ordinary  $a_0/4\langle 111 \rangle$  dislocations and associated APB trails on the slip planes. They attributed this deformation behavior to a relatively low APB energy, allowing slip of individual dislocations. More recent studies [27-30] have shown that a number of different dislocation arrangements may occur, depending on alloy composition, deformation temperature, and work hardening stage. Leamy and co-workers [27,28] have related a 5 stage work

hardening process in single crystals to changes in dislocation behavior. They found that initially perfect superdislocations (four  $a_0/4\langle 111 \rangle$  dislocations) predominated. Later, imperfect dislocations of the two  $a_0/4\langle 111 \rangle$  type and associated NNNAPB's occurred. Finally, single  $a_0/4\langle 111 \rangle$  dislocations with NNAPB were predominant. Crawford et al. [29,30] found that as the aluminum composition was increased, dislocations changed from perfect four  $a_0/4\langle 111 \rangle$  superdislocations to imperfect two  $a_0/4\langle 111 \rangle$  superdislocations. They attributed this behavior to a decrease in NNNAPB energy with increasing Al content while the NNAPB energy increases to some degree. Thus, below a given energy (i.e. at higher Al contents), the NNN interaction no longer restrict dislocation motion.

#### FeAl Fracture, Ductility and Yielding

Although B2 FeAl alloys have a reputation for being brittle materials, very little work has been performed on their mechanical behavior. The earliest work on this material was performed by Sainfort and co-workers [31] who studied tensile properties of a 40 at% alloy, with 100  $\mu\text{m}$  grain size, as a function of temperature. This study found the ductility increased from 8% at ambient temperature to 50% at 1073 K. The corresponding yield strength remained essentially constant to 973 K, then fell off rapidly.

A number of more recent studies have examined materials

produced by extrusion of rapidly solidified powder. Mendiratta et al. [32] have reported tensile elongations of 6% and 2.5% for alloys containing 35 and 40 at% Al respectively. These alloys had grain sizes of approximately 20  $\mu\text{m}$ . Also Baker and Gaydos [33] have reported yield behavior consistent with Sainfort et al. [31] with a Fe-36.9Al-2.2Ni alloy. Unfortunately, this paper only reported reduction in area and not tensile elongation as a measure of ductility. Baker [34] has also tested a Fe-48Al alloy and has found no yielding before fracture below 500 K. The general trend of decreasing ductility with increasing aluminum content has also been observed in melt spun ribbons [35]. Using a simple bend test, the strain to failure of as-spun ribbons was 6% for Fe-40Al, 1.5% for 45Al and essentially 0 at 50Al. The ductility of the 40Al and 45Al ribbons was found to increase to a large degree with heat treatment at 1273 K for one hour. However, the reasons for this behavior have not been given, and may either be related to some type of recovery, or to increases in grain size such that the grains extend completely across the ribbons. The ribbons were found to fail in an intergranular manner. All of these studies suggest that the ductility of B2 FeAl is a strong function of aluminum concentration. However, no explanation has been proposed for this behavior.

Westbrook [36] has studied the effect of alloy stoichiometry on the hardness of FeAl. He has found that as the aluminum content is decreased from stoichiometry, the hardness decreases

rapidly. Aluminum additions above stoichiometry increase the hardness dramatically. This behavior is found from room temperature, up to 600 °C, where the hardness is relatively constant with composition. These results are contrary to those for the B2 alloys NiAl and CoAl where deviations on either side of stoichiometry cause dramatic hardening [36]. Westbrook has attributed this effect in NiAl and CoAl to defect hardening as the alloys are moved away from stoichiometry. However, he has given no explanation for the behavior observed in FeAl.

#### FeAl Substructure and Dislocations

A large number of studies have examined the substructure of B2 FeAl in both single crystal and polycrystalline forms. In neither of these cases has the occurrence of thermal antiphase domains been observed. This suggests that the equilibrium domain size is extremely large, and complications due to domains do not have to be considered.

A number of studies have used single crystals to study the nature of dislocations. The first of these studies was carried out on a series of single crystals with a composition of 35.5 at% Al [37]. This study used rectangular single crystals to determine the slip plane by trace analysis. The observed slip plane from 77 K to room temperature was  $(\bar{1}01)$ . The slip direction was determined to be  $[111]$  by determining the orientation of "zero contrast" where the slip direction is parallel to the surface. In



this temperature range, no [001] type slip was observed. Although this study used TEM micrographs to relate work hardening to dislocation densities, no burgers vector determination by contrast analysis was reported.

Yamagata and Yoshida [38] used this same type of trace analysis to determine the deformation characteristics at a much higher aluminum content, 48 at%. Using a number of different orientations, they found that while the slip direction was constant at [111], the slip plane could be {110}, {123}, or {112}. These multiple slip planes were dependent on orientation and temperature. Multiple slip was predominant at 77 K but decreased with temperature. At room temperature, {110} was the dominant slip plane with {112} being the only other slip plane observed, and this only when oriented so that the resolved shear stress was at a maximum on {112}. Yamagata [39] followed up this investigation with transmission electron microscopy. He concluded that because FeAl has a large elastic anisotropy factor,  $A = 2C_{44}/(C_{11} - C_{12}) = 2.94$  ( $\alpha$ -iron has a value of 2.33), that  $\vec{G} \cdot \vec{b} = 0$  invisibility criteria is not applicable. Head et al. [40,41] have discussed this problem in detail and have predicted double images for  $\vec{G} \cdot \vec{b} = 0$  in  $\beta$ -brass. Yamagata [39] has observed this behavior in FeAl and concluded that the burgers vector in these studies is  $\langle 111 \rangle$ . (It should be noted that the double images presented by Yamagata are in weak contrast, and the  $\vec{G} \cdot \vec{b} = 0$  criteria may be applied to images with residual contrast.)

Umakoshi and Yamaguchi have also studied the slip directions in single crystal FeAl [42,43]. These studies have examined compositions ranging from 47.2 to 49.2 at% Al and confirm that  $\langle 111 \rangle$  is the dominant slip direction at room temperature. However, the slip direction was observed to change to  $\langle 001 \rangle$  at higher temperatures. This transition temperature was found to increase from around 600 K at 47.2 at% Al to around 800 K at 49.2 at% Al and was also found to be dependent upon the crystal orientation. The observed slip plane in this study was  $\{110\}$  throughout the temperature range studied with occasional cross slip of  $\langle 111 \rangle$  dislocations onto  $\{211\}$  planes noted.

A similar study of slip directions as a function of deformation temperature has been undertaken over a much wider composition range, 35 at% Al to 50 at% Al, using polycrystalline compression samples [44]. This study confirmed the transition from  $\langle 111 \rangle$  to  $\langle 001 \rangle$  slip with temperature. However, the slope of the transition temperature versus composition was opposite to that which was found in single crystals [43]. In the polycrystal study, no transition was observed at 35 at% Al. The transition was observed at 700 °C in Fe-40Al and decreased to 400 °C at Fe-50Al. No explanation has been given for these differences in transition observations.

The observation of  $\langle 111 \rangle \{110\}$  slip has an important implication with regards to the mechanical behavior of these alloys. It is well known that the combination of  $\langle 111 \rangle$  slip on

{110} planes provides a sufficient number of slip systems for polycrystalline compatibility. That is, von Mises criteria is satisfied. Thus, the limited ductility in these alloys is clearly not a result of insufficient slip systems. Therefore, other factors must be involved in the limited ductility in B2 FeAl.

Another consequence of the  $\langle 111 \rangle$  dislocations is that in B2 alloys, these must move in pairs of  $1/2 \langle 111 \rangle$  dislocations, or leave APB trails. None of the studies on these materials have observed any APB trails in electron microscopy [37,39,42-44]. Thus, the dislocation motion must occur in pairs. Ray, Crawford, and Cockayne [45] first observed these pairs in Fe-35Al using weak beam microscopy. Crawford and Ray [30] then calculated the APB energy by measuring dislocation separations in alloys from 27 to 36 at% Al in alloys displaying both DO<sub>3</sub> and B2 order. They have shown that for B2 order, the APB energy varies from 28 ergs/cm<sup>2</sup> at 27% Al to 105 ergs/cm<sup>2</sup> at 36% Al. Further analysis by Crawford [46] has shown that the relationship

$$\gamma_{\text{APB}} (\text{B2}) = (\gamma_{\text{NNAPB}} - 1/2 \gamma_{\text{NNNAPB}})(\text{DO}_3) \quad [1]$$

is predicted by ordering theory, and that experimental data fit this expression well.

Vidoz and Brown [47] have proposed a mechanism for work

hardening in ordered alloys which involves the formation of APB tubes. These are formed by the intersection of 2 superdislocations on different slip planes, which results in jogs. If the jogs do not lie in the slip plane, or if they have low mobilities, they will be left behind as the dislocations continue to slip. This leaves behind a thin ribbon of APB material known as an APB tube. These APB tubes have been observed by Crawford [37] in highly deformed Fe-35.5 at% Al as fine lines in the [111] direction on dark field micrographs. Corresponding to these, streaking was observed in the  $[1\bar{2}1]$  directions on selected area diffraction patterns. Chou and Hirsch [48] have also observed these in a Fe-30.5 at% Al alloy displaying B2 long range order. This study used weak-beam microscopy using superlattice reflections to image these tubes properly. Attempts to determine the thickness of these tubes resulted in estimates of approximately 0.4 nm on the order of a few burgers vectors.

#### Effect of Boron on Ni<sub>3</sub>Al

Recently, a considerable amount of research has studied the effect of small amounts of boron additions to Ni<sub>3</sub>Al. This material, which has the L1<sub>2</sub> structure, is characterized by no ductility and brittle intergranular failure at room temperature. This is in spite of the fact that single crystals display substantial ductility and enough slip systems are available to satisfy von Mises criteria.

Aoki and Izumi [49] were the first to report that small additions of boron greatly improved the room temperature ductility of polycrystalline  $\text{Ni}_3\text{Al}$ . This effect was then studied in greater detail by Liu et al. [50,51] for Al compositions ranging from 24 to 26 at% and boron levels up to 0.4 wt%. This study found that the boron ductilizing effect was critically dependent on deviations from alloy stoichiometry, with the best effect occurring at substoichiometric 24 at% Al. At this stoichiometry, a maximum tensile elongation of 50% was possible by using a boron addition of 0.1 wt%. Associated with a large increase in ductility, the fracture mode changed from brittle intergranular fracture to transgranular fracture.

The question then arises, what is the boron doing to effect such a dramatic change? The boron has in some way strengthened the  $\text{Ni}_3\text{Al}$  grain boundary adhesion such that brittle fracture is inhibited. Two possibilities exist: (1) that impurity effects are weakening the grain boundaries and boron is acting as a scavenger of these detrimental contaminants or (2) the grain boundaries in  $\text{Ni}_3\text{Al}$  are intrinsically weak (poor adhesion) and the boron is strengthening these weak bonds. The second situation is particularly applicable to ordered alloys where wrong neighbor bonds may cause certain grain boundary structures to be inherently weak [52].

This question has been examined in detail in a number of recent studies. Although early studies using Auger Electron

Spectroscopy (AES) have indicated that sulfur can segregate to grain boundaries in  $\text{Ni}_3\text{Al}$ , and almost certainly has a detrimental effect [53]. recent studies have suggested impurity effects are not the cause of weak grain boundaries in  $\text{Ni}_3\text{Al}$ . Using high purity  $\text{Ni}_3\text{Al}$ , Obura, Hanada, Masumoto, and Izumi [54] found that  $\text{Ni}_3\text{Al}$  still failed by intergranular fracture. Subsequent AES found no Auger peaks other than those of Ni and Al, proving that there was no segregated impurity at grain boundaries. This suggests that grain boundary brittleness in  $\text{Ni}_3\text{Al}$  is an inherent property and not due to harmful impurities. Other studies [54,55] have also shown that intergranular failure of  $\text{Ni}_3\text{Al}$  persists even though no impurities are detected using AES. Thus, the role of boron in strengthening  $\text{Ni}_3\text{Al}$  grain boundary adhesion is one of increasing the boundary strength, and not due to scavenging of impurities. The above studies by Liu et al. [50,55] have also shown that the boron segregates to grain boundaries in  $\text{Ni}_3\text{Al}$ , and this segregation is stronger at substoichiometric compositions where the best mechanical properties are observed. Along with this, the segregation of boron is stronger to grain boundaries than to free surfaces [56], which is opposite than that observed for C and S. This agrees with the theory of Rice [57] which predicts enhancement of grain boundary adhesion for elements which segregate strongly to grain boundaries, but not to free surfaces.

In addition to improving the adhesion of  $\text{Ni}_3\text{Al}$  grain boundaries, boron also plays another role. When the yield stress

is plotted as a function of (grain size)<sup>-1/2</sup> (i.e. Hall-Petch plot), the slope of the resulting lines are different for Ni<sub>3</sub>Al than for Ni<sub>3</sub>Al + B [58,59]. The slope,  $K_y$ , of the boron containing alloys is significantly less than that for the alloys without boron. This suggests that boron makes propagation of slip across grain boundaries easier [58]. Thus, in addition to increasing the adhesive strength of Ni<sub>3</sub>Al grain boundaries, boron also allows slip to move across grain boundaries easily, rather than initiating intergranular cracks. This effect has been attributed to boron increasing the mobility of grain boundary dislocations [59].

Because boron segregation to grain boundaries is so important to the ductility of Ni<sub>3</sub>Al, Choudary, White, and Brooks [60] have examined this segregation as a function of thermal history. Using AES, this study found that water quenching inhibited boron segregation and resulted in increased intergranular failure. By contrast, step annealing resulting in enhanced boron segregation and a correspondingly greater amount of transgranular failure. Another finding was that in samples that displayed mixed mode failure, the intergranular facets had a correspondingly lower boron content than those associated with transgranular facets.

#### Boron Effects in other Materials

Although boron has not been studied as a grain boundary strengthener in many materials, a few studies are worth noting.

The susceptibility of nickel to hydrogen embrittlement was found to decrease with the addition of boron [61]. This was observed as an increase in fracture stress and elongation for a given hydrogen charging time in Ni containing boron versus Ni without any boron. Intergranular fracture was also suppressed significantly in the samples containing boron. This study was unable to conclude whether the beneficial effect was due to increased grain boundary bond strength, or due to a scavenging of residual impurities such as Sb or Sn which may be related to hydrogen cracking of Ni.

In contrast to this, boron has no beneficial effect on the room temperature mechanical properties of 316 stainless steel [62]. The boron was found to have no effect on the grain boundary state in terms of diffusion and free energy. This was attributed to most of the boron being tied up in the form of  $M_{23}(C,B)_6$  carbides.

One other limited study on the effect of boron additions should be noted. Using rapidly solidified powder, boron has been found to strengthen  $Fe_3Al$  [63]. This strengthening has been attributed to precipitation of borides.

### The Present Study

The review of the current literature reveals an incomplete understanding of a number of aspects of B2 FeAl alloys. To begin with, it has been demonstrated that the ductility of FeAl decreases with increasing Al content. However, the reasons for



this have not been studied. Secondly, although the quenching in and subsequent annealing of vacancies has been studied in FeAl, the effect these vacancies have on the mechanical behavior has not been addressed. Thirdly, because the addition of boron has such a dramatic effect on  $\text{Ni}_3\text{Al}$ , it is important to determine if this effect is applicable to other ordered aluminides. Thus, this study has three primary objectives. The first is to gain a better understanding of the relationships between yielding, ductility, and fracture of B2 FeAl. This will be accomplished by studying the mechanical behavior at two compositions; Fe-40Al and Fe-50Al. Powder processed polycrystalline behavior will be related to that observed in single crystals. These results will be discussed in terms of changes in dislocation behavior as a function of stoichiometry.

The second goal is to study the effect of prior thermal history on the mechanical behavior. As has been described, large numbers of vacancies can be quenched into B2 FeAl. The effect of these vacancies on the deformation behavior will be related to the general behavior of polycrystals and single crystals.

The third objective of this study is to examine the effect of boron on the mechanical behavior of these alloys. The effect of boron will be observed as a function of stoichiometry and of thermal history in both powder processed materials, and cast and extruded materials.

## EXPERIMENTAL PROCEDURE

### Material

A number of different materials and processing techniques were used in this study, including extrusions of FeAl powder and castings, and single crystals.

### Powder Extrusions

Three different series of powder extrusions were used in this investigation. All of the powders were manufactured by gas atomizing pre-alloyed FeAl to the desired stoichiometry. The resulting powders were spherical in shape and -80 mesh in size. Figure 5 shows the appearance of the initial powder. Boron additions were made by elementally blending -200 mesh boron powder. Extrusions were carried out by NASA Lewis Research Center, Brookpark, Ohio.

The first series of powder extrusions consisted of 2 alloys produced from powder supplied by Alloy Metals Inc., Troy, Michigan. The first extrusion was produced from the as received powder while the second was produced by adding 0.1 wt% B. Both of these batches received a 2 hour mix in a vee blender. Extrusions were made by filling 1 pound of powder into a mild steel can with an inside diameter of 2 inches, an outside diameter of 3 inches, and an overall length of 5.6 inches. These cans were evacuated and welded shut. The cans were then extruded at 1250 K using an

ORIGINAL PAGE IS  
OF POOR QUALITY

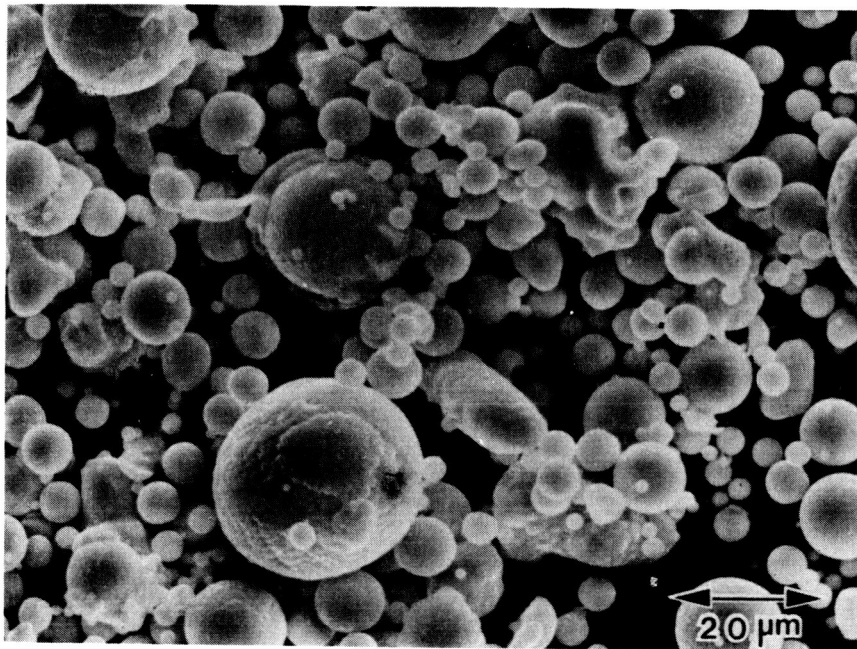


Figure 5. SEM micrograph displaying the typical starting powder used in this study.

area reduction ratio of 16:1. A schematic representation of the extrusion process is shown in fig. 6. The extrusions had the following chemical compositions and designations.

	<u>Al</u>	<u>O</u>	<u>B</u>	<u>Fe</u>
1.A	33.0 wt%(50.4 at%)	0.059 wt%	-	balance
1.B	31.5 wt%(46.4 at%)	0.074 wt%	0.24 wt%	balance

The second series of powders consisted of 8 different compositions Fe-40Al and Fe-50Al, each containing 0, 0.05, 0.1, and 0.2 wt% B. These powders were also supplied by Alloy Metals. The powder lot designations were Lot #A12218 for the Fe-50Al powder and Lot #A18115 for the Fe-40Al. Boron additions were made in the same manner as before. Three pounds of each powder were put into mild steel cans with 3" I.D. and 4" O.D.. These were extruded at 1250 K with a diameter ratio of 8:1. Four inch sections were cut from these extrusions and placed in 2" I.D. cans. These were then re-extruded at 1075 K and 1350 K at a ratio of 6:1. The chemistries and designations of these materials are given in table I. It should be noted that this series of extrusions contained significant amounts of metallic contaminants.

The third series of powder extrusions was produced using Alloy Metals Lot #A188767 which contained no measurable metallic impurities. These extrusions were produced in the one step method as in series 1, with an extrusion temperature of 1250 K and a

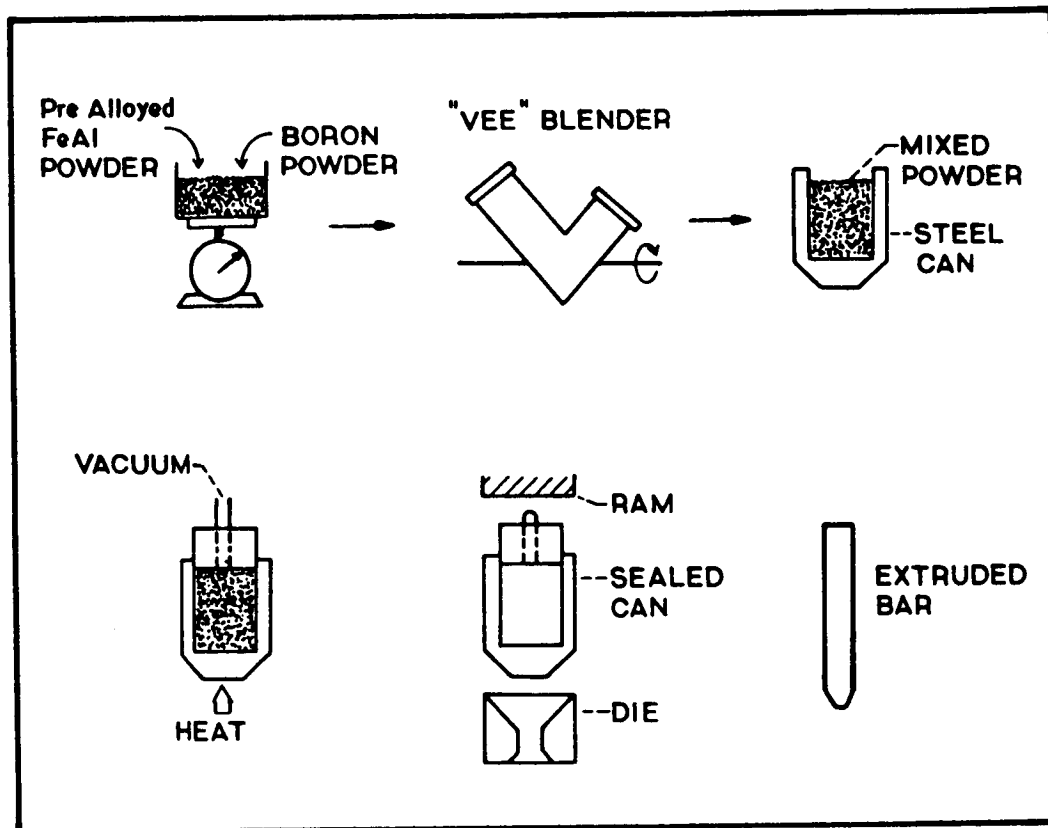


Figure 6. Illustration of the hot extrusion process used in consolidation of metallic powders.

Table I  
Chemical compositions and designations of second series  
extrusions.

	<u>2nd extrusion temperature</u>	<u>Al*</u>	<u>Co*</u>	<u>Cr*</u>	<u>Mn*</u>	<u>La*</u>	<u>N*</u>	<u>O*</u>	<u>B*</u>	<u>Fe*</u>
2.B	1350 K	24.4 wt% (40.0 at%)	0.08	0.1	0.1	0.3	0.004	0.061	-	balance
2.BL	1073 K	"	"	"	"	"	"	"	-	"
2.C	1350 K	"	"	"	"	"	"	0.062	0.072	"
2.CL	1073 K	"	"	"	"	"	"	"	"	"
2.D	1350 K	"	"	"	"	"	0.006	"	0.100	"
2.DL	1073 K	"	"	"	"	"	"	"	"	"
2.E	1350 K	"	"	"	"	"	0.004	0.066	0.190	"
2.EL	1073 K	"	"	"	"	"	"	"	"	"
2.F	1350 K	32.8 wt% (50.2 at%)	-	0.02	0.01	-	0.002	0.058	-	"
2.FL	1073 K	"	-	"	"	-	"	"	-	"
2.G	1350 K	"	-	"	"	-	"	0.062	0.62	"
2.GL	1073 K	"	-	"	"	-	"	"	"	"
2.H	1350 K	"	-	"	"	-	"	0.064	0.11	"
2.HL	1073 K	"	-	"	"	-	"	"	"	"
2.I	1350 K	"	-	"	"	-	0.001	0.062	0.18	"
2.IL	1073 K	"	-	"	"	-	"	"	"	"

\* in weight percent

reduction ratio of 16:1. The designation and chemistries of these alloys are:

	<u>Al</u>	<u>N</u>	<u>O</u>	<u>B</u>	<u>Fe</u>
3.A	25.03 wt%(40.83 at%)	0.0006	0.028	-	*
3.B	25.03 wt%(40.83 at%)	0.0006	0.028	0.10	*

\* = balance is Fe

#### Cast Extrusions

FeAl castings approximately 2" in diameter and 4" in length were provided by Armco Metals Inc., Cincinnati, Ohio. The compositions of these castings were

#### Fe-40Al cast:

<u>Al</u>	<u>B</u>	<u>C</u>	<u>O</u>	<u>H</u>	<u>N</u>	<u>P</u>
22.8 wt%(37.9 at%)	-	0.0154	0.0005	0.0002	0.0003	0.003

#### Fe-40Al-B cast:

22.9 wt%(38.0 at%)	0.13	0.0214	0.0009	0.003	-	0.001
(balance Fe)						

These castings were sealed in 2" I.D. extrusion cans and evacuated. They were also extruded at 1250 K using a ratio of 16:1.

Details of all of the extrusion runs are given in Appendix A.

Single crystal specimens were also cut from this material.

### Heat Treatments

After removing the extrusion cans by centerless grinding, heat treatments varying from 1073 K to 1473 K for 24 hours were performed on the extruded specimens. These were performed to homogenize the extrusions, vary their grain sizes, and to study the effects of cooling rate. All heat treatments were carried out in a tube furnace in flowing Ar. The exit gas was monitored using a  $\text{ZrO}_2$  detector and was found to have an oxygen pressure of approximately  $1 \times 10^{-3}$  atm. Heat treatments were followed by a number of different cooling treatments as listed below:

- [1] Slow cooling: 50 K /30 min steps down to 500 °C, then furnace cooled to room temperature.
- [2] Tube cooling: slowly removing from furnace at approximately 1 inch per minute.
- [3] Air quenching: quickly removed from furnace and cooled in moving air.
- [4] Oil quenching: quickly removed from furnace and quenched in oil at room temperature.
- [5] Water quenching: quickly removed from furnace and quenched in water at room temperature.

After cutting to the desired dimensions, single crystal



These extrusion sheets include information press pressure, extrusion time, heat time and other details.

### Single Crystals

Two sources of single crystals were used in this study. The first was a rectangular casting approximately 6"x2"x0.5" containing large grains provided by TRW Inc., Euclid, Ohio. The composition and designation of this bar was:

#### Fe-50Al:

<u>Al</u>	<u>O</u>	<u>P</u>	<u>Fe</u>
31.6 wt%(48.8 at%)	0.0008	0.004	balance

Single crystal specimens were cut out of this polycrystalline casting using a low speed diamond saw.

The second source of single crystals was a rectangular casting approximately 6"x1"x1", also with large grains. This bar was supplied by NASA Lewis Research Center, Brookpark, Ohio and had a composition of:

#### Fe-40Al:

<u>Al</u>	<u>O</u>	<u>C</u>	<u>N</u>
23.8 wt%(39.2 at%)	0.0009	0.005	0.0005
balance is Fe			

specimens received heat treatments of 1273 K for 24 hours with the cooling steps slow cooled and oil quench designated above.

### Optical Microscopy

Optical microstructures were revealed using an etchant of 100 parts water, 20 parts  $\text{HNO}_3$ , 3 parts HF, and 2 parts HCl. This was effective in revealing the grain structure and precipitates.

Optical microstructures were examined using Nomarski interference contrast which brought out the grain structure in greater detail.

Grain sizes were determined using standard intercept methods on optical microstructures. The grain size is given by:

$$\text{Grain Size} = \frac{L}{M \times N} \quad [2]$$

where: L is the length of the test line

N is the number of intersections

M is the magnification.

A grid of test lines was used in an effort to maintain objectivity in determining the grain sizes.

Following heat treatment, round tensile bars were centerless ground out of the extruded specimens. The tensile bars had a diameter of 0.120" and a gauge length of 1.25" with the tensile direction corresponding to the extrusion direction. Figure 7 gives the dimensions of these tensile bars.

Prior to testing, these tensile bars were electropolished to

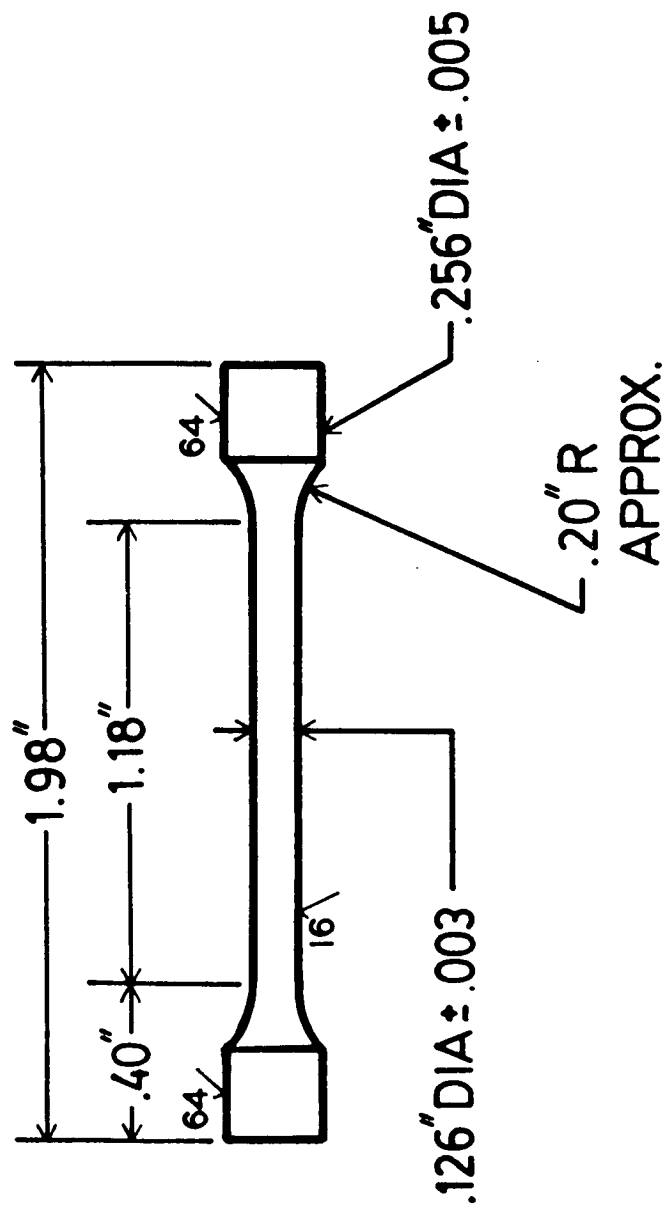


Figure 7. Schematic representation of tensile bars used in this study.

minimize the effects of surface flaws due to machining. the electrolyte used was 10% perchloric acid in methanol, cooled to  $-20^{\circ}\text{C}$ . The tensile bar was used as the cathode and a stainless steel beaker as the anode. The best polish was found to occur at a voltage of 18 V, with the tensile bar being rotated at 4 rpm.

Tensile tests were run using a crosshead speed of 0.005 "/min, a chart speed of 0.5 "/min, and a full scale load of 2000 lbs. Room temperature tests were performed in air while high temperature tests were carried out in vacuum.

The resulting fracture surfaces were examined using scanning electron microscopy (SEM) using an accelerating voltage of 25 kV. Compression samples 0.25 " in length and 0.12 " in diameter were also produced by centerless grinding and the ends ground parallel. These were tested at room temperature using tool steel compression pads. A crosshead speed of 0.001 "/min, a chart speed of 0.5 "/min, and a full scale load of 5000 lbs was used.

Rectangular single crystal compression samples approximately 3mm x 3mm x 10mm were cut from the single crystal material described above. These were hand polished through 600 grit and then their orientations determined by the back reflection Laue technique using an accelerating voltage of 26 kV, a current of 36 mA, and a Mo X-ray tube. These were then electropolished using the same set of conditions as those used for the tensile bars. Compression tests were carried out using a crosshead speed of 0.005 "/min, a chart speed of 2"/min, and a 2000 lb full scale

load. These single crystals were strained to approximately 2%. Slip lines were examined using Nomarski interference contrast and the slip plane determined by slip trace analysis.

#### Transmission Electron Microscopy

Thin foils for electron microscopy were produced by cutting thin sections from the materials and grinding by hand to a thickness of approximately 300  $\mu\text{m}$ . In the case of the deformed single crystals, these slices were made parallel to the slip plane, while they were made perpendicular to the deformation axis in polycrystalline samples. When necessary, 3 mm disks were cut from the thinned material using a Gatan ultrasonic disk cutter and boron nitride abrasive. Final electropolishing of the thin foils was carried out using a Struers Tenupol twin jet electropolishing cell and Polypower power supply. The electrolyte used was 30%  $\text{HNO}_3$  in methanol and was used only on the day it was made. The polishing was carried out at  $-30^\circ\text{C}$  using a voltage of 12 V. This resulted in a polishing current of approximately 0.1 A. The best polish was achieved by starting with a pump speed of 8, until the specimens faces became dished, then reducing the speed to 3 to avoid damaging the foil as it became thinner.

Transmission electron microscopy was performed on a Phillips EM 400T electron microscope equipped with a double tilt specimen holder and operated with an accelerating voltage of 120 kV. Burgers vector analysis was carried out using the  $\vec{g} \cdot \vec{b} = 0$  and

$\vec{g} \cdot \vec{b} \times \vec{u} = 0$  criteria. A complete analysis was carried out by using all of the available g-vectors in a combination of {100}, {110}, {111} poles.

Extraction replicas were produced for precipitate analysis. These were made by applying Fullam replicating tape to deeply etched samples, removing the tape, and carbon coating it. This resulted in the precipitates lying in the tape/carbon interface. The tape was placed on a Cu grid and then placed in an acetone evaporator. This dissolved the replicating tape and left behind a carbon film containing the precipitates supported on the Cu grid.

These replicas were examined in the TEM. X-ray energy dispersive spectroscopy (EDS) was performed on the extracted precipitates. Light elements were identified by performing wavelength dispersive spectroscopy (WDS) in a JEOL 840 SEM.

#### Texture Determination

Qualitative texture measurements were made by x-ray diffraction. Diffractometer scans were made of transverse and longitudinal sections of the extruded polycrystals. The relative peak heights in each orientation were then compared with each other, and to those published for FeAl, to give an indication of the texture of the material.

## EXPERIMENTAL RESULTS

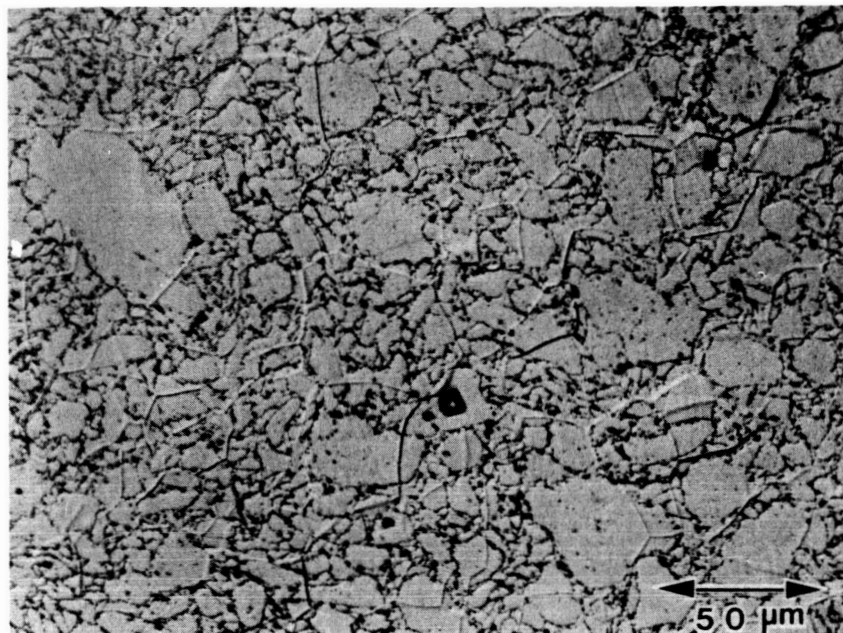
### Optical Microstructures

#### Powder Extrusions

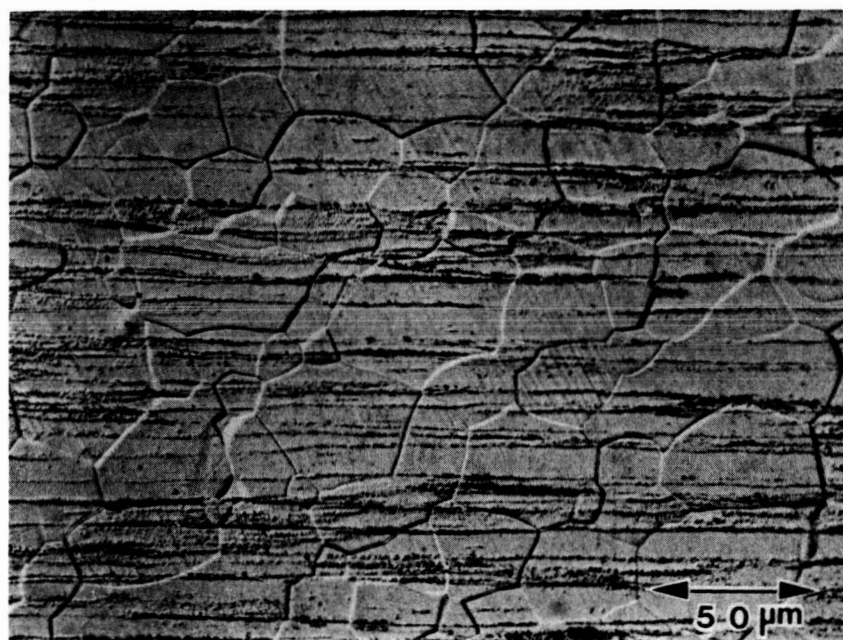
The hot extrusion technique used for consolidation of the starting powders has resulted in a fully dense material. Figure 8 shows typical transverse and longitudinal sections of this extruded material. The microstructure is characterized by an equiaxed grain structure and an underlying structure of oxide particles. These oxides, which are a result of oxidation of the alloy powder surfaces prior to extrusion, will be referred to as prior powder particle boundaries. In the transverse section these prior powder particle boundaries appear as circular rings of varying sizes. In the longitudinal sections, they are evident as long lines of particles strung out in the extrusion direction. This type of structure was typical of all of the extruded powder materials. However, some variations occurred with the different series of extrusions and various thermal treatments and these will be discussed in more detail.

The first series of extrusions, Fe-50Al and Fe-50Al + 0.2B, were all given a standard heat treatment of 1323 K for 48 hours, and all data from this series are from this thermal treatment. The microstructure of the Fe-50Al is shown in figs. 8a and b and has already been discussed. The microstructure obtained by addition of boron to this material is shown in figs 8c and d.

ORIGINAL PAGE IS  
OF POOR QUALITY



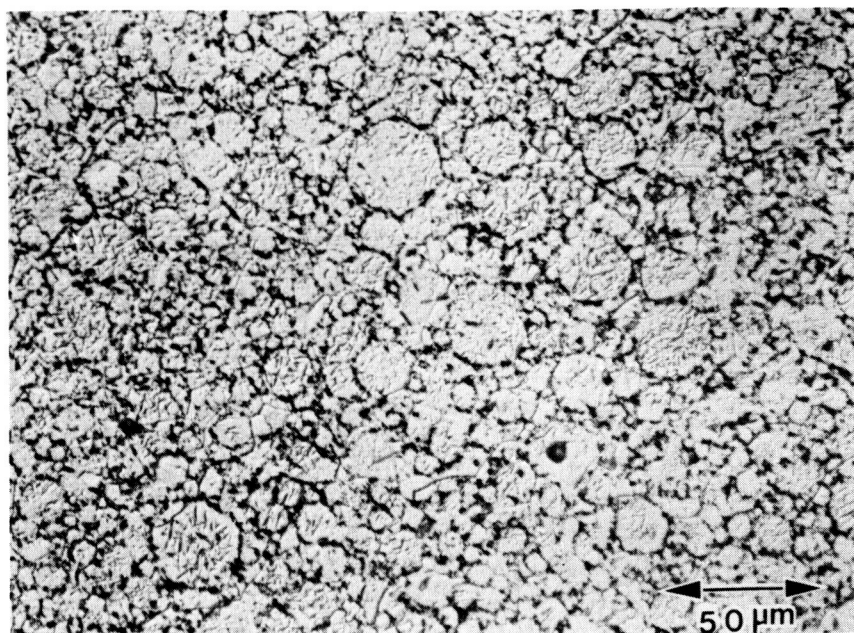
(a)



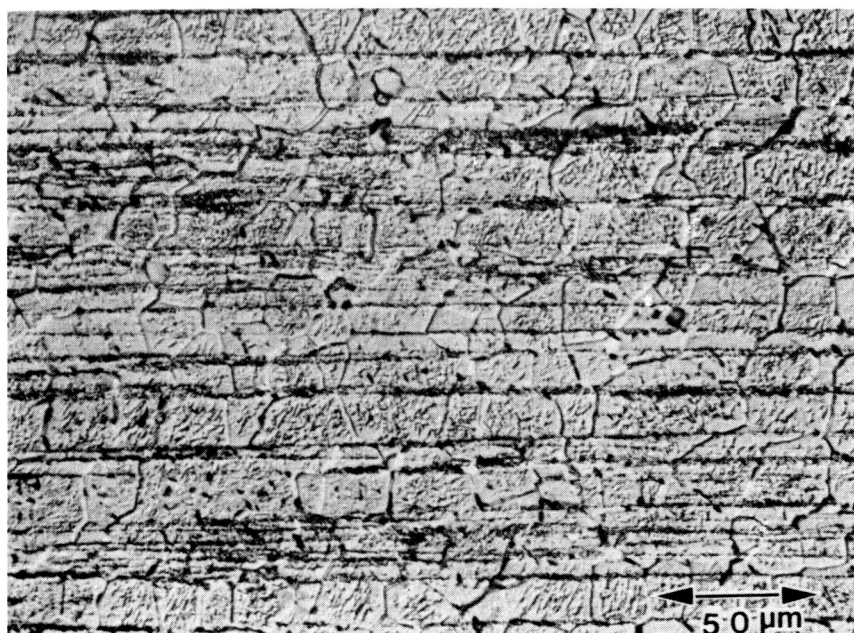
(b)

Figure 8. Optical micrographs showing a) transverse and b) longitudinal sections of the first series Fe-50Al and c) and d) Fe-50Al-B.





(c)



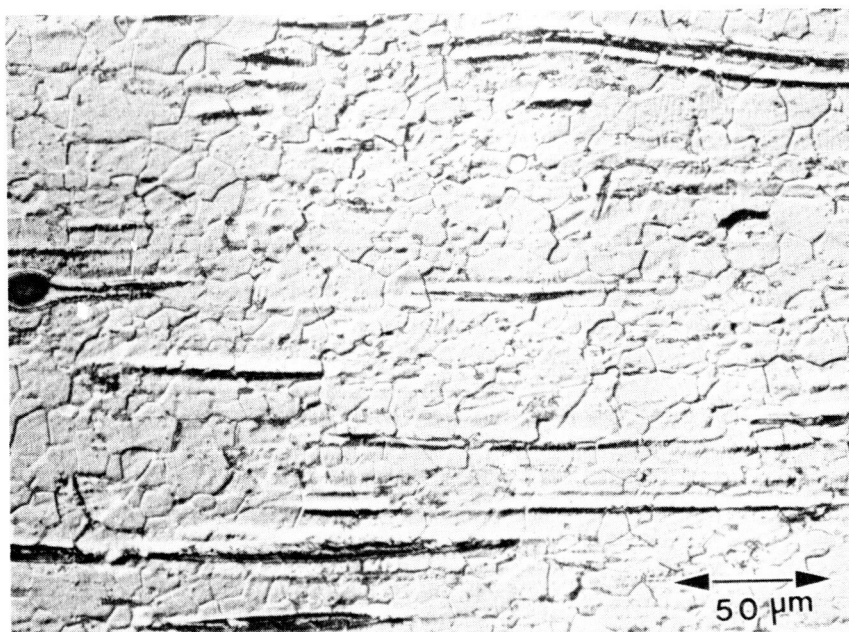
(d)

Figure 8 (cont.)

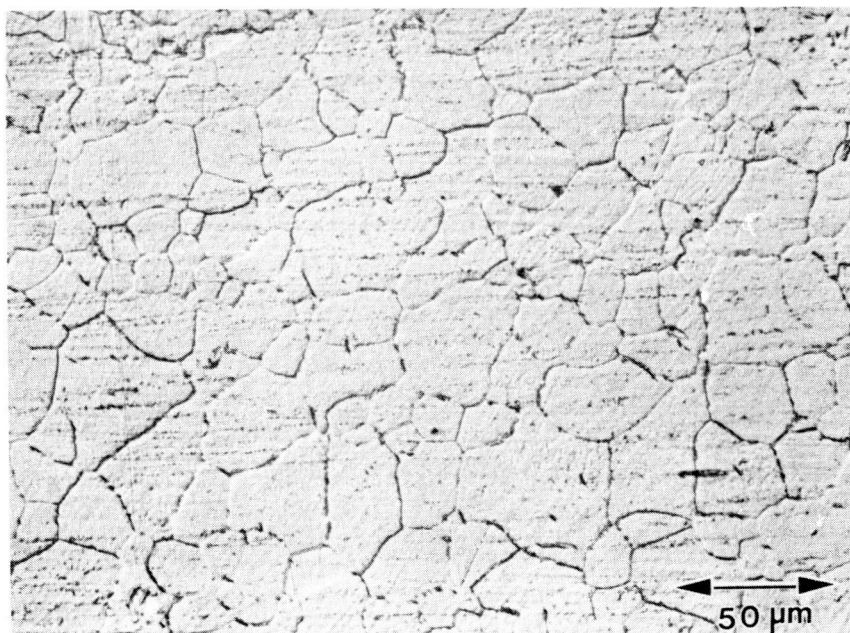
Although the basic grain and prior powder particle boundary structure are essentially the same, the addition of boron resulted in precipitation of a second phase which is revealed in the form of a fine needle-like distribution.

A number of interesting observations can be made from the microstructures of the second series of powder extrusions. It should be remembered that this series contained significant amounts of metallic impurities. Figures 9a and b show the microstructures of the Fe-40Al alloy of this series extruded at low (9a) and high (9b) temperatures. Evident in the low temperature extrusions are ribs of material which etched differently than the surrounding material. These stringers are often associated with inclusions and are suspected to be a result of the impurities. In the high temperature extrusions, these impurity stringers are not observed, suggesting that the material has become more homogeneous. Additionally, heat treatments performed on the low temperature extrusions result in a decrease in the amount of ribs observed. Some grain boundary precipitation was also observed, presumably as a result of the impurities. In extrusions of the second series, which were Fe-50Al, the starting powder had fewer contaminants, and these types of stringers were not observed.

The addition of boron to this second series of extrusions resulted in precipitation similar to the first series. However, this amount of precipitation was a function of composition, heat



(a)



(b)

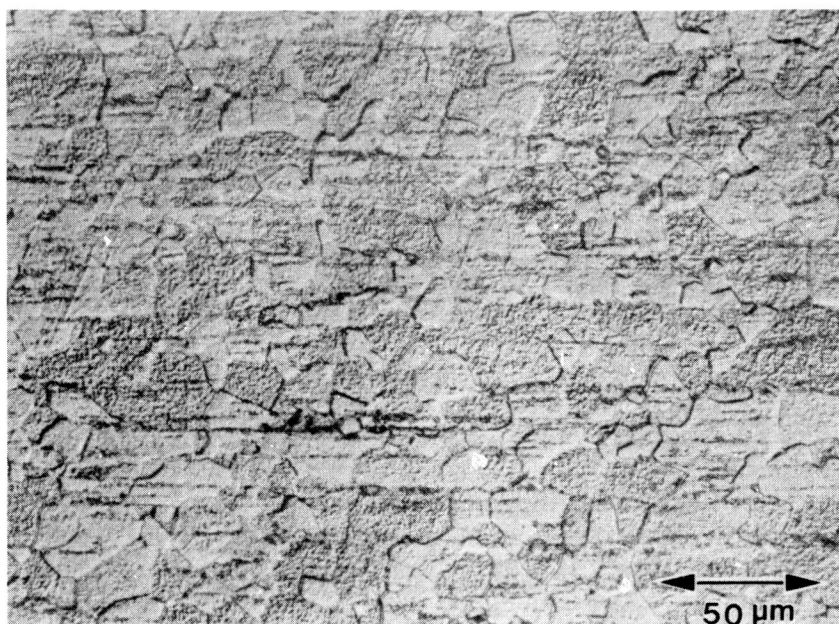
Figure 9. Optical micrographs of second series Fe-40Al extruded at a) 1073 K and b) 1350 K.

treatment, extrusion temperature, and boron level. In general, more precipitation was observed at the stoichiometric composition of Fe-50Al, than at off-stoichiometric Fe-40Al. This is displayed in fig. 10 where 2 alloys containing 0.1 wt%B which were subjected to the same thermal treatments are shown. The amount of precipitation was found to increase with extrusion temperature and with heat treatment at both stoichiometry levels. Additionally, the amount of boron added had a direct effect on the amount of precipitation observed. It should be noted however, that in all cases, the addition of boron caused some precipitation, indicating that the solubility limit of boron in the matrix has been reached even at the lowest level of 0.05 wt%B. The cooling rate following heat treatment had no noticeable effect on precipitation.

The third series of powder extrusions displayed a much more even microstructure than the second series in the as-extruded form. This is probably due to the fact that the third series did not contain any significant amounts of contamination. The addition of boron also resulted in significant precipitation. Figure 11 shows an example of this clean material, Fe-40Al-0.1B.

#### Cast Extrusions

The microstructures of the cast extrusions differ somewhat from the powder processed material. Figures 12a and b show optical micrographs of the cast material prior to extrusion. Although the chemistries indicate that the castings have



(a)



(b)

**Figure 10.** Optical micrographs displaying boron related precipitation in the second series a) Fe-50Al and b) Fe-40Al.

ORIGINAL PAGE IS  
OF POOR QUALITY

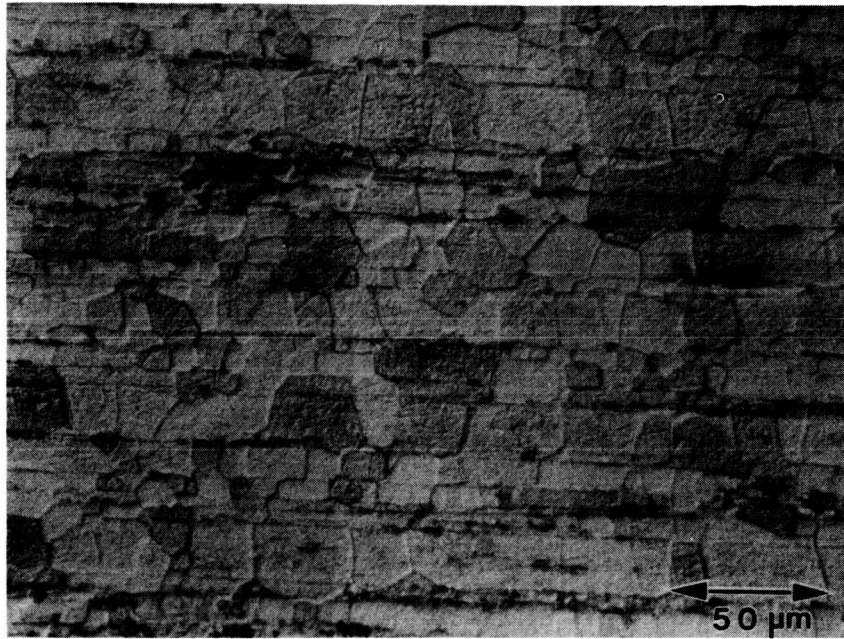
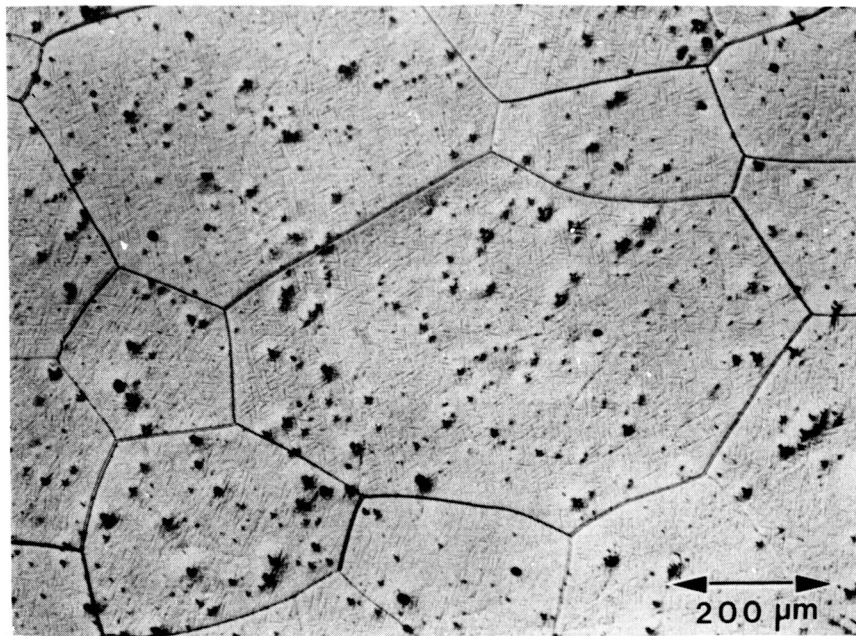


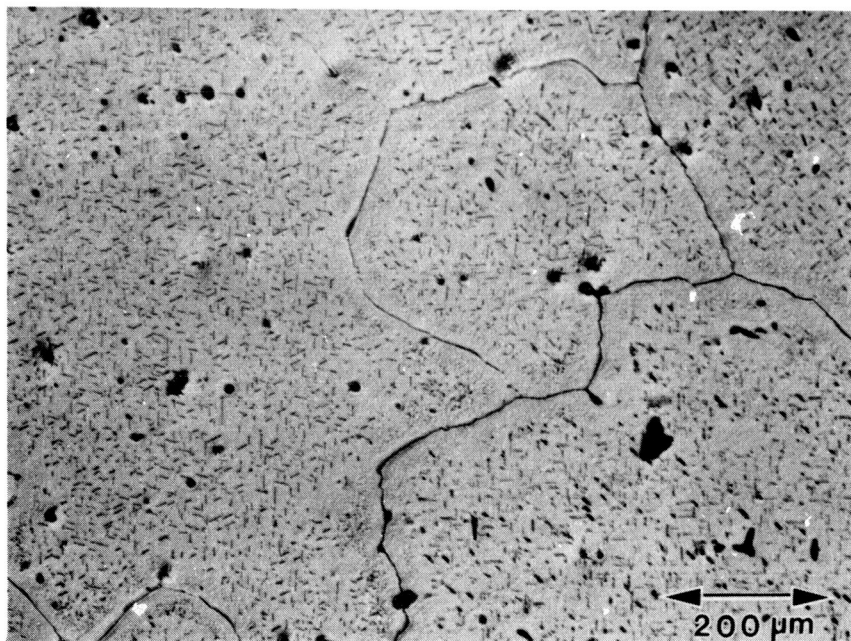
Figure 11. Optical micrograph displaying microstructure of the third extrusion series Fe-40Al-0.10B.



ORIGINAL PAGE IS  
OF POOR QUALITY



(a)



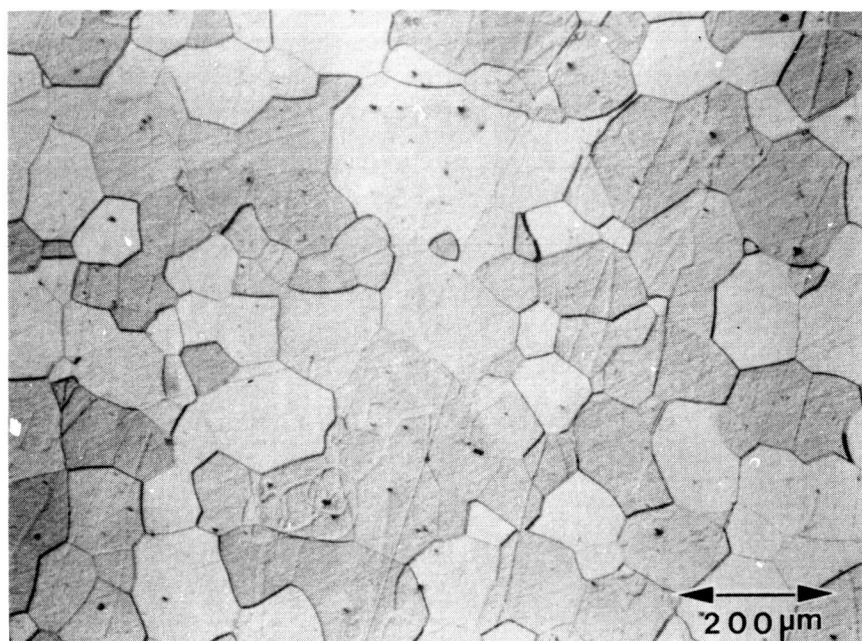
(b)

Figure 12. Optical micrographs of as-cast a) Fe-40Al and b) Fe-40Al-B.

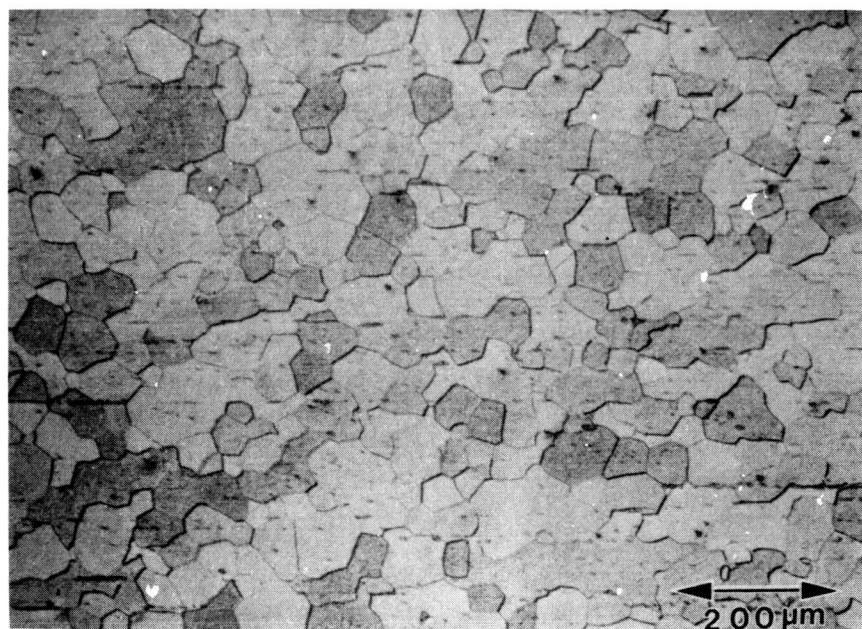
relatively high purities, it can be seen that significant amounts of debris are found in both castings. It should be noted however, that these micrographs were taken from the ends of the castings, and the inclusions may not be representative of the bulk. Some differences can be noted between the castings with and without boron. The casting without boron displays straight grain boundaries and a mottled background. This background when viewed at higher magnifications, appears to be an etching effect. By contrast, the casting containing boron displayed curved grain boundaries which may be a result of boride related pinning. Additionally, significant precipitation is observed in the casting with boron. These precipitates are observed to lie on 3 variants and are similar in appearance, but much larger in size, to those observed in the powder processed material.

Extrusion of these castings resulted in equiaxed grain structures as shown in fig. 13. The only significant differences between the extrusions is that the boron containing alloy has a considerably finer grain size. No precipitation is evident in either alloy in the as-extruded condition. Subsequent heat treatment results in considerable grain growth as displayed in fig. 14. As with the as-cast materials, Fe-40Al displayed straight grain boundaries while Fe-40Al-0.1B was characterized by curved boundaries which probably results from pinning effects. Heat treatment also resulted in some precipitation in the boron containing alloy. However, instead of appearing plate- or





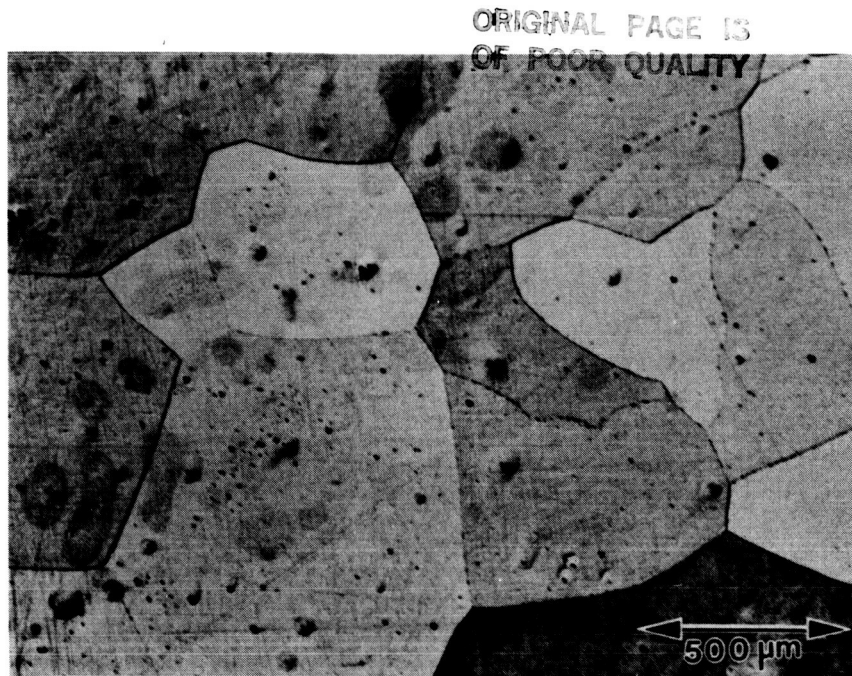
(a)



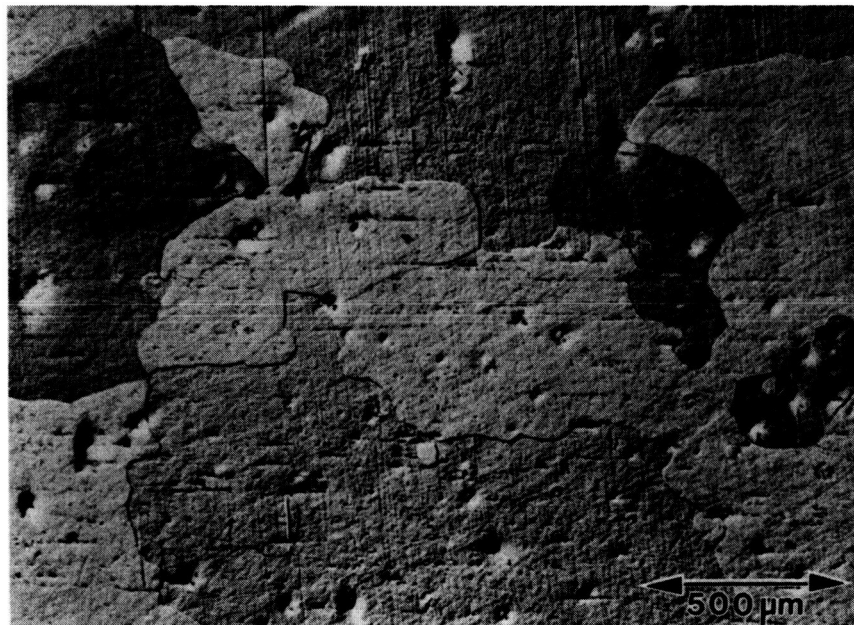
(b)

Figure 13. Optical micrographs of cast and extruded a) Fe-40Al and b) Fe-40Al-B.

ORIGINAL PAGE IS  
OF POOR QUALITY



(a)



(b)

Figure 14. Optical micrographs of cast and extruded a) Fe-40Al and b) Fe-40Al-B following heat treatment at 1273 K for 24 hours.

needle-like, this precipitation was observed as spherical shaped particles (fig. 15). Cooling rate had no noticeable effect on the amount, distribution or morphology of these precipitates.

### Grain Growth

As mentioned, a number of different heat treatments with different cooling rates were performed on the extruded materials. These heat treatments have a significant effect on the grain size of these materials.

The results of the grain size measurements are presented in table II. It should be noted that in the as-extruded form, all of the materials display equiaxed grain structures indicating recrystallization has occurred as a result of extrusion. The grain size data allows a number of observations to be made concerning grain growth in extruded materials.

To begin with, in the as-extruded condition, the grain size appears to be strongly related to the prior powder particle boundaries. These boundaries appear to be restricting the grain boundary movement at the temperature of extrusion. Increasing the extrusion temperature results in only small increases in the grain size, from  $\approx 10 \mu\text{m}$  to  $\approx 15 \mu\text{m}$ . By contrast, in the cast and extruded materials, prior powder particle boundaries are not present, and the as-extruded grain size is much larger (55-100 $\mu\text{m}$ ) (However, it should be noted that the cast material had a much larger initial grain size). Boron tends to decrease the

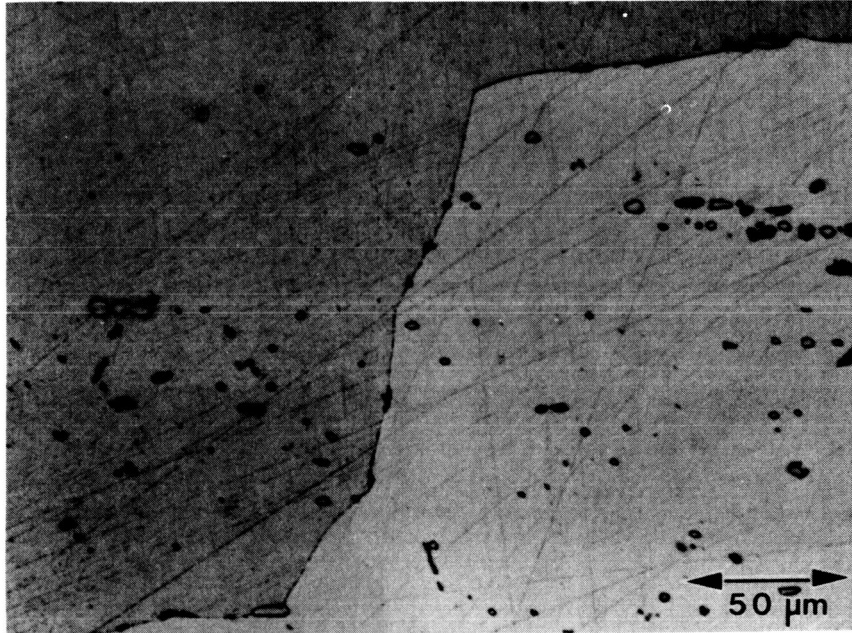


Figure 15. Higher magnification micrograph showing spherical precipitation in Fe-40Al-B heat treated at 1273 K for 24 hours.

Table II

Grain sizes of as-extruded materials and following various heat treatments (in microns).

Alloy	As extruded	1073 K/24 hrs		1173 K/24 hrs		1273 K/24 hrs		24 hrs	1323 K 48 hrs
		Tube	Cooled	Tube	Cooled	slow cooled	air		
1.A Fe-50Al	-	-	-	-	-	-	-	-	27.7
1.B Fe-50Al-0.20B	-	-	-	-	-	-	-	-	18.7
2.B Fe-40Al (HT) (1350 K)	16.7	15.7	17.0	17.0	-	-	-	21.5	23.1
2.BL Fe-40Al (LT) (1073 K)	10.3	13.0	11.1	11.1	14.0	11.0	14.7	-	-
2.C Fe-40Al-0.05B (HT)	18.0	-	-	-	-	-	-	-	354
2.CL Fe-40Al-0.05B (LT)	10.1	11.3	-	-	14.1	-	14.8	-	-
2.D Fe-40Al-0.10B (HT)	13.9	-	-	-	-	-	-	-	16.6
2.DL Fe-40Al-0.10B (LT)	9.9	11.5	-	-	11.6	-	12.3	-	-
2.E Fe-40Al-0.20B (HT)	10.7	11.9	11.3	11.3	-	11.5	-	945	469
2.EL Fe-40Al-0.20B (LT)	10.0	9.7	8.9	8.9	13.2	13.2	12.8	-	-
2.F Fe-50Al (HT)	24.5	24.0	29.1	29.1	-	30.5	-	44.6	34.5
2.FL Fe-50Al (LT)	11.0	12.8	17.4	17.4	13.2	17.0	15.2	-	-
2.G Fe-50Al-0.05B (HT)	16.8	-	-	-	-	-	-	-	1026
2.GL Fe-50Al-0.05B (LT)	8.5	10.5	-	-	44.8	-	37.5	-	-
2.H Fe-50Al-0.10B (HT)	16.4	-	-	-	-	-	-	-	-
2.HL Fe-50Al-0.10B (LT)	8.7	7.8	-	-	14.8	-	14.7	-	267
2.I Fe-50Al-0.20B (HT)	9.8	8.4	9.6	9.6	-	10.7	-	51	-
2.IL Fe-50Al-0.20B (LT)	9.2	8.0	11.5	11.5	11.6	11.5	12.7	17.2	13.2
3.A Fe-40Al	18.7	-	-	-	28.7	24.6	23.7	27.0*	850**
3.B Fe-40Al-0.10B	14.8	-	-	-	25.9	21.6	21.3	25.3*	240**
Fe-40Al cast	103	-	-	-	455	544	468	-	-
Fe-40Al-0.10B cast	55	-	-	-	602	678	842	-	-

\* = 1373 K \*\* = 1473 K

as-extruded grain sizes in both the powder and cast extrusions. This may be due to boron (or related borides) pinning grain boundaries and thus limiting growth.

Heat treatment is found to increase the grain size in all of the materials. However, in the powder processed materials, this grain growth is very sluggish at temperatures below 1273 K. Above this temperature, very rapid grain growth takes place. This growth occurs in an abnormal manner, with a few very large grains present in a distribution of fine equiaxed grains. An example of this abnormal grain growth is illustrated in fig. 16. Abnormal grain growth was found to start with heat treatment at 1273 K, and was observed to some degree at all heat treatment temperatures above that. This abnormal growth was not observed in the cast materials and may be related to the lack of prior powder particle boundaries. However, equiaxed grain growth was observed to occur readily in the cast and extruded material.

#### Texture Observations

Although a study of the texture of the extruded material was not a main focus of this investigation, some qualitative observations are worth discussing. Table III shows the peak intensity ratio for FeAl from the published powder diffraction file. Along with these published values are data obtained from longitudinal and transverse sections of Fe-50Al and Fe-50Al-0.2B. While the experimental diffraction scans displayed high background

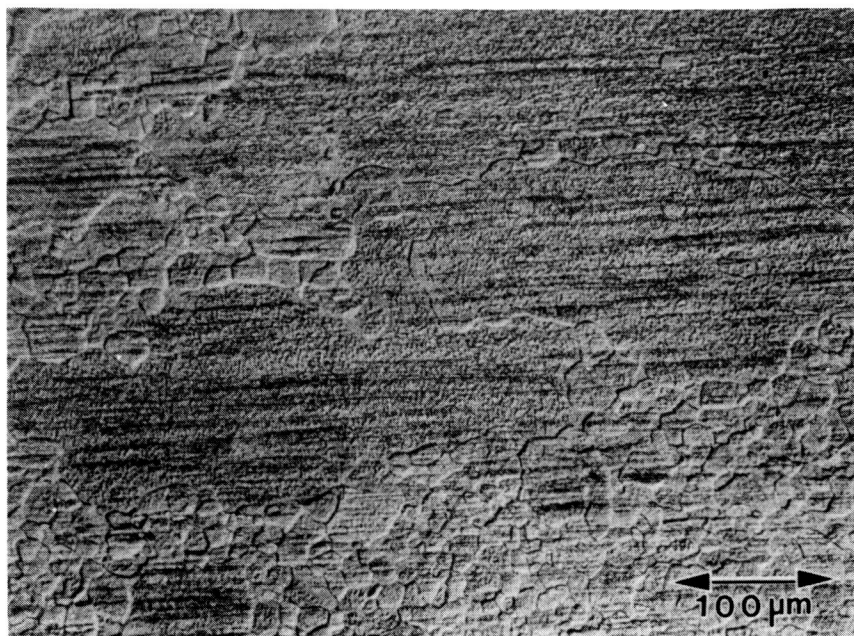


Figure 16. Optical micrograph of second series Fe-50Al-0.05B illustrating abnormal grain growth due to heat treatment at 1273 K for 24 hours.

Table III  
Intensity ratios  $I/I_1$  indicating texture.

		<u>hkl</u>	<u>100</u>	<u>110</u>	<u>111</u>	<u>200</u>	<u>210</u>	<u>211</u>
<u>Published Powder</u> <u>Diffraction Data</u>			12	100	4	8	3	20
<u>Fe-50Al (1A)</u>	longitudinal	-	100	2.6	2.3	3.8	16.5	
	transverse	-	100	51.5	-	-	13.3	
<u>Fe-50Al-0.2B (1B)</u>	longitudinal	-	100	2.4	1.8	1.6	15.8	
	transverse	-	100	82.6	-	-	36.4	



levels making exact quantification difficult, it can be seen that the ratios of the peaks recorded from longitudinal sections agree well with the published figures. By contrast, the transverse sections displayed {111} peaks which were very large in relation to the other peaks, while {200} and {210} peaks were not observed. This suggests that the extruded powder material displays a strong {111} wire texture.

Further evidence of this texture was observed in TEM. In studying foils made from transverse sections, a majority of grains were found to have orientations very near {111}. In these specimens, it was difficult to tilt to {110} orientations, and {100} orientations typically were outside of the tilting capacity of the microscope ( $\pm 45^\circ$  and  $\pm 30^\circ$ ). This texture was observed in all of the powder processed extrusions.

### Mechanical Behavior

#### Tensile Tests

The first series of extrusions were tensile tested following a standard homogenization treatment of 48 hours at 1323 K. The results of the tensile tests for Fe-50Al and Fe-50Al-0.2B are displayed in figs. 17a and 17b respectively. It should be noted that these curves, along with all of the other stress strain curves presented hereafter, do not accurately represent the elastic behavior of the materials. This is due to the inherent elasticity of the tensile testing frame. The critical parameters

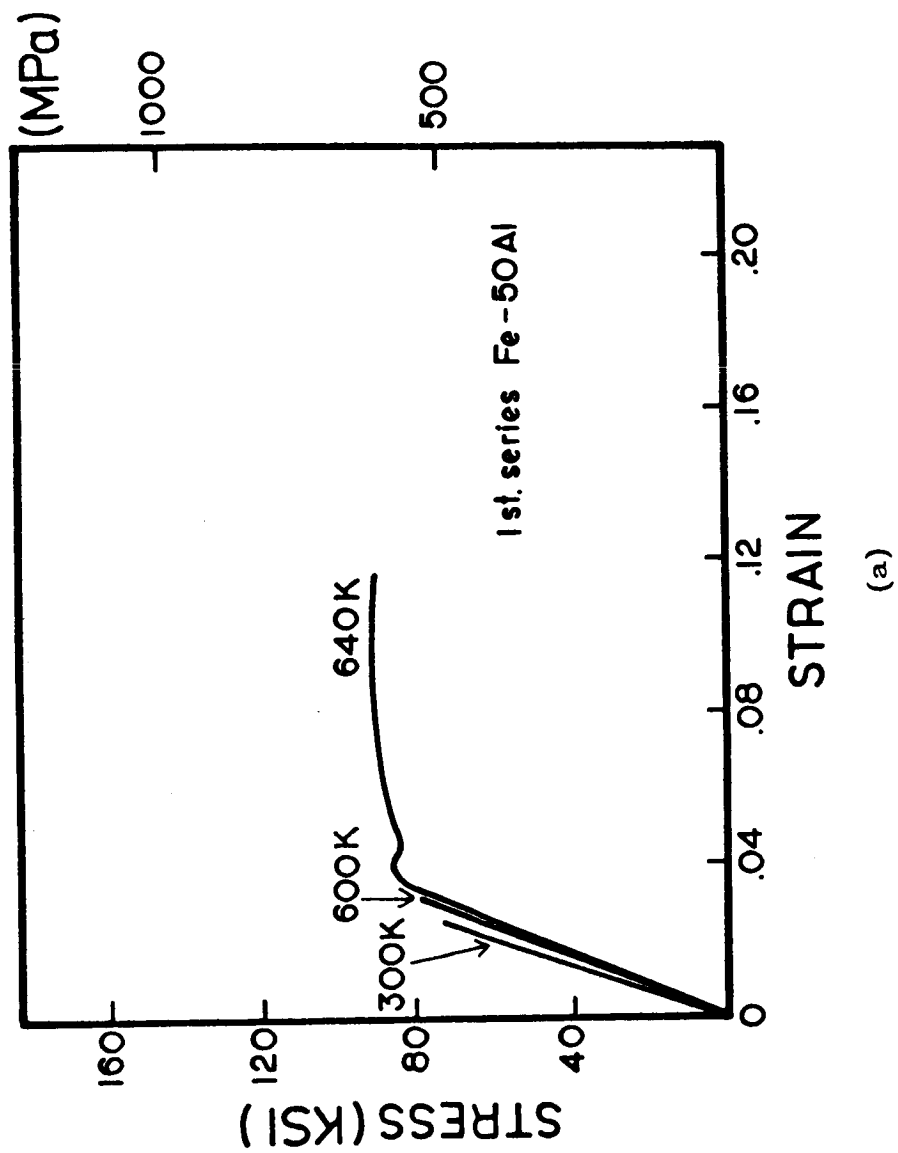


Figure 17. Tensile stress-strain curves for the first series extrusions a) Fe-50Al and b) Fe-50Al-B.

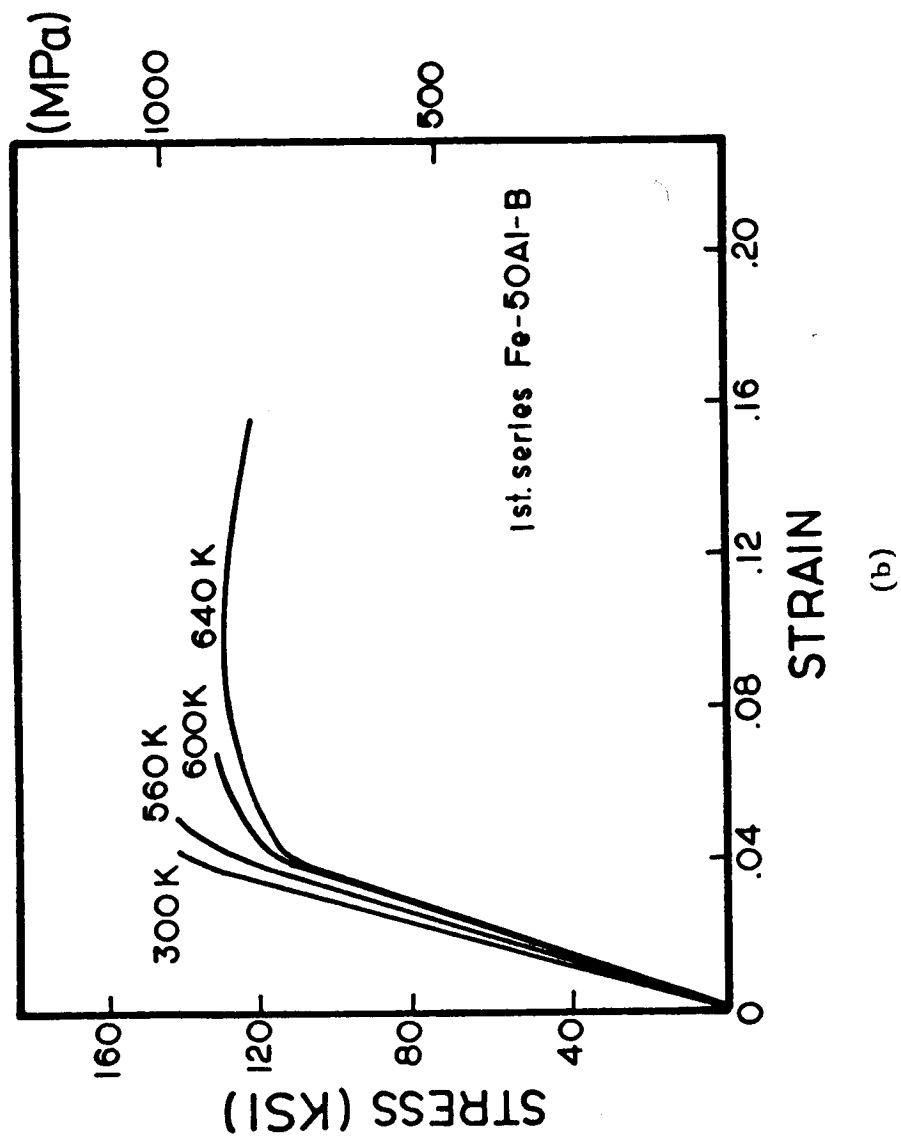


Figure 17 (cont..)

of these tests are given in table IV. The plastic strain,  $\epsilon_p$ , given in this and subsequent tables is the observed strain following yielding, taking into account the specimen and tensile testing frame elasticity. As can be seen, at room temperature, both alloys displayed brittle tensile behavior. However, the alloy containing boron fractured at a significantly higher stress. At higher temperatures, this brittle behavior gives way to ductility, and significant elongation can be observed in both of the alloys. The temperature where this ductile to brittle transition takes place is somewhat lower in the alloy containing boron (560 K versus 640 K). At these higher temperatures where plastic behavior begins, the alloys containing boron continue to show increased fracture strengths suggesting fracture is being somewhat delayed. Furthermore, when yielding takes place, the addition of boron has increased the yield strength to a large degree.

The second series of extrusions was tested in a large variety of heat treatments and cooling rates, with all of the tensile tests being performed at room temperature. Because of the number of tests, all of the data will be displayed in tables, with only example stress strain curves being presented.

The results of the tensile tests of the Fe-40Al base alloys of the second series of extrusions are presented in table V. This table presents data for the behavior of the as-extruded material, as well as for a number of heat treatments and cooling rates.

Table IV

Tensile test data for first series Fe-50Al extrusions.

	<u>Test T (K)</u>	<u><math>\sigma_y</math> (ksi)</u>	<u><math>\sigma_{UTS}</math> (ksi)</u>	<u><math>\epsilon_y</math></u>	<u><math>\epsilon_p</math></u>	<u>Brittle/Ductile</u>
Fe-50Al	300	-	76	-	-	B
"	600	-	80	-	-	B
"	640	88	93	0.037	0.073	D
Fe-50Al-B	300	-	142	-	-	B
"	560	135	144	0.045	0.006	D/B
"	600	119	130	0.045	0.023	D
"	640	117	129	0.044	0.112	D
"	680	108	120	0.037	0.079	D

Table V

Tensile test data for second series Fe-40Al extrusions.

Extrusion	Heat treat	Cooling	$\sigma_y^*$	$\sigma_{UTS}^*$	$\epsilon_y$	$\epsilon_p$	Brittle/Ductile
2.BL	as ext.	-	81	96	0.012	0.018	D
2.CL	"	-	85	129	"	0.047	"
2.DL	"	-	83	122	"	0.041	"
2.EL	"	-	84	125	"	0.037	"
2.B	as ext.	-	76	99	0.013	0.019	D
2.C	"	-	82	116	0.014	0.029	"
2.D	"	-	83	124	0.013	0.031	"
2.E	"	-	83	117	0.013	0.027	"
2.BL	1073 K/24 hrs	tube	83	83	0.015	0.008	D
2.CL	"	"	82	116	0.016	0.036	"
2.DL	"	"	82	117	0.015	0.038	"
2.EL	"	"	83	118	0.014	0.038	"
2.B	1323 K/24 hrs	tube	78	90	0.013	0.011	D
2.D	"	"	80	109	0.013	0.020	"
2.BL	1273 K/24 hrs	S.C.	68	83	0.011	0.017	D
2.CL	"	"	65	96	"	0.030	"
2.DL	"	"	66	92	"	0.029	"
2.EL	"	"	60	93	"	0.024	"
2.B	"	"	60	80	0.009	0.017	D
2.C	"	"	59	103	"	0.033	"
2.D	"	"	60	101	"	0.031	"
2.E	"	"	58	96	"	0.026	"
2.BL	1273 K/24 hrs	air	86	94	0.012	0.006	D
2.B	"	"	85	88	0.011	0.006	"
2.B	"	oil	-	118	-	-	B
2.BL	"	"	-	117	-	-	"
2.CL	"	"	108	136	0.013	0.008	D
2.DL	"	"	117	141	"	0.010	"
2.EL	"	"	117	136	"	0.008	"
2.DL	"	water	-	99	-	-	B
2.EL	"	"	-	123	-	-	"

\* -  $\sigma$  is calculated in ksi

Figure 18 shows the stress strain behavior of the as-extruded low temperature extrusions. This figure is typical of all of the as-extruded materials as well as those homogenized at 1373 K and air cooled or slow cooled. It is seen that Fe-40Al yields and displays some ductility. The yielding occurs with a significant amount of Luders strain followed by a region of smooth work hardening. The addition of boron does not affect the yield and work hardening behavior to any substantial degree under any of the various thermal conditions. However, boron has increased the ductility of the material by a significant amount. Without boron, the observed elongations were in the range of 2 to 3%, while with boron, elongations up to 6% have been observed. Variations in the amount of boron added does not appear to effect the observed ductility in any consistent manner. The alloy with 0.05B results in slightly better behavior under some conditions and the alloy with 0.2B results in slightly better behavior under other conditions. Any differences can be attributed to experimental scatter. Thus, it appears that an optimum amount of boron necessary for an improvement in ductility has been reached with 0.05B and additional amounts have no effect.

Subsequent heat treatments followed by air cooling had little effect on the tensile behavior. One noticeable change was a slight decrease in the yield strengths, which can be attributed to grain growth. Associated with these lower yield stresses, the amount of Luders strain was observed to decrease which is to be

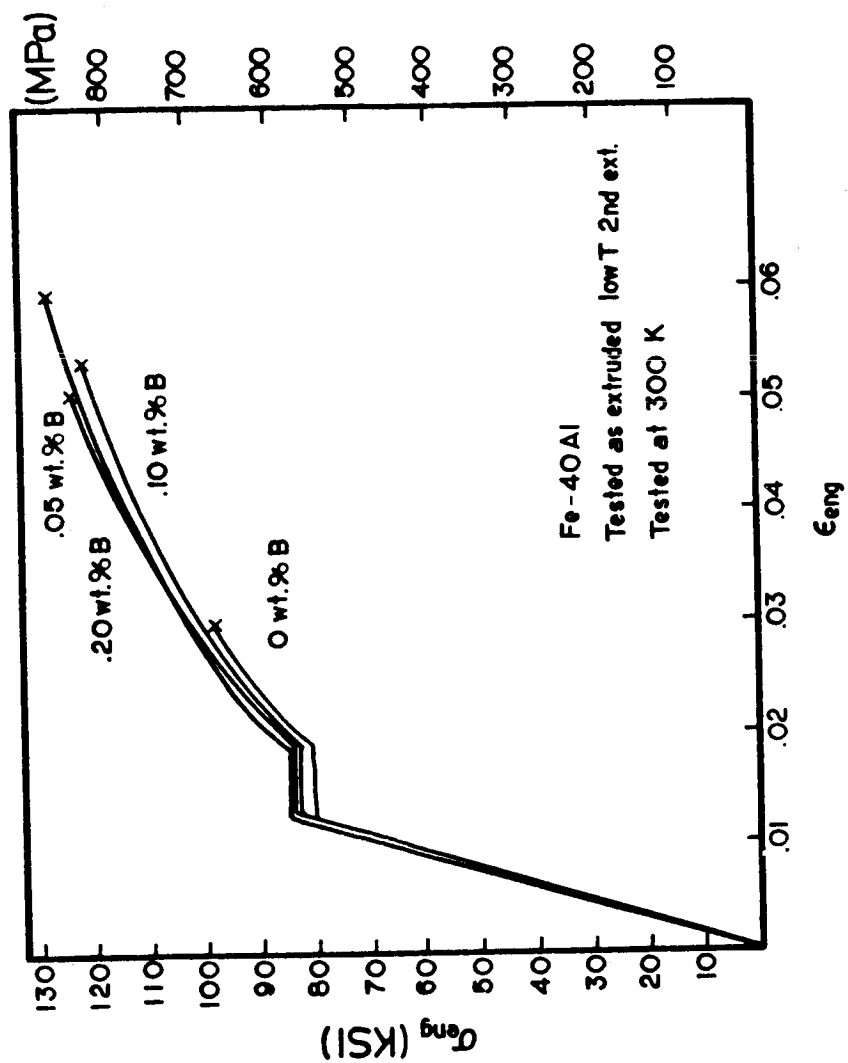


Figure 18. Tensile stress-strain curves for the second series extrusions of Fe-40Al with various boron levels.



expected with an increasing grain size. These heat treatments had no substantial effect on the overall elongation or on the boron effects.

While the homogenization heat treatments followed by a standard air cooling treatment did not have a significant effect on the mechanical behavior of Fe-40Al and Fe-40Al-B, the subsequent cooling rate did. Figure 19 shows the effect in detail. Slow cooling at 50 K per half hour resulted in behavior similar to the as-extruded materials. However, as the cooling rate is increased through air quenching to oil and water quenching, a dramatic change is observed. The faster the cooling rate, the higher the observed yield stress. Correspondingly to this increasing yield strength, the ductility decreased until totally brittle behavior was observed in water quenched samples. It should be noted that water quenching resulted in some microcracking which limited the mechanical testing that could be performed on these specimens.

As with the first series of extrusions, the second series of Fe-50Al extrusions also displayed brittle behavior at room temperature. Figure 20 shows an example of this behavior for Fe-50Al with various boron levels. All of the tensile behavior for these materials are presented in table VI. No evidence of yielding was observed under any of the conditions tested. Because the materials were so brittle, many attempts to make tensile bars failed. It should be pointed out that contrary to the first

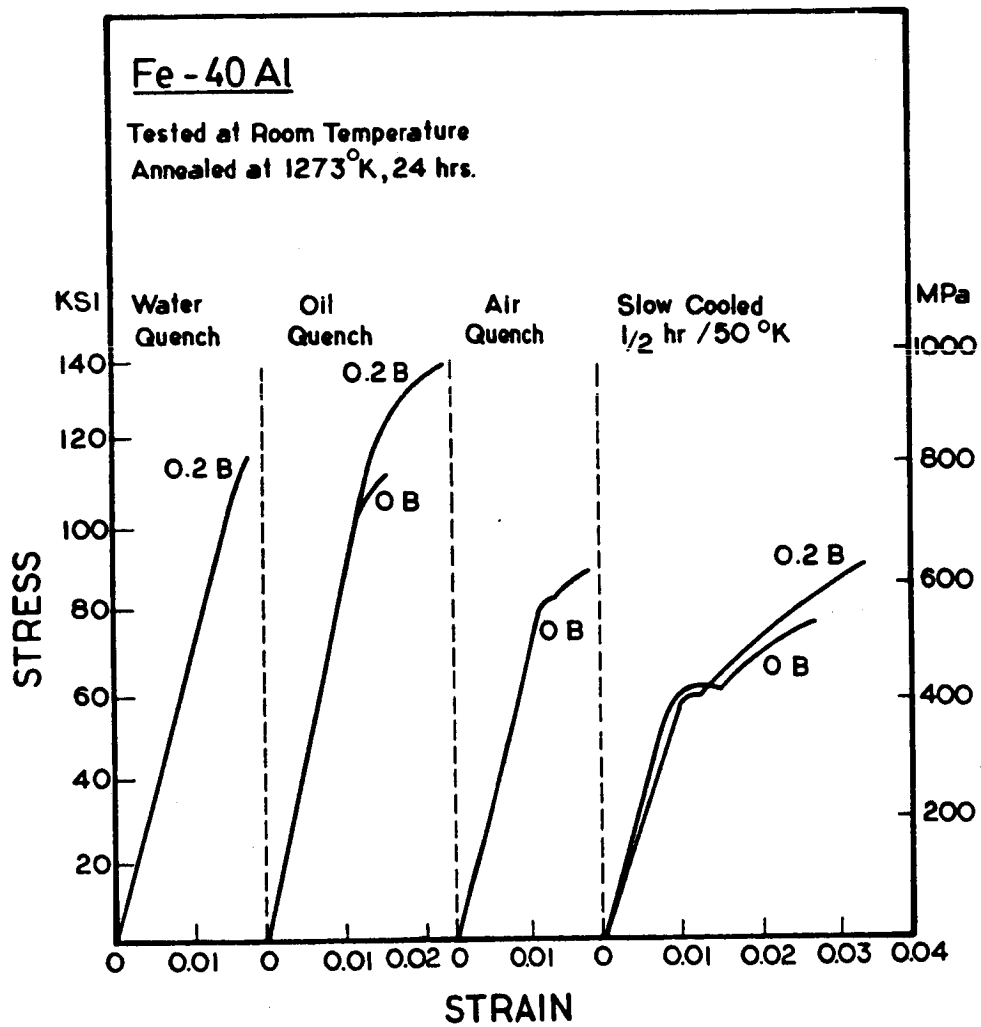


Figure 19. The effect of cooling rate on tensile stress-strain behavior of second series Fe-40Al alloys.

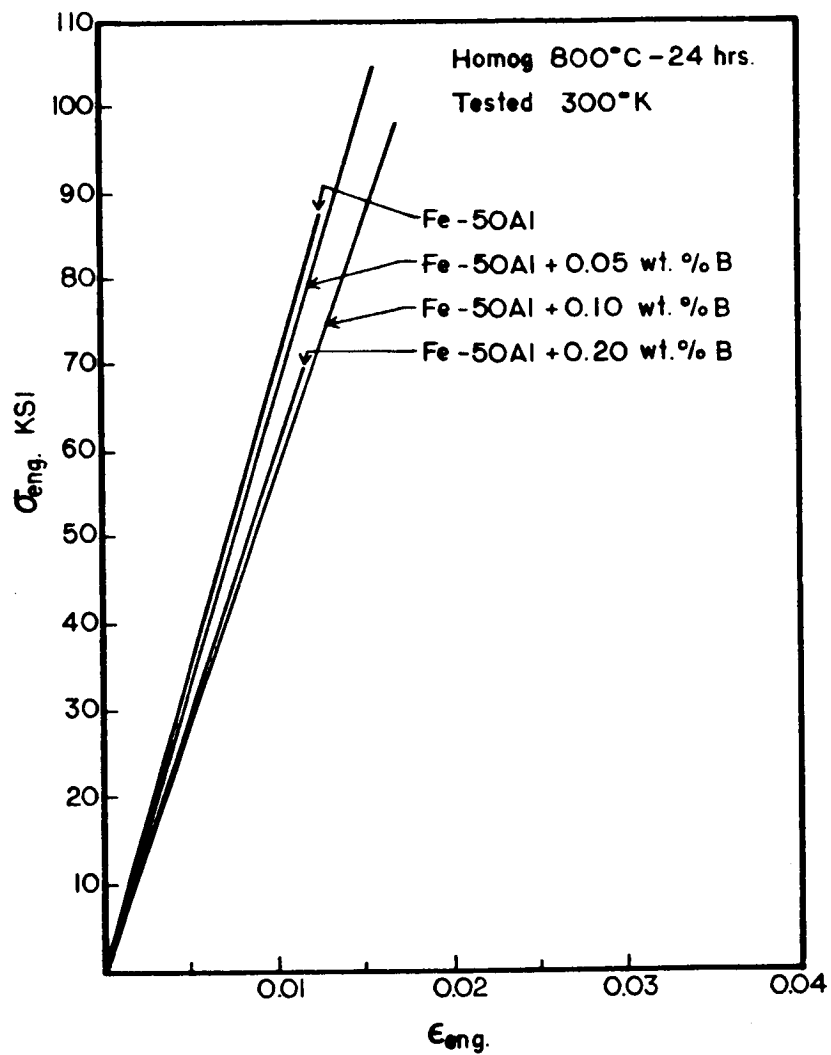


Figure 20. Tensile stress-strain curves for the second series extrusions of Fe-50Al with various boron levels.

Table VI

Tensile test data for second series Fe-50Al extrusion.

<u>Extrusion</u>	<u>Heat Treat</u>	<u>Cooling</u>	$\sigma_y^*$	$\sigma_{UTS}^*$	$\epsilon_y$	$\epsilon_p$	<u>Brittle/Ductile</u>
2.FL	as ext.	-	-	77	-	-	B
2.GL	"	-	-	104	-	-	"
2.HL	"	-	-	109	-	-	"
2.IL	"	-	-	125	-	-	"
2.F	"	-	-	90	-	-	"
2.G	"	-	-	83	-	-	"
2.FL	1073 K/24 hrs	tube	-	82	-	-	"
2.GL	"	"	-	105	-	-	"
2.HL	"	"	-	97	-	-	"
2.IL	"	"	-	69	-	-	"
2.F	1373 K/24 hrs	"	-	64	-	-	"
2.G	"	"	-	76	-	-	"
2.HL	"	"	-	68	-	-	"
2.IL	"	"	-	103	-	-	"
2.FL	1273 K/24hrs	S.C	-	86	-	-	"
2.GL	"	"	-	79	-	-	"
2.HL	"	"	-	101	-	-	"
2.IL	"	"	-	104	-	-	"

\* -  $\sigma$  is calculated in ksi

series of extrusion, the addition of boron had no effect on the room temperature fracture stress of Fe-50Al. Because of the extreme brittleness of the material, all attempts to study the effects of fast cooling by quenching failed.

The third series of extrusions showed tensile behavior similar to the Fe-40Al alloys of the second series except for some small differences. It should be remembered that the third series contains much lower amounts of impurities than the second series. The tensile data for the third series are given in table VII. In the as-extruded form, the Fe-40Al alloys without boron displayed greater ductilities in the cleaner material (third series). However, while the addition of boron to the third series improved the ductility slightly, this increase was not as significant as in the second series.

The effects of cooling rate were also duplicated in the third series of alloys. This indicates that these effects are not related to the presence of impurities in the Fe-40Al alloys. Another important fact is that samples in the third series indicate that the strengthening due to increased cooling rate is reversible. Figure 21 shows the stress-strain curves for an oil quenched sample which was re-heated and slow cooled. While the oil quenched sample is characterized by high strength and low ductility, the sample which was first oil quenched and then slow cooled reverts to a lower yield strength and significant ductility.

Table VII

Tensile test data for third series Fe-40Al extrusions.

<u>Extrusion</u>	<u>Heat Treat</u>	<u>Cooling</u>	$\sigma_y^*$	$\sigma_{UTS}^*$	$\epsilon_y$	$\epsilon_p$	<u>Brittle/Ductile</u>
3.A	as ext.	-	75	96	0.011	0.024	D
3.A	"	-	74	93	0.010	0.023	"
3.B	"	-	84	105	0.011	0.017	"
3.B	"	-	86	120	"	0.027	"
3.A	1273 K/24 hrs	S.C	59	93	0.009	0.042	"
3.B	"	"	57	82	"	0.022	"
3.A	"	air	75	86	0.010	0.012	"
3.B	"	"	93	119	0.013	0.016	"
3.A	"	oil	-	93	-	-	D/B
3.B	"	"	123	139	0.017	0.007	D
3.A	1273 K/24 hrs	oil					
followed by 1273 K/24 hrs S.C			64	86	0.010	0.028	D
3.B	1273 K/24 hrs	oil					
followed by 1273 K/24 hrs S.C			58	81	"	0.017	D
3.A	1373 K/24 hrs	S.C	62	89	"	0.033	"
3.B	"	"	57	87	"	0.022	"
3.A	"	oil	106	113	0.015	0.003	D/B
3.B	"	"	140	152	0.018	0.005	D/B
3.A	1473 K/24 hrs	S.C	34	52	0.006	0.050	D
3.B	"	"	58	77	0.010	0.015	D
3.A	"	air	51	69	0.007	0.047	D
3.B	"	"	66	91	0.010	0.018	D
3.A	"	oil	-	96	-	-	D/B
3.B	"	"	-	124	-	-	"

\* -  $\sigma$  is calculated in ksi.

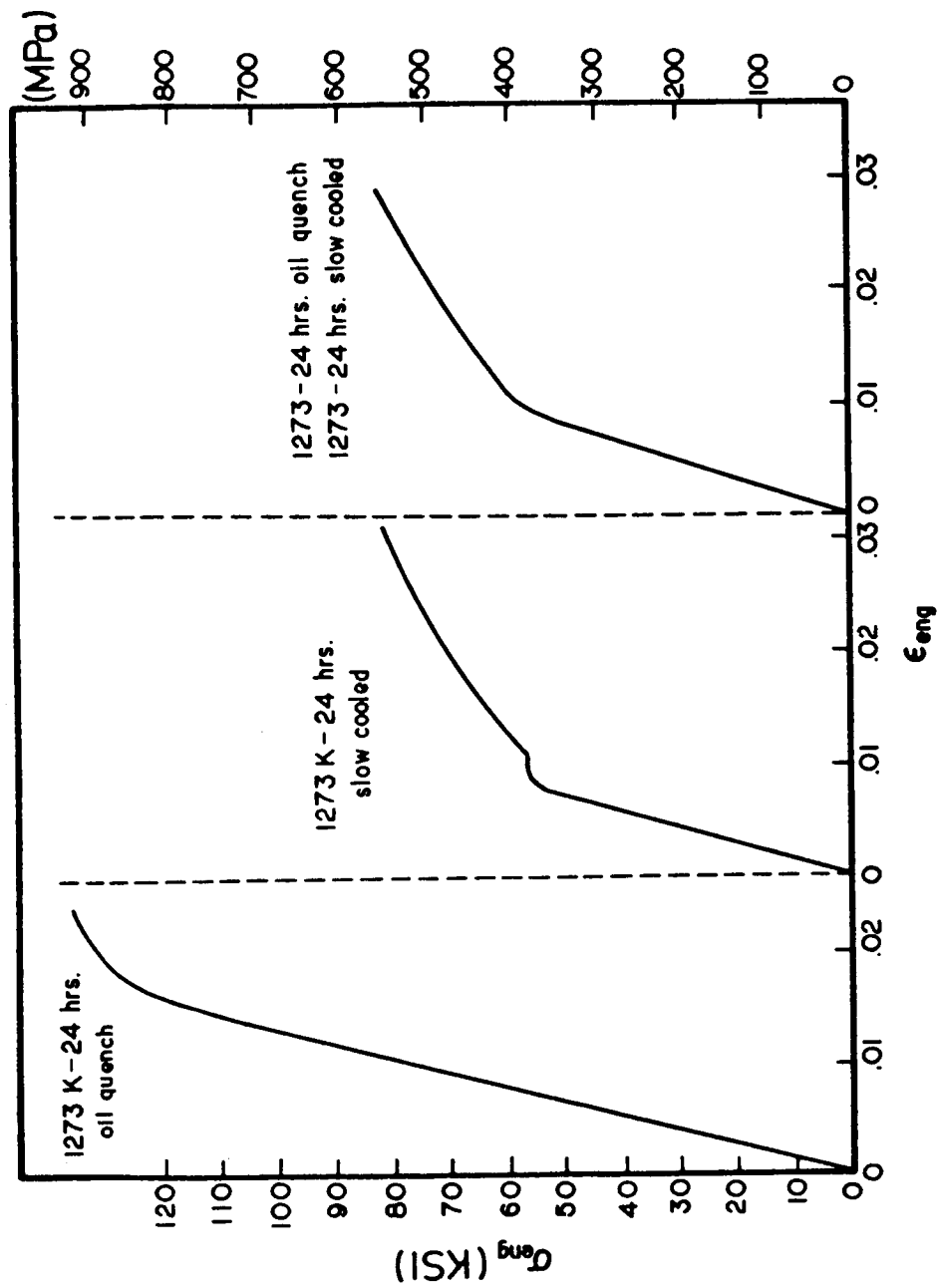


Figure 21. Tensile stress-strain curves for the third series extrusion Fe-40Al-0.10B showing the reversibility of the cooling rate effects.

The tensile deformation data for the cast extrusions was presented in table VIII. The deformation was similar to that observed in the Fe-40Al powder extrusions. However, the overall ductility was considerably greater in the cast materials than in the powder processed materials (tensile elongations of 6% were observed in the as-extruded condition compared with  $\approx 3\%$  in the powder processed Fe-40Al). Also, the Luder strain was essentially absent in the cast materials. The addition of boron however, had no noticeable effect on the tensile behavior of the cast materials. In all conditions, the yield strength and ductility of cast and extruded Fe-40Al, with and without B, displayed similar behavior.

Although boron effects were not observed in the cast materials, the cooling rate effects observed in the powder processed materials were duplicated. Figure 22 displays stress-strain curves of Fe-40Al-cast heat treated at 1273 K and cooled by slow cooling, air quenched and oil quenched. As can be seen, the faster cooling rates result in an increase in strength and corresponding decreases in ductility. Although oil quenching increases the yield strength, some ductility is still observed.

#### Tensile Fracture Surfaces

The resulting tensile fractures have been studied using scanning electron microscopy (SEM). Two different fracture modes, intergranular and transgranular, are the general modes that have



Table VIII

Tensile test data for cast and extruded Fe-40Al alloys.

<u>Extrusion</u>	<u>Heat Treat</u>	<u>Cooling</u>	$\frac{\sigma}{y}^*$	$\sigma_{UTS}^*$	$\frac{\epsilon}{y}$	$\frac{\epsilon}{p}$	<u>Brittle/Ductile</u>
Cast							
Fe-40Al	as ext.	-	75	118	0.010	0.049	D
"	"	-	69	114	0.010	0.051	"
Cast							
Fe-40Al-B	"	-	62	129	0.008	0.058	"
"	"	-	69	109	"	0.030	"
Cast							
Fe-40Al	1273 K/24 hrs	S.C	45	74	0.007	0.030	"
Cast							
Fe-40Al-B	"	"	42	69	0.008	0.028	"
Cast							
Fe-40Al	"	air	71	99	0.010	0.026	"
Cast							
Fe-40Al-B	"	"	59	68	"	0.008	"
Cast							
Fe-40Al	"	oil	96	109	0.014	0.010	"
Cast							
Fe-40Al-B	"	"	91	104	"	0.008	"

\* -  $\sigma$  is calculated in ksi.

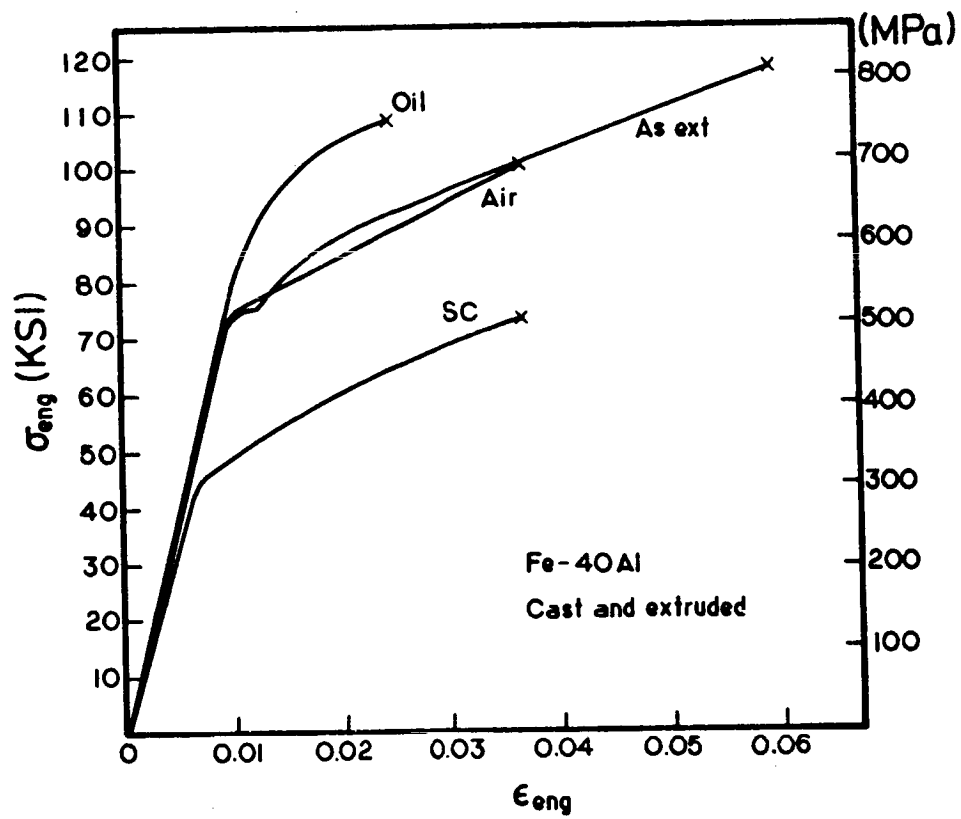


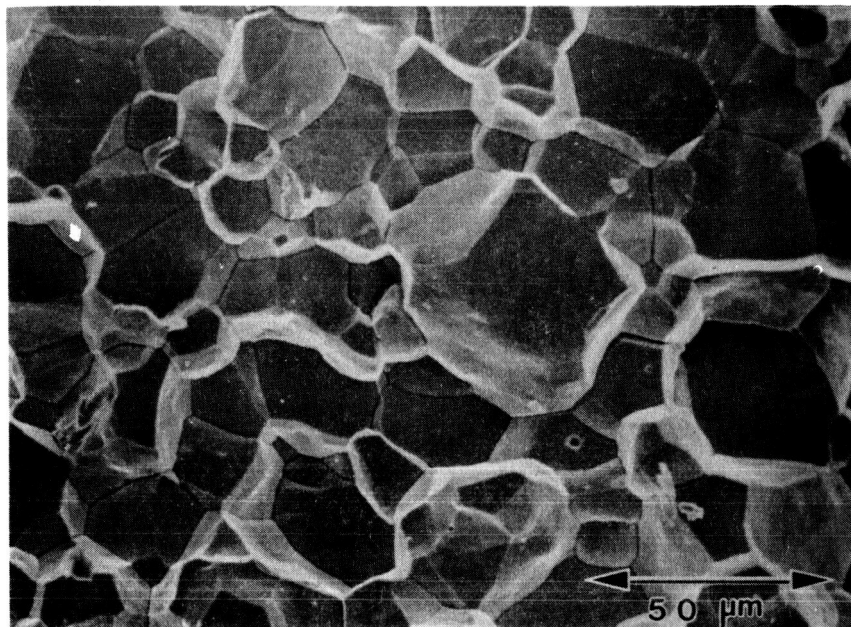
Figure 22. Tensile stress-strain curves for cast and extruded Fe-40Al.

been observed. However, some of the details vary and will be discussed.

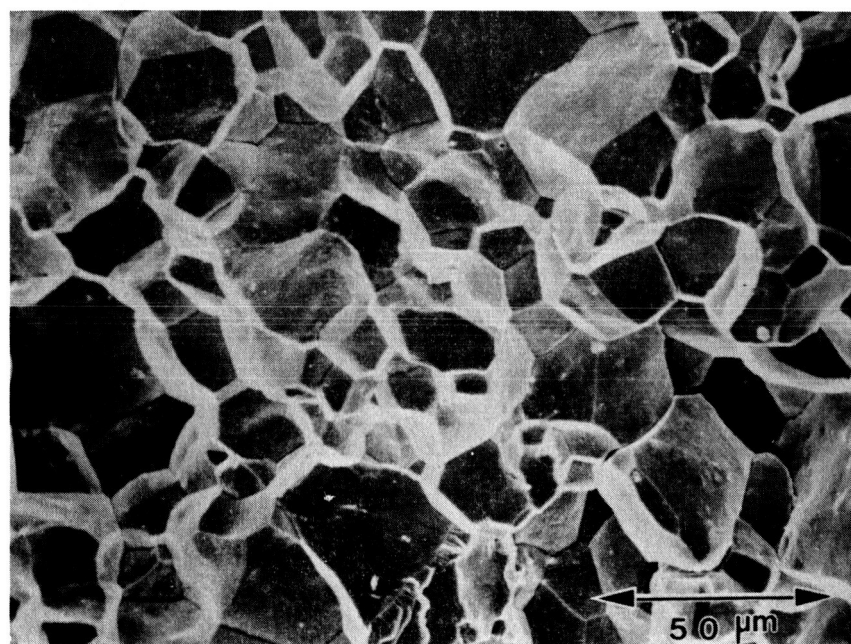
In the first series of extrusions, two distinct fracture types have been observed. In Fe-50Al, pure intergranular fracture was observed both at low temperatures, and at high temperatures where ductility is observed. This is shown in figs. 23a and 23b. The addition of boron has changed this fracture mode, again at low and high temperatures, to pure cleavage/transgranular (figs. 24a and 24b). Also, all of the boron-containing Fe-50Al alloys had noticeable pores on the fracture surfaces (fig. 25) which have not been observed in alloys without boron.

A number of interesting observations were noted in the second series of extrusions. In the as-extruded Fe-40Al without boron, the fracture was intergranular, but not as crisp as in the first series (fig. 26a). The addition of boron has again resulted in a change in fracture mode, but in this material, transgranular tearing (quasi-cleavage) was observed instead of pure cleavage (fig. 26 b).

The cooling rate has a significant effect on the fracture behavior of the second series extrusions of Fe-40Al. While at slow cooling rates, the fracture surfaces were similar to those discussed above, the faster cooling rates resulted in more distinct fracture modes. Figure 27 shows Fe-40Al and Fe-40Al-0.05B after oil quenching from 1273 K. It is seen that the Fe-40Al shows a more distinct intergranular fracture than the

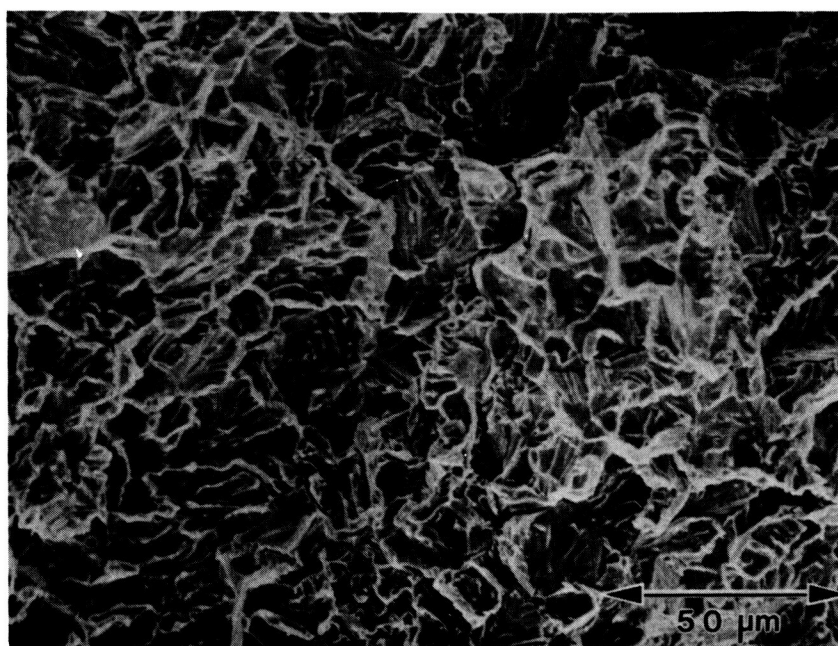


(a)

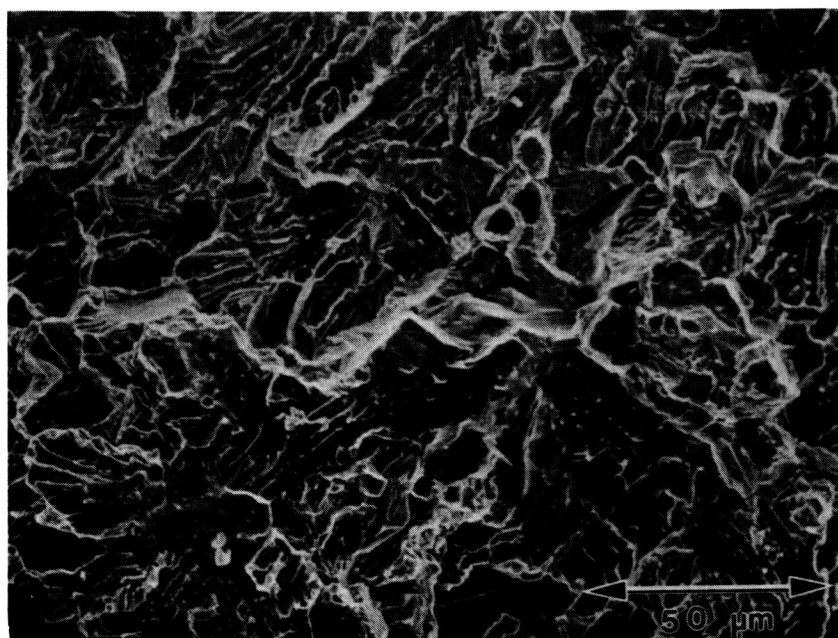


(b)

Figure 23. SEM micrographs displaying fracture surfaces for the first series Fe-50Al tested at a) 300 K and b) 680 K.



(a)



(b)

Figure 24. SEM micrographs displaying fracture surfaces for the first series Fe-50Al-B tested at a) 300 K and b) 600 K.

ORIGINAL FROM IS  
OF POOR QUALITY

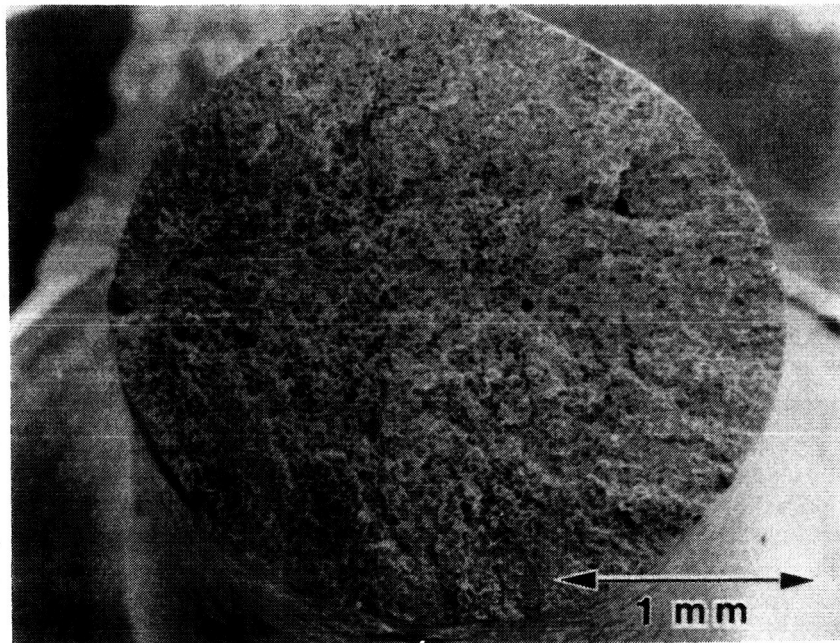
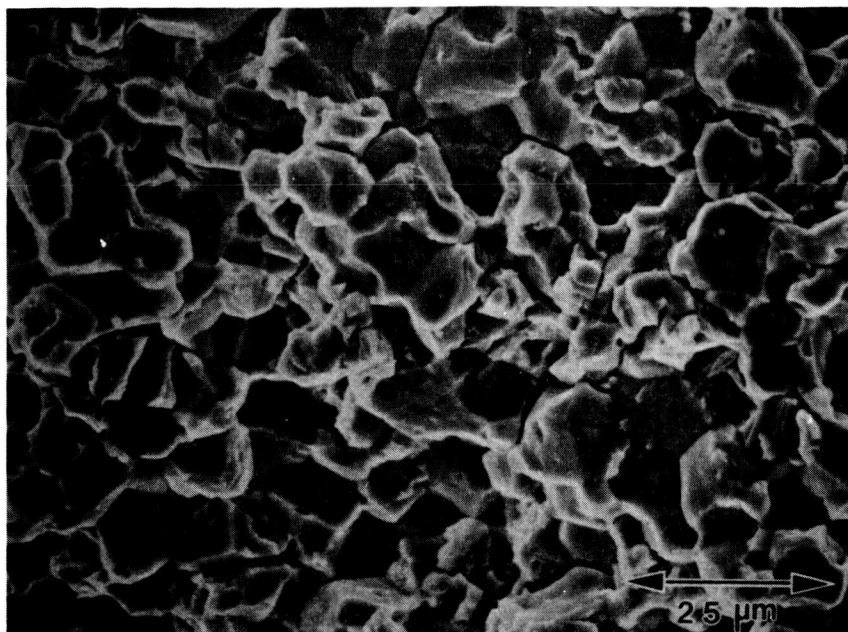
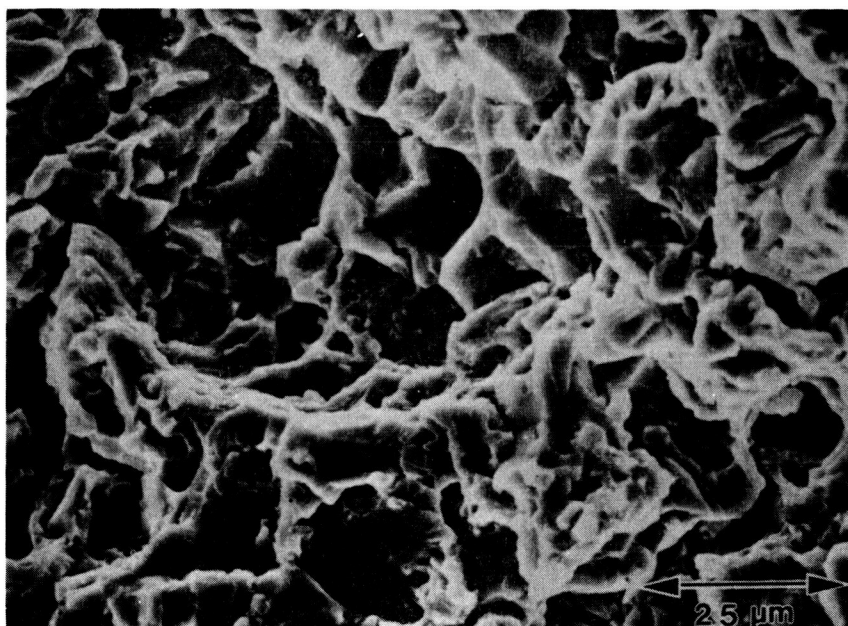


Figure 25. SEM micrograph of the first series Fe-50Al-B displaying boron related voids.

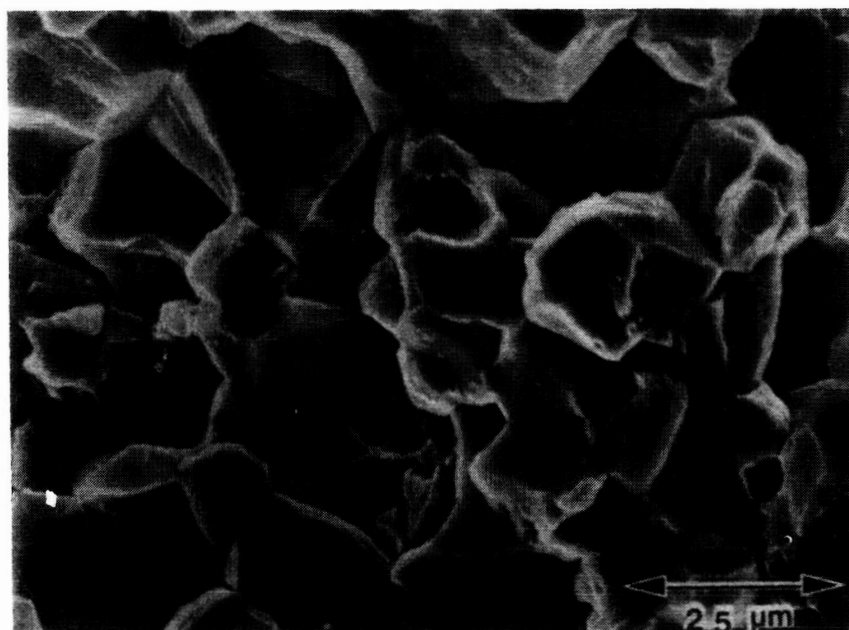


(a)

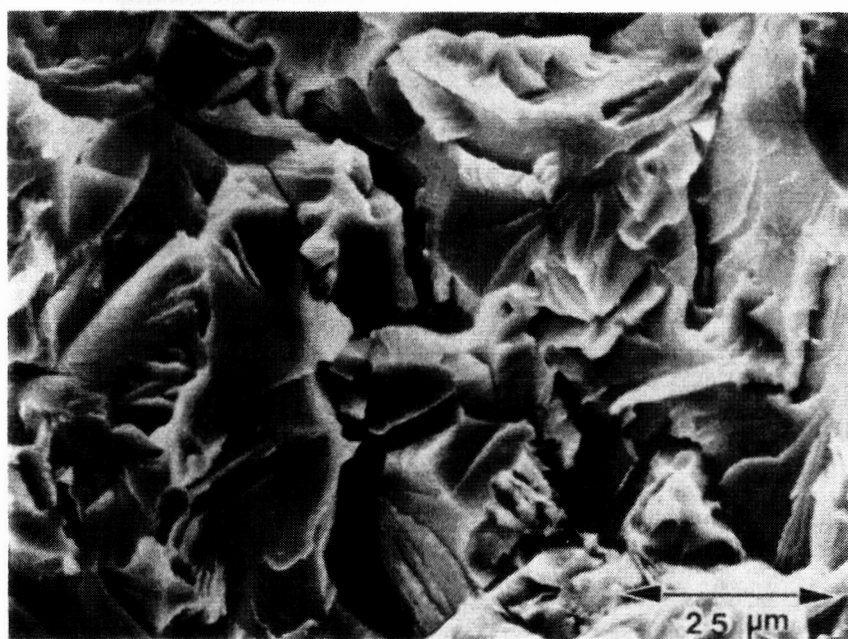


(b)

Figure 26. SEM micrographs displaying fracture surfaces of as-extruded second series a) Fe-40Al and b) Fe-40Al-0.05B.



(a)



(b)

Figure 27. SEM micrographs displaying fracture surfaces of second series a) Fe-40Al and b) Fe-40Al-0.05B heat treated at 1273 K oil quenched.



as-extruded Fe-40Al. In the Fe-40Al-0.05B it can be seen that oil quenching changes the fracture to total cleavage from transgranular tearing.

For the Fe-50Al alloys of the second series, all the samples regardless of boron level and/or cooling, displayed brittle intergranular fracture. This is contrary to what was observed in the first extrusion series of Fe-50Al. The reasons for this will be discussed later. One interesting observation of fracture in this series is related to the abnormal grain growth. Although the predominant fracture mode was intergranular in all of the Fe-50Al second series alloys, the very large grains associated with abnormal grain growth fail by cleavage. This is shown in a SEM micrograph in fig. 28 and an optical micrograph in fig. 29.

The third series of extrusions, Fe-40Al alloys with low impurity levels, was characterized by more distinct fracture modes than those in the second series. Without boron, the fracture mode was total intergranular fracture (fig. 30). The alloys containing boron showed an interesting fracture behavior. The fracture appeared to be initiated at pores and/or inclusions, with the area around the pore being characterized by cleavage fracture. As the distance from the pore is increased, the fracture tends to change to a more tearing type of fracture. This type of fracture is illustrated in fig. 31. Fracture surfaces of this type were observed in all of the alloys containing boron. It is important to note that the various cooling rates had no noticeable effect on

ORIGINAL PHOTO IS  
OF POOR QUALITY

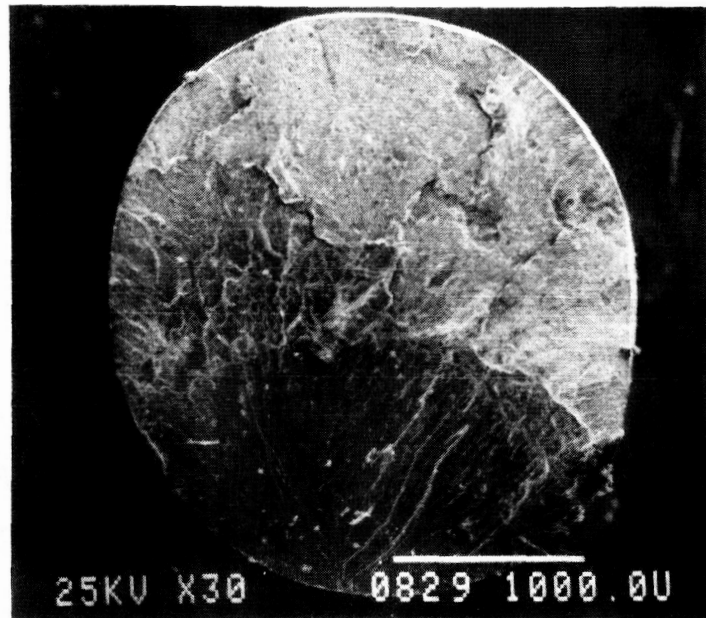


Figure 28. SEM micrograph showing cleavage of large grains and intergranular fracture of small grains in second series Fe-50Al-0.05B with abnormal grain growth.

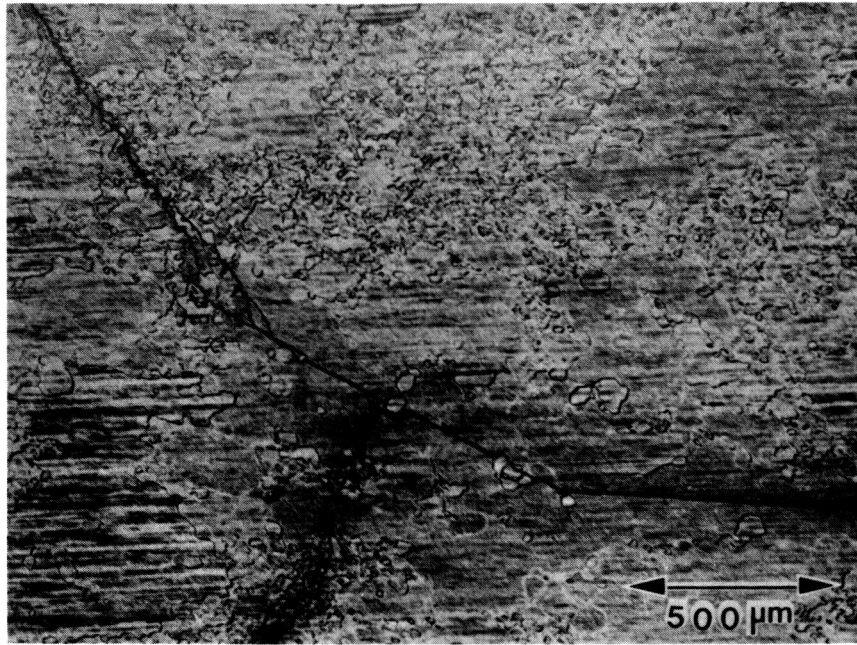


Figure 29. Optical micrograph showing crack path around fine grains and through large grains in second series Fe-50Al-0.05B with abnormal grain growth.

ORIGINAL PAGE IS  
OF POOR QUALITY

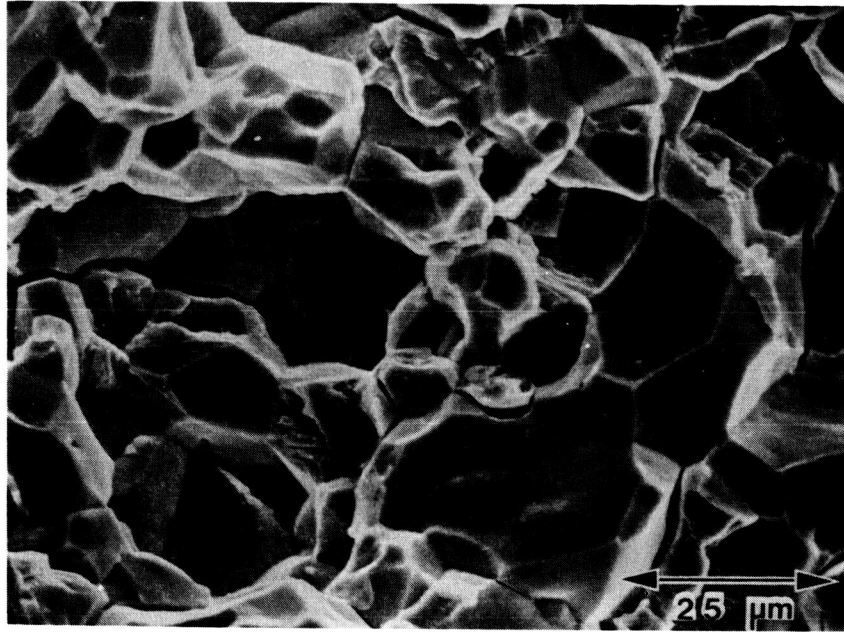


Figure 30. SEM micrograph showing pure intergranular fracture in the third series Fe-40Al.

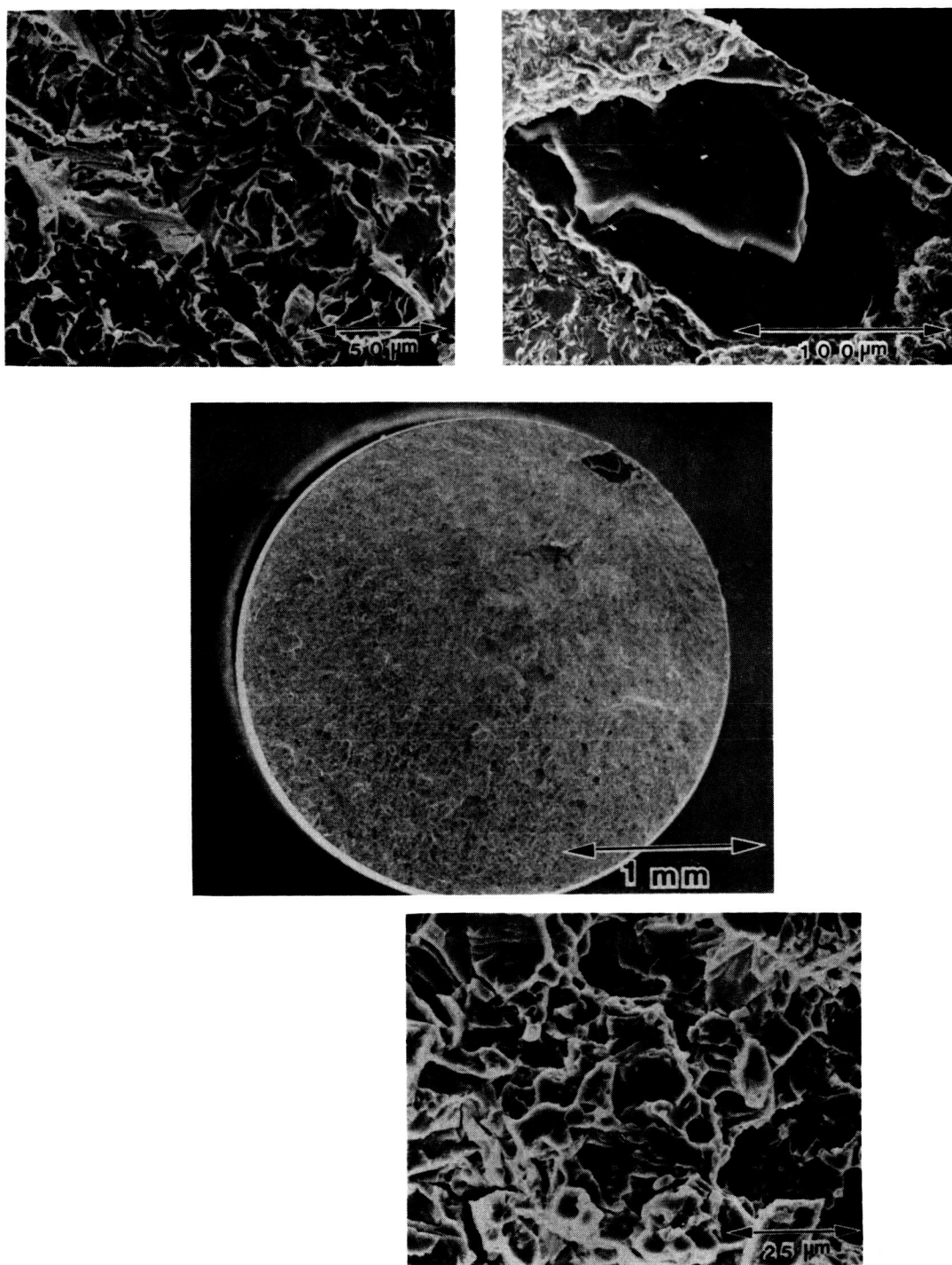


Figure 31. SEM micrographs showing the fracture behavior of the third series Fe-40Al-0.1B alloys.

the fracture modes observed in the third extrusion series.

The cast and extruded materials were characterized by predominantly cleavage fracture modes with only occasional intergranular facets observed. This transgranular failure was observed in both the alloys with and without boron and appears to be related to the large grain sizes observed in these samples (fig. 32). Variations in the cooling rate have produced no changes in this fracture behavior.

#### Compression Tests

While tensile testing provides considerable information on the mechanical behavior of materials, including ductility and fracture, compression testing merits consideration because it provides complimentary data. In materials which fail in a brittle manner in tension, the compression test allows some information on the yield behavior to be obtained.

Table IX displays the yield stresses determined in compression for the second series, Fe-40Al extrusions. In the as-extruded and 1073 K- 24 hour heat treatment condition, the yield stresses are in relatively good agreement with those found in tension and are presented in table V. The yield stresses found in compression are slightly higher, which may be a result of end effects associated with compression testing. Figure 33 illustrates the effect of cooling rate on the yield behavior of Fe-40Al. The same general effects observed in tension are

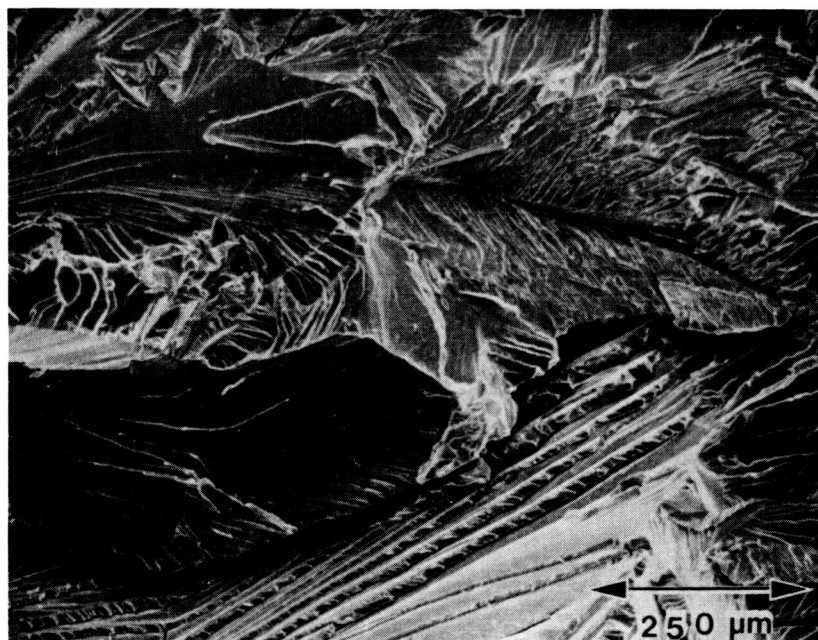
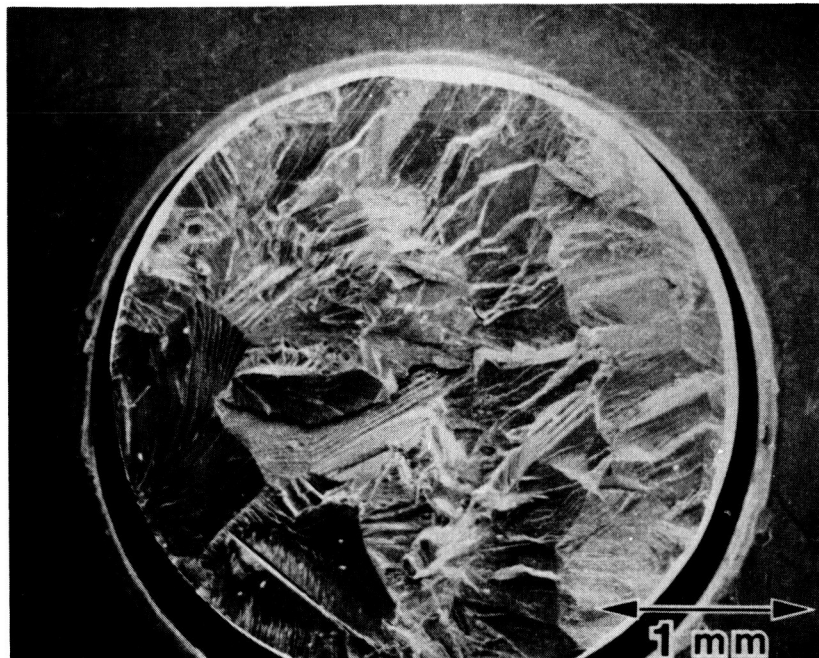


Figure 32. SEM micrographs of Fe-40Al cast and extruded followed by heat treatment of 1273 K for 24 hours.

Table IX

Compression test data for second series Fe-40Al extrusions.

<u>Extrusion</u>	<u>Heat Treat</u>	<u>Cooling</u>	<u><math>\sigma_y</math> (ksi)</u>
2.BL	as ext.	-	97
2.CL	"	-	102
2.DL	"	-	106
2.EL	"	-	100
2.BL	1073K/24hrs	tube	115
2.CL	"	"	92
2.DL	"	"	94
2.EL	"	"	116
2.BL	1273 K/24 hrs	S.C.	71
2.BL	"	air	101
2.BL	"	oil	145
2.BL	"	water	142
2.EL	"	S.C.	74
2.EL	"	oil	155



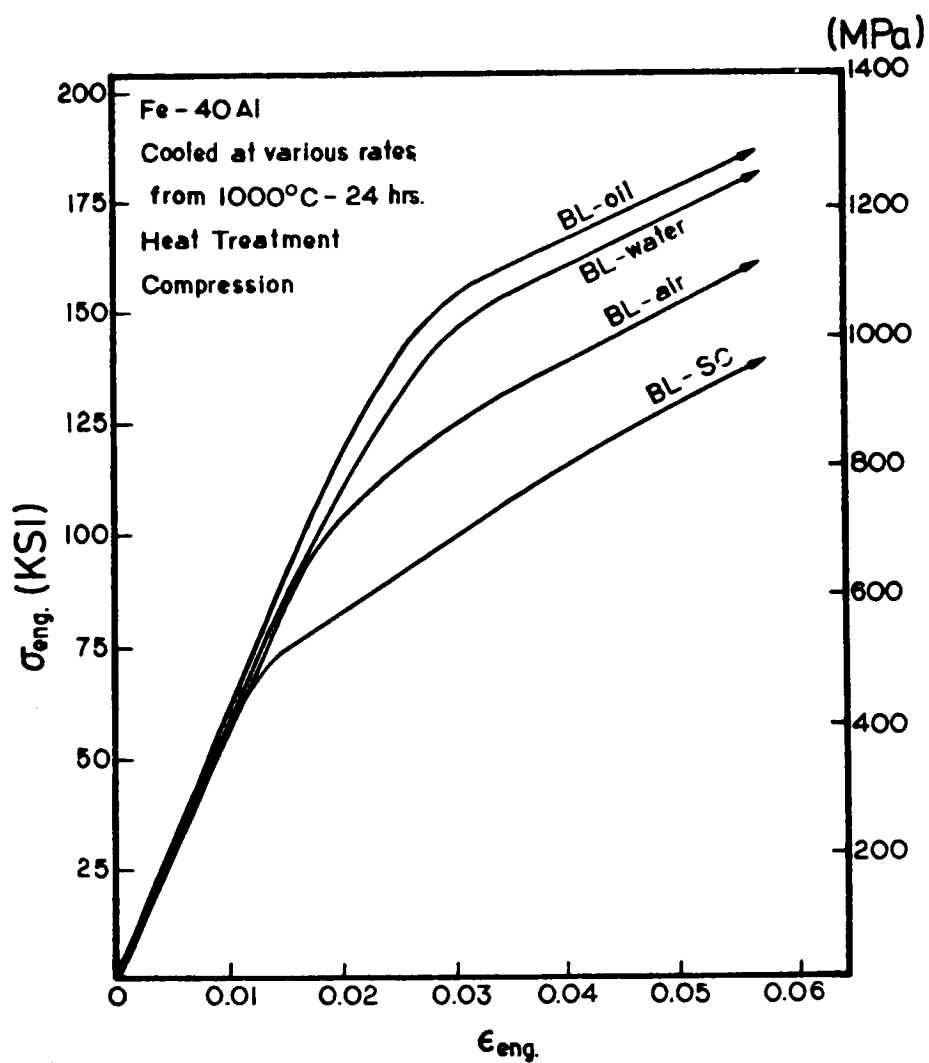


Figure 33. Compressive stress-strain curves for second series Fe-40Al cooled at various rates.

uplicated in compression, with the faster cooling rates increasing the yield strength. However, instead of fracturing near these high yield stresses, considerable ductility is observed in compression. The tests were stopped when the specimens started to tilt, and not at failure.

The advantage of the compression test is better observed in the Fe-50Al second series extrusions. These samples all failed in a totally brittle manner in tension. Figure 34 shows that in compression, these alloys are able to yield and display ductility. The yield stresses for a number of these alloys are presented in table X. It should be noted that these yield stresses are very high, approximately double of those observed in Fe-40Al. Unfortunately, due to quenching cracks, it was impossible to make compression samples of many of the heat treated samples. Thus, very little information is available on the effects of cooling rate on the yield behavior of Fe-50Al alloys.

#### Single Crystal Compression Tests

Single crystal compression tests resulted in load elongation behavior similar in appearance to those of polycrystals. Two different nominal compositions of single crystals were studied, Fe-40Al and Fe-50Al. Each of these were subjected to a standard 1273 K - 24 hour heat treatment followed by either slow cooling or oil quenching. The orientations of these 4 different conditions, as determined by back reflection Laue analysis, are shown in figs.

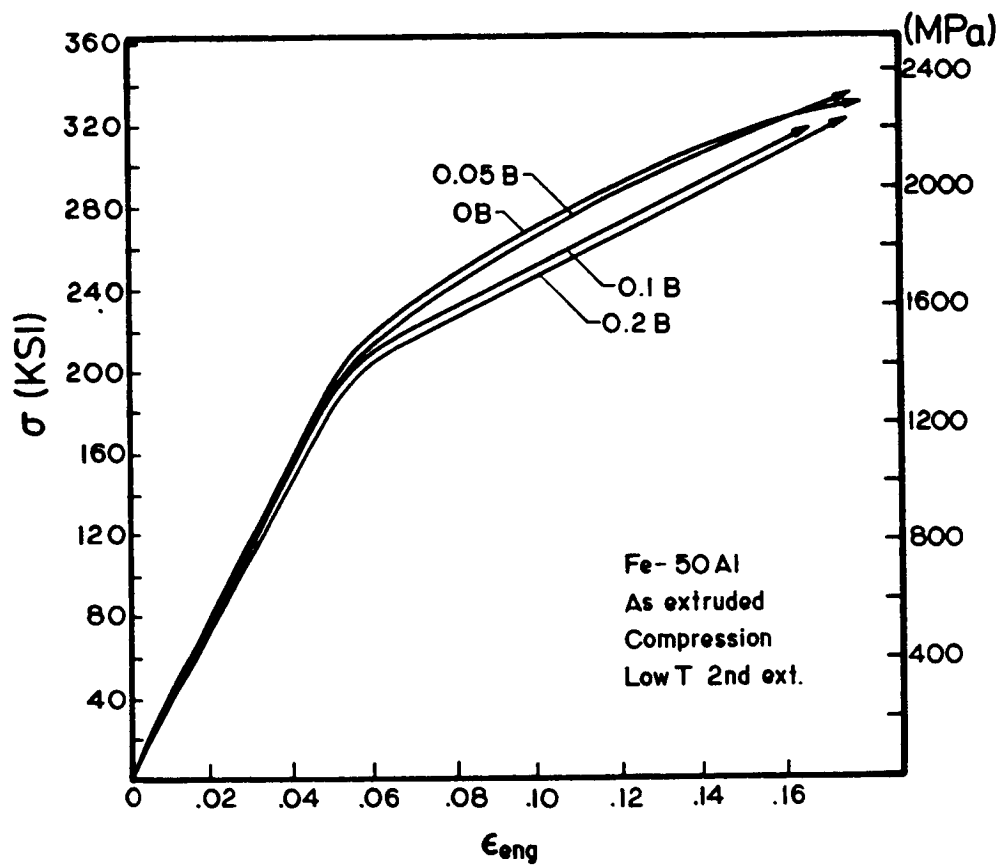


Figure 34. Compressive stress-strain behavior of second series Fe-50Al alloys with various boron levels.

Table X

Compression test data for second series Fe-50Al extrusions.

<u>Extrusion</u>	<u>Heat Treat</u>	<u>Cooling</u>	<u><math>\sigma_y</math> (ksi)</u>
2. FL	as ext.	-	208
2. GL	"	-	203
2. HL	"	-	199
2. IL	"	-	197
2. FL	1073 K/24 hrs	tube	215
2. GL	"	"	208
2. HL	"	"	205
2. IL	"	"	198
2. FL	1273 K/24 hrs	S.C.	162

35 through 38. As can be seen, most of the orientations of the compression axis lie near (001).

Following compression of about 1% plastic strain, the single crystals were examined optically to reveal slip traces. An example of this is shown in figs. 39a and b. These slip lines were generally straight indicating planar slip. However, in a number of cases, more than one set of lines was observed. This is probably due to activation of slip on more than one system in samples with orientations near the border of crystallographic triangles. The slip planes were determined by trace analysis using the method described by Barrett [64]. An example of this analysis will be given. The angles  $\alpha$  and  $\beta$  are measured on a pair of micrographs showing the front and right faces of the rectangular compression sample as shown in fig. 40. The angles are then plotted on the stereographic projection of the front face in the manner shown in fig. 41. The two points define the plane which causes the slip trace on the single crystal. The plane and its pole ( $90^\circ$  from the plane) are shown on the stereographic projection. In all of the samples where slip traces were observed, {110} was the slip plane. In two samples, some {211} slip traces were also observed indicating some cross-slip has occurred. In a few samples, no distinct slip lines were observed. This usually occurred at orientations very close to (001) where 4 different systems may be activated, thus causing obliteration of the slip lines.

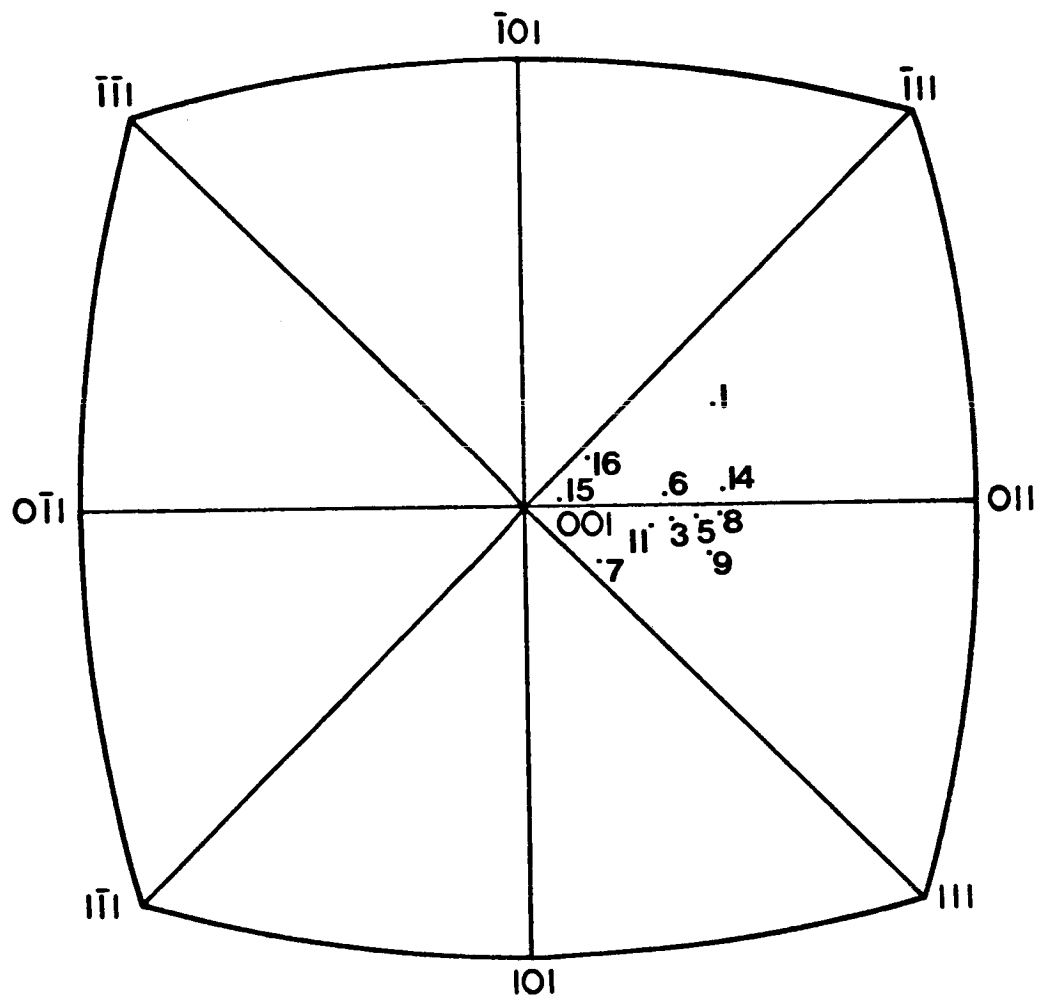


Figure 35. Orientations of compression axis's of Fe-40Al slow cooled single crystals determined by back-reflection Laue.

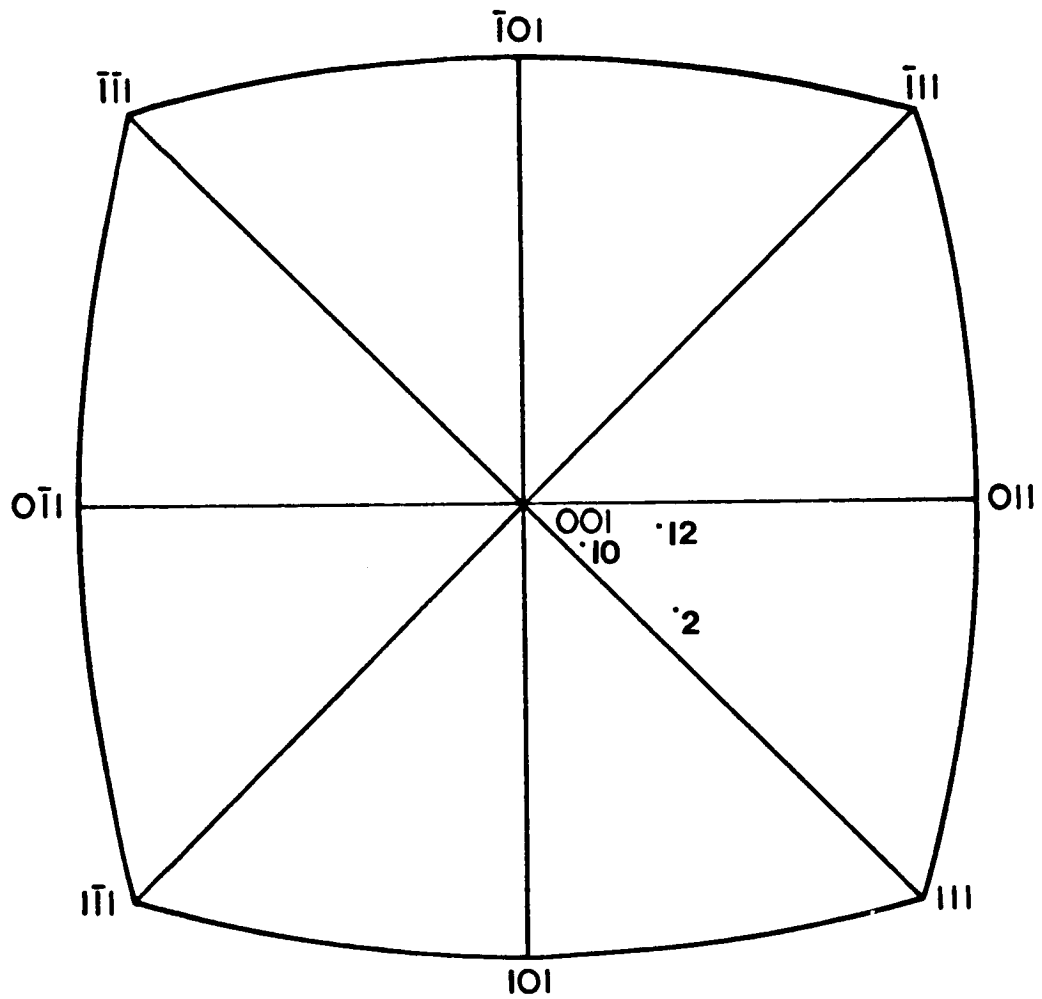


Figure 36. Orientations of compression axis's of Fe-40Al oil quenched single crystals determined by back-reflection Laue.

C-2

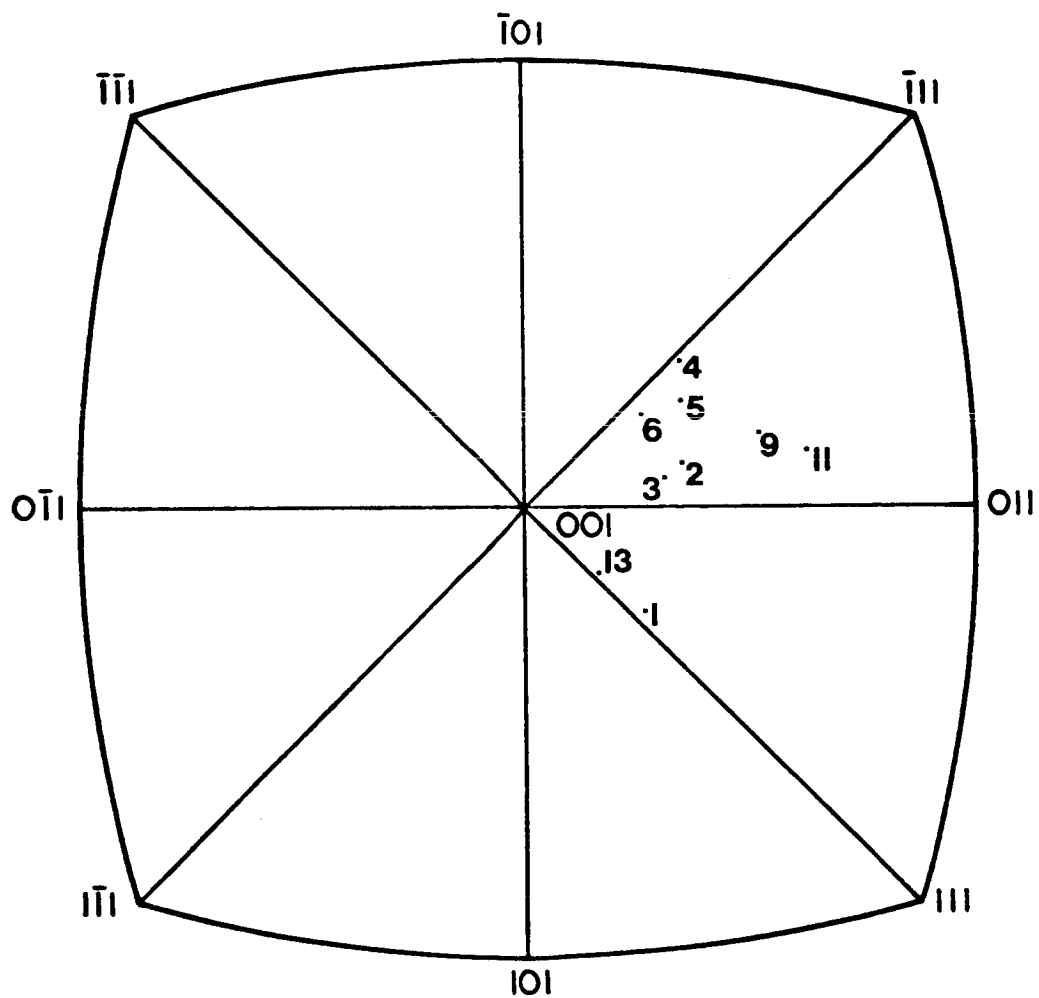


Figure 37. Orientations of compression axis's of Fe-50Al slow cooled single crystals determined by back-reflection Laue.



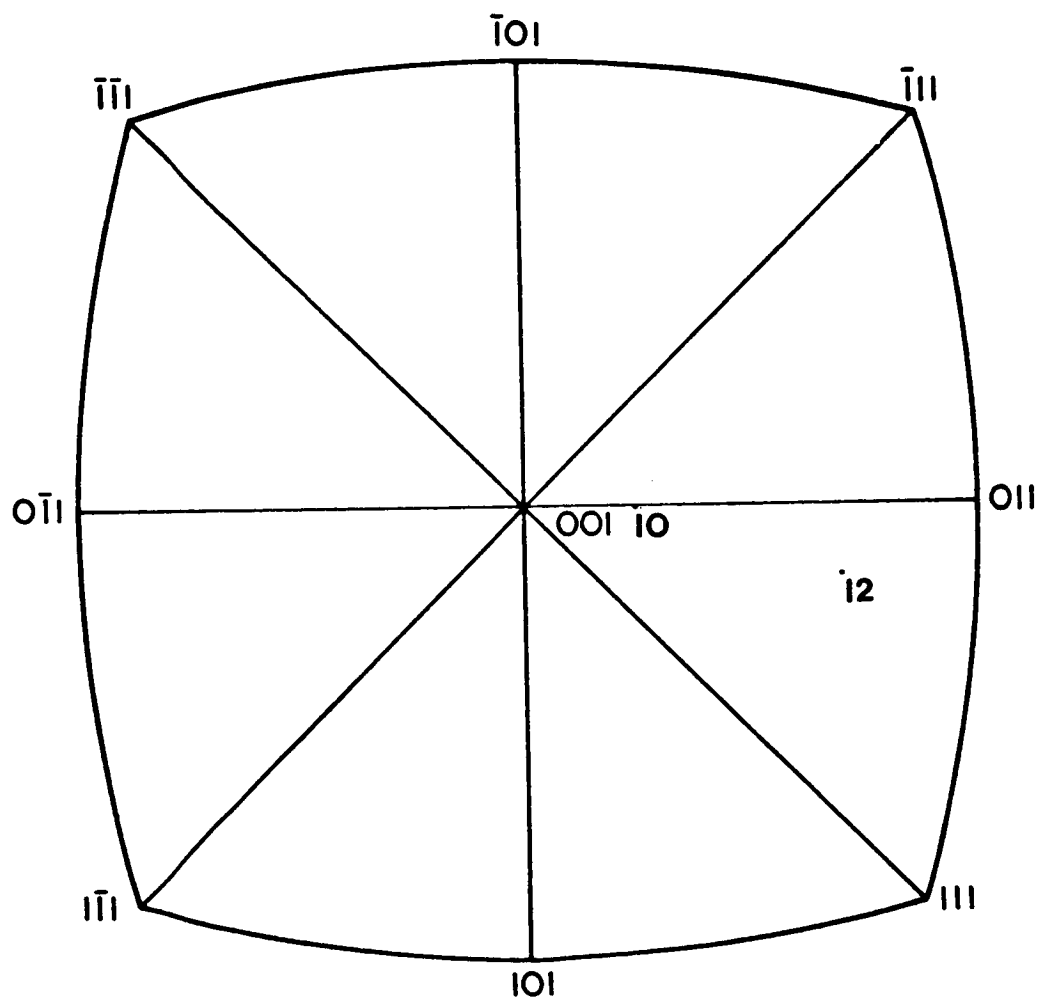
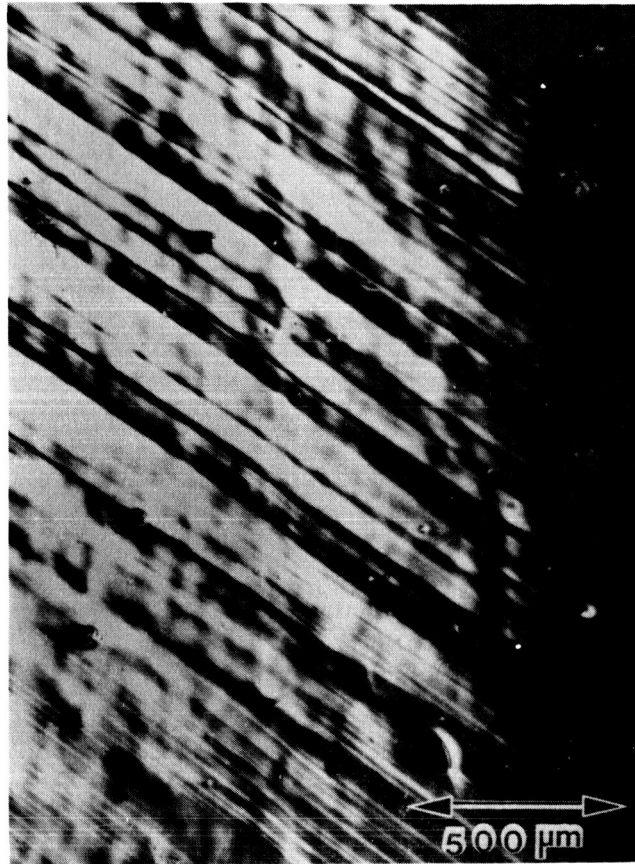


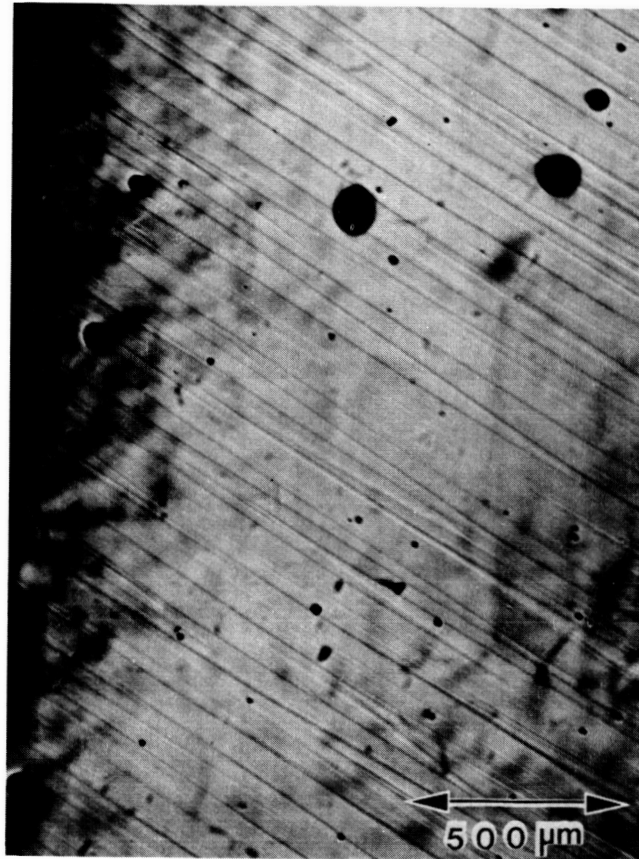
Figure 38. Orientations of compression axis's of Fe-50Al oil quenched single crystals determined by back-reflection Laue.

ORIGINAL PAGE IS  
OF POOR QUALITY



(a)

Figure 39. Fe-40Al slow cooled single crystal displaying slip traces on a) front and b) right faces.



(b)

Figure 39 (cont.)

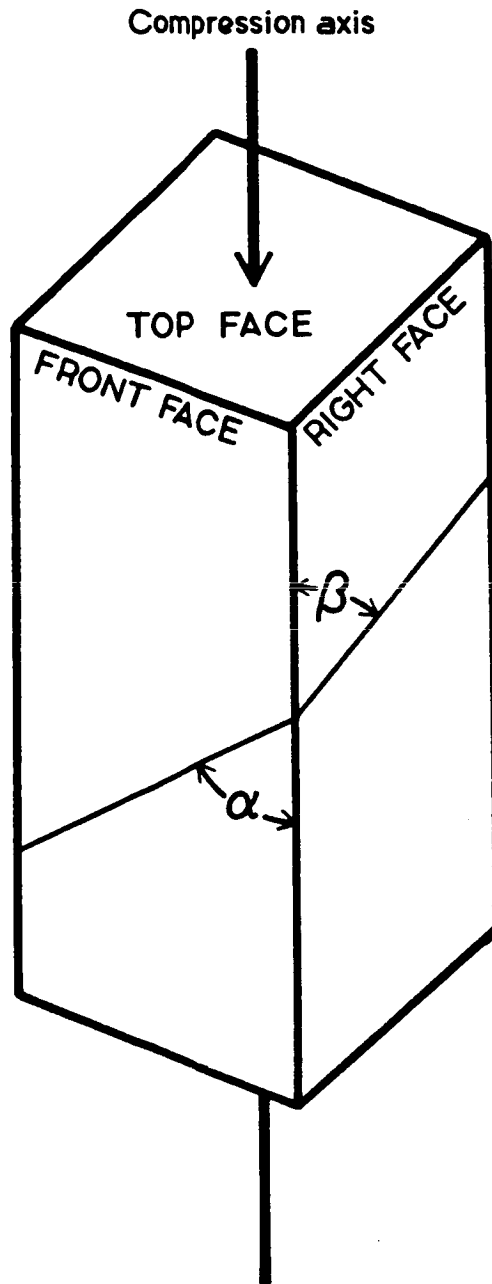


Figure 40. Schematic representation of a single crystal compression sample displaying the measurement of  $\alpha$  and  $\beta$  used in determining the slip plane.

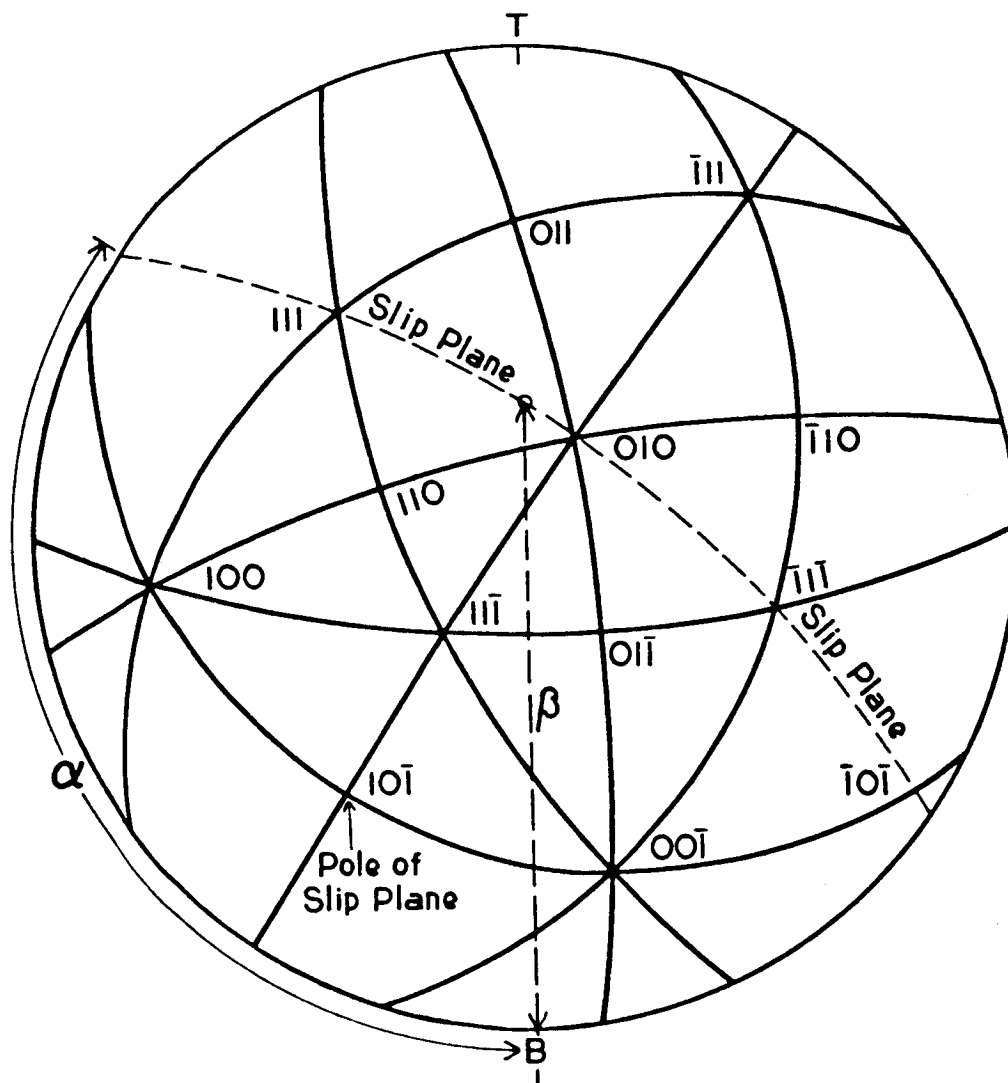


Figure 41. Stereographic projection of the single crystal shown in fig. 39 displaying the plotting of angles  $\alpha$  and  $\beta$  to determine slip plane.

The critical resolved shear stress ( $\tau_{crss}$ ) was determined for the single crystal orientations assuming  $\{110\}\langle 111 \rangle$  slip (TEM analysis confirmed  $\langle 111 \rangle$  slip and will be discussed later). The critical resolved shear stress is given by:

$$\tau_{crss} = \frac{P \cos \alpha \cos \gamma}{A} \quad [3]$$

where:  $P$  = applied load

$A$  = cross-sectional area

$\alpha$  = angle between slip direction and compression axis

$\gamma$  = angle between slip plane and compression axis.

The results of these calculations are given in tables XI-XIV. Also presented in these tables are calculated primary (P) and secondary (S) slip systems and whether they were observed (O) or not observed (NO). These data lead to a number of important conclusions. First, the critical resolved shear stress is much lower for Fe-40Al (14.1 ksi) than for Fe-50Al (29.3 ksi). Also, the cooling rate has a significant effect on the critical resolved shear stress. In Fe-40Al, oil quenching increases  $\tau_{crss}$  to 44.1 ksi from 14.1 ksi in the slow cooled state. An increase to 46.2 ksi from 29.3 ksi is observed in the case of Fe-50Al.

#### Transmission Electron Microscopy

##### Burgers Vector Analysis

Table XI

Compression data for Fe-40Al slow cooled single crystals.

#	$(\bar{1}01)[111]$		$(101)[\bar{1}11]$		CRSS Primary (ksi) (MPa)		$\{211\}$ observed
B-1	P	O	S	NO	17.3	119	NONE
B-3	S	O	P	O	10.6	73	NONE
B-5	S	NO	P	O	13.3	92	NONE
B-6	P	NO	S	O	14.0	96	NONE
B-7	P	O	S	NO	17.2	118	NONE
B-8	S	NO	P	NO	14.7	102	NONE
B-9	S	NO	P	O	13.8	95	NONE
B-11	S	O	P	O	12.5	86	NONE
B-14	P	O	S	NO	13.1	90	NONE
B-15	P	NO	S	NO	15.0	103	NONE
B-16	P	O	S	NO	13.5	93	NONE
					14.1±1.9	97±13	

P and S indicate primary and secondary calculated slip systems respectively. O and NO indicate if the slip system was observed or not observed.

Table XII

Compression data for Fe-40Al oil quenched single crystals.

#	<u>(<math>\bar{1}01</math>)[111]</u>		<u>(101)[<math>\bar{1}11</math>]</u>		CRSS Primary		<u>{211} observed</u>
					<u>(ksi)</u>	<u>(MPa)</u>	
B-2	S	NO	P	O	42.9	295	NONE
B-10	S	NO	P	NO	46.9	323	NONE
B-12	S	O	P	NO	42.7	294	NONE
					<u>44.1±2.3</u>	<u>304±16</u>	

P and S indicate primary and secondary calculated slip systems respectively. O and NO indicate if a slip system was observed or not observed.



Table XIII

Compression data for Fe-50Al slow cooled single crystals.

#	$(\bar{1}01)[111]$		$(101)[\bar{1}\bar{1}1]$		CRSS Primary		$(211)$ observed
					(ksi)	(MPa)	
A-1	S	O	P	O	26.3	181	NONE
A-2	P	NO	S	O	33.7	232	NONE
A-3	P	O	S	NO	29.8	205	NONE
A-4	P	NO	S	O	27.6	190	$(\bar{1}21)[\bar{1}\bar{1}1]$
A-5	P	O	S	NO	30.8	212	$(\bar{2}11)[111]$
A-6	P	NO	S	O	30.6	211	NONE
A-9	P	O	S	NO	27.9	192	NONE
A-11	P	NO	S	NO	30.9	213	NONE
A-13	S	O	P	NO	26.4	182	NONE
					<u>29.3±2.5</u>	<u>202±17</u>	

P and S indicate primary and secondary calculated slip systems respectively. O and NO indicate if the slip system was observed or not observed.

Table XIV

Compression data for Fe-50Al oil quenched single crystals.

#	<u>(101)[111]</u>		<u>(101)[111]</u>		<u>CRSS Primary</u> <u>(ksi) (MPa)</u>		<u>(211) observed</u>
A-7	-	-	-	-	CRACKED		-
A-10	S	NO	P	O	44.6	307	NONE
A-12	S	NO	P	O	47.7	329	NONE
A-14	-	-	-	-	CRACKED		-
					<u>46.2±2.3</u>	<u>318±15.6</u>	

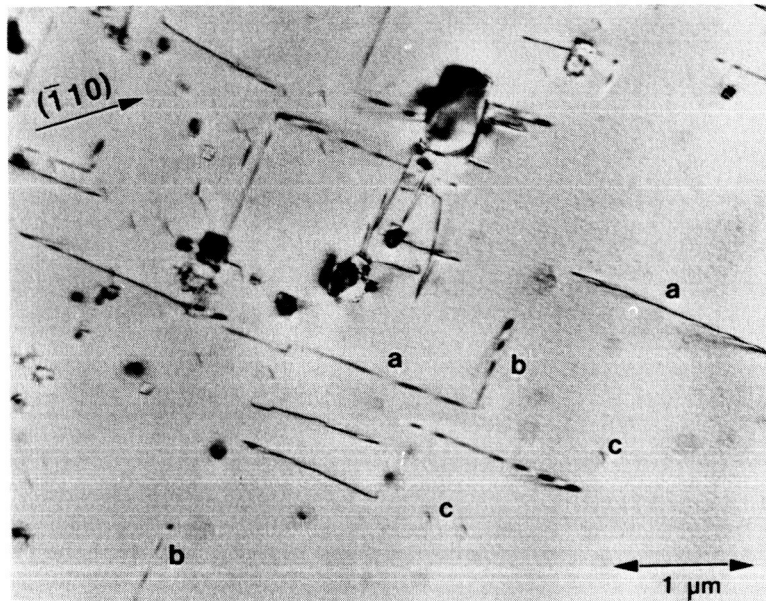
P and S indicate primary and secondary calculated slip systems respectively. O and NO indicate if the slip system was observed or not observed.

TEM contrast analysis using  $\vec{g} \cdot \vec{b} = 0$  and  $\vec{g} \cdot \vec{b} \times \vec{\mu} = 0$  criteria was used to determine the Burgers vectors in these alloys. For this analysis, only regular lattice spots were used in setting up two-beam conditions. This is because superlattice reflections have very large extinction distances which result in broad dislocation images with weak contrast which make interpretation difficult. To obtain a sufficient number of g-vectors, the primary spots of 3 poles, usually (001), (011) and ( $\bar{1}11$ ) were used.

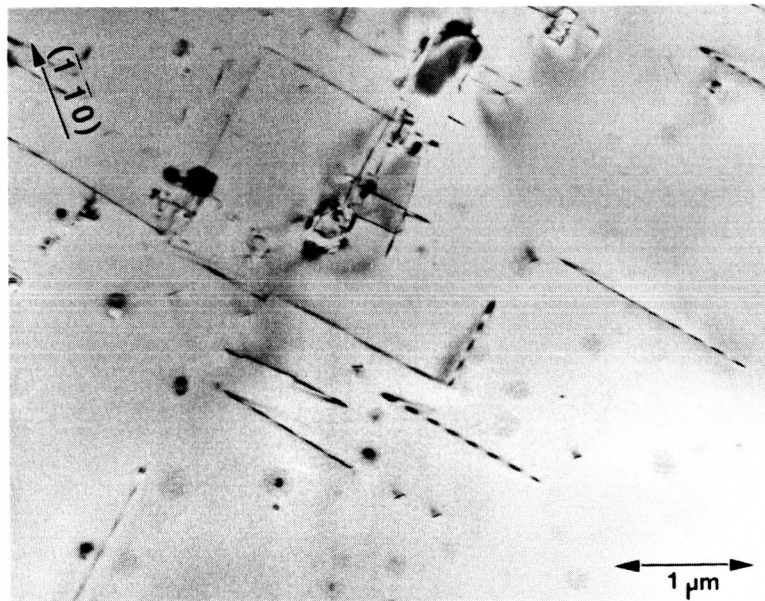
In the as-extruded condition, the residual dislocations in Fe-50Al, are  $\langle 100 \rangle$  type. Figure 42 shows a burgers vector analysis for the first series extrusion Fe-50Al. The residual dislocations are seen to lie on 3 distinct orientations labeled types "a", "b", and "c". Dislocations are out of contrast with  $\vec{g} = (0\bar{2}0)$ , in residual contrast with  $\vec{g} = (0\bar{1}1)$  and in good contrast for the other reflections. Thus, type "a" dislocations have  $[100]$  slip directions. Similar analysis shows type "b" dislocations are  $[010]$  and type "c" dislocations are  $[100]$ . These dislocations are predominantly edge in character.

In contrast with the as-extruded Fe-50Al, the as-extruded Fe-40Al contained a majority of  $\langle 111 \rangle$  dislocations with a small number of  $\langle 100 \rangle$  dislocations. Figure 43 displays the burgers vector analysis for the second series extrusion 2.BL (Fe-40Al with no boron). As can be seen, the residual dislocations in this alloy are not as strictly oriented as those in Fe-50Al. Also, a

ORIGINAL PAGE IS  
OF POOR QUALITY

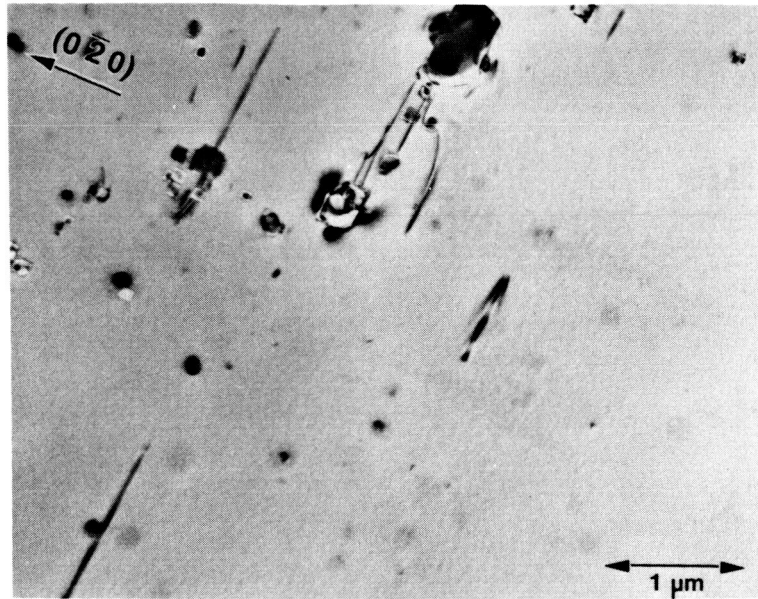


(a)



(b)

Figure 42. TEM burgers vector analysis for as-extruded first series Fe-50Al. a), b), c), are near  $(001)$ , d), e) are near  $(011)$ , and f) is near  $(111)$ .



(c)

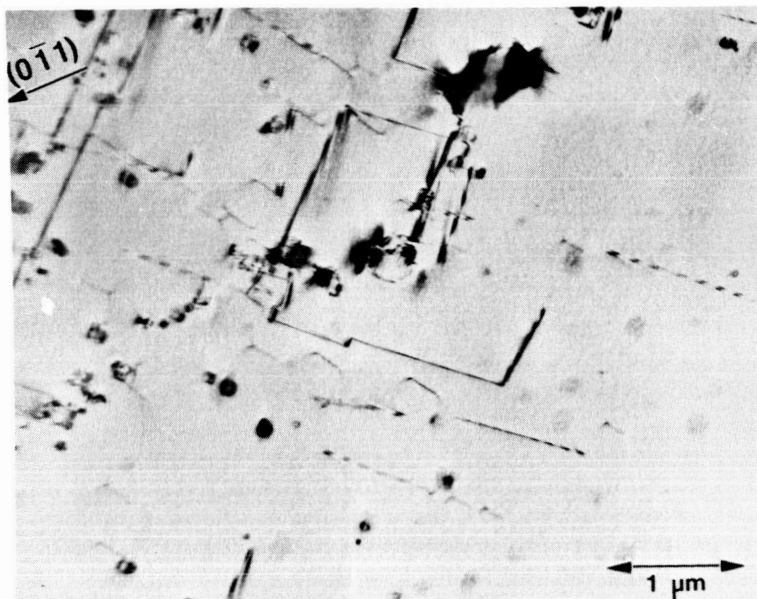


(d)

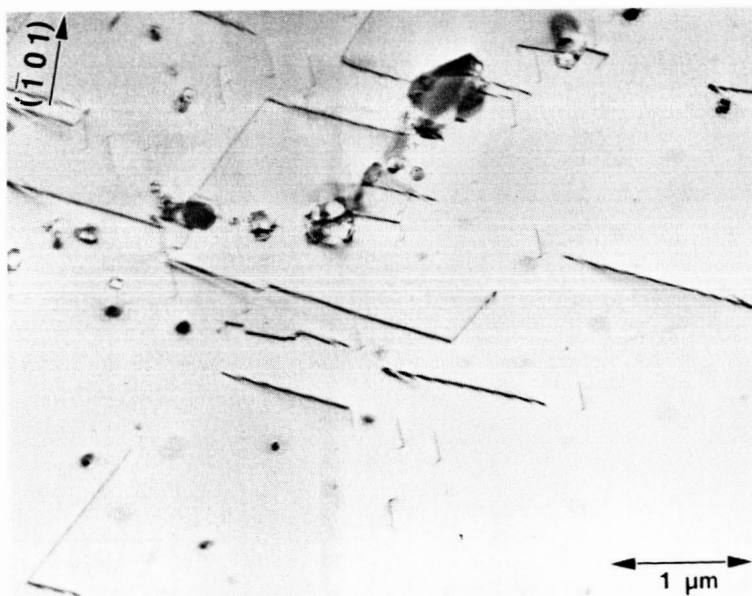
Figure 42 (cont.)

ORIGINAL PAGE IS  
OF POOR QUALITY

ORIGINAL PAGE IS  
OF POOR QUALITY

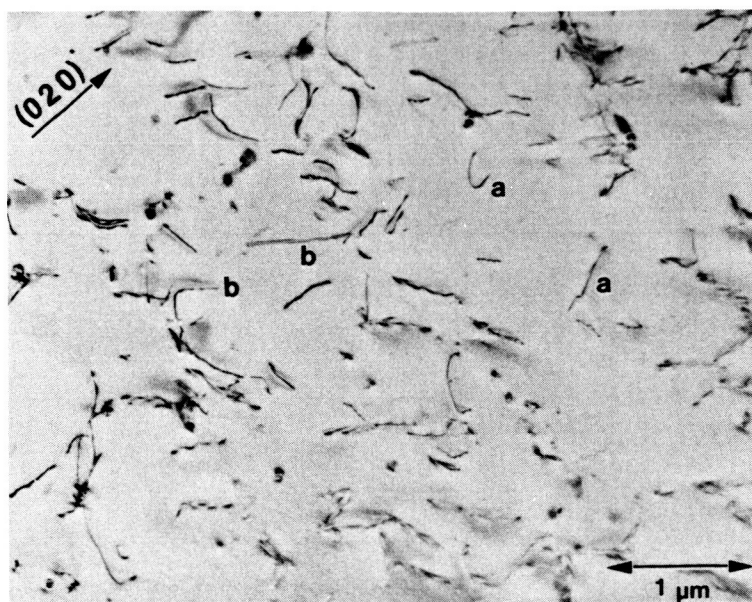


(e)

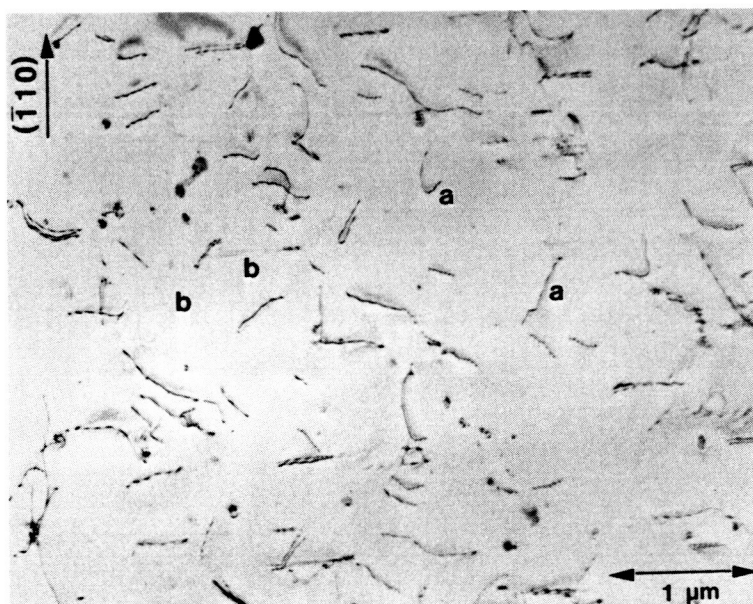


(f)

Figure 42 (cont.)



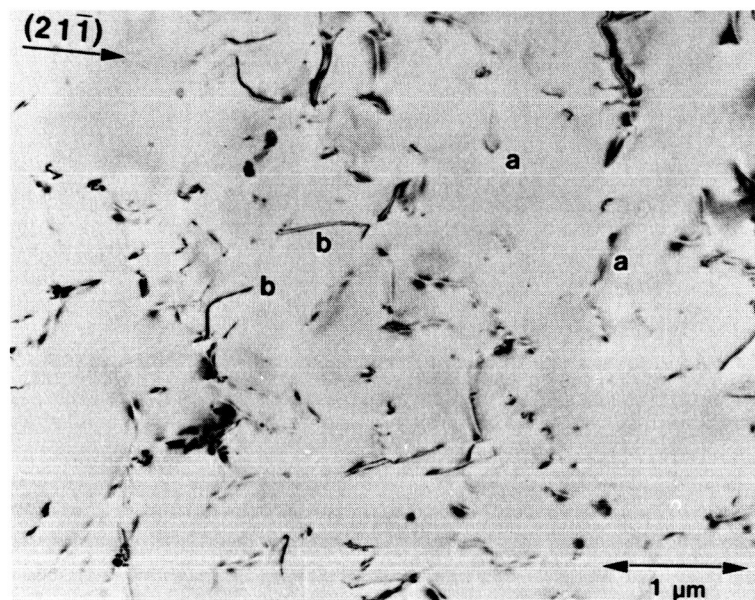
(a)



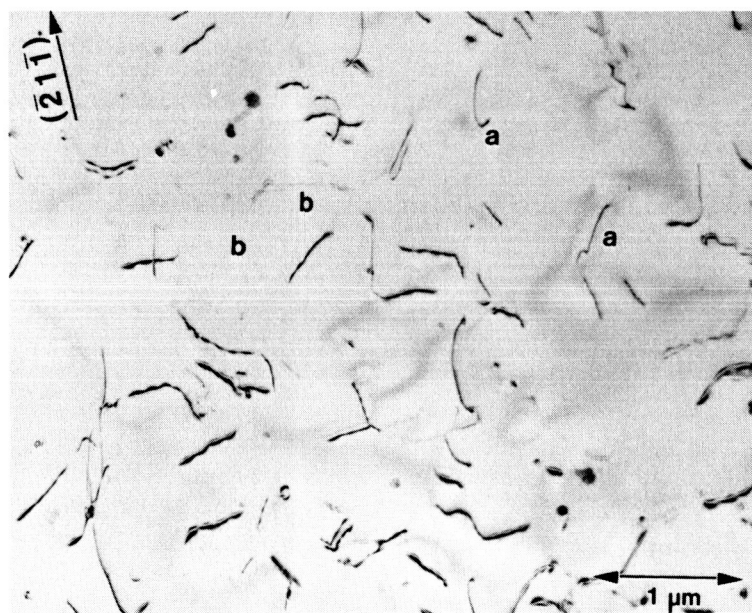
(b)

Figure 43. TEM burgers vector analysis for as-extruded second series Fe-40Al. a), b) are near (001), c), d), e) are near (011), f), g), h) are near ( $\bar{1}11$ ).

ORIGINAL PAGE IS  
OF POOR QUALITY



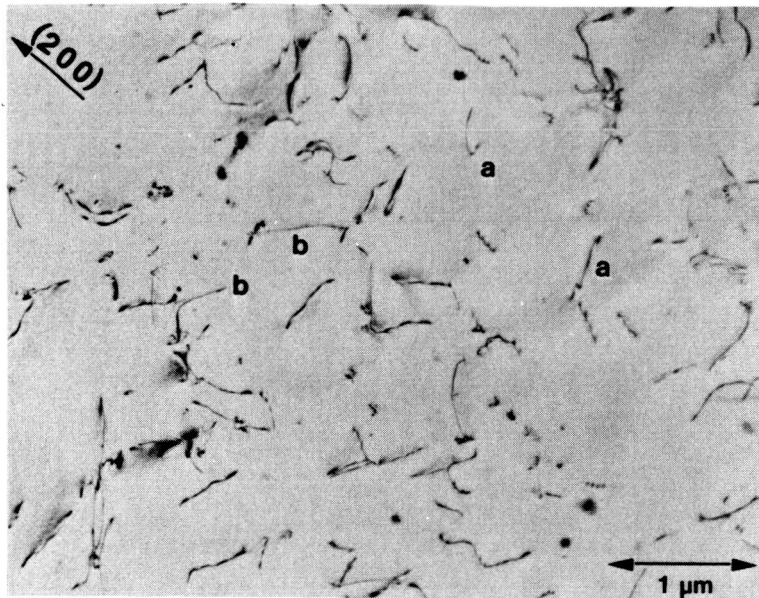
(c)



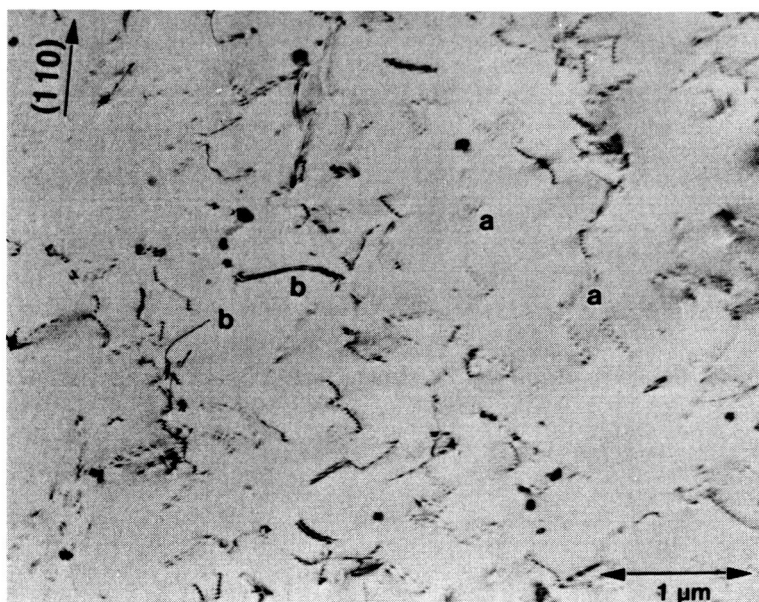
(d)

Figure 43 (cont.)



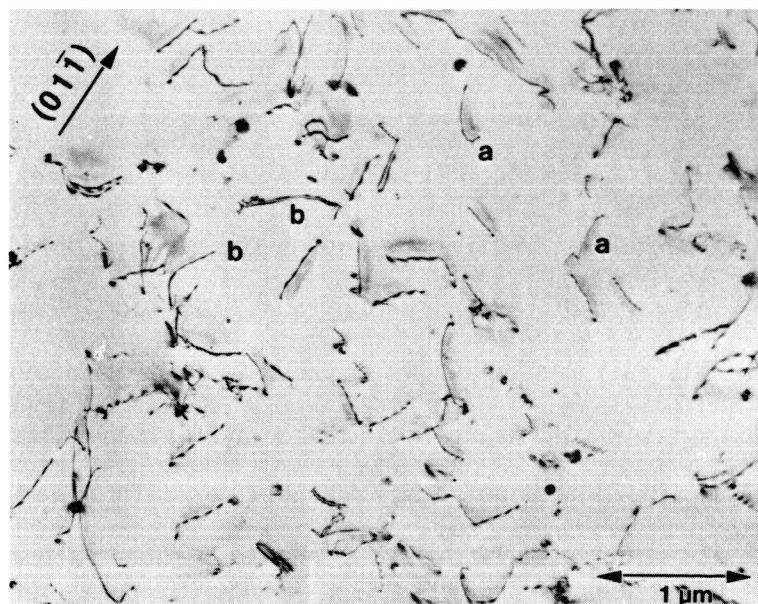


(e)

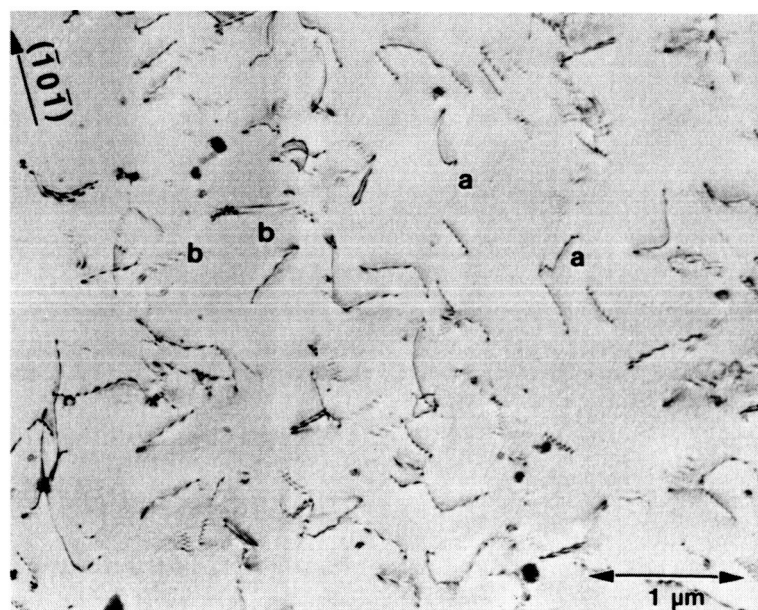


(f)

Figure 43 (cont.)



(g)



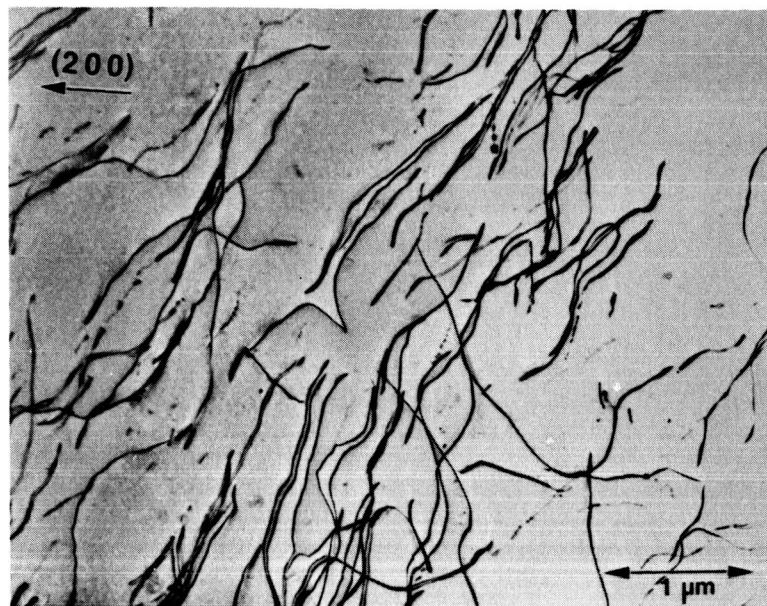
(h)

Figure 43 (cont.)

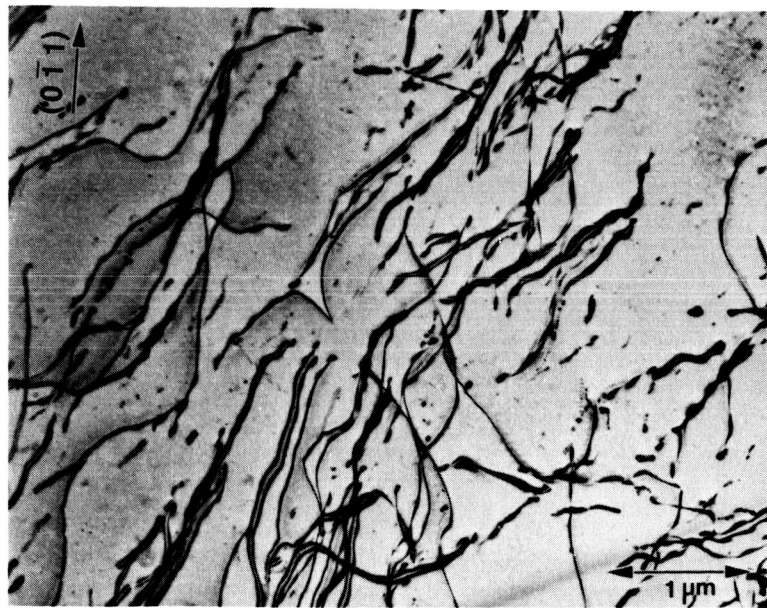
number of double images, from superdislocation pairs, are evident. The dislocations labelled "a" are seen to be in contrast for  $(01\bar{1})$ ,  $(\bar{1}0\bar{1})$ ,  $(200)$ , and  $(020)$  reflections. They are in weak, residual contrast with double images for  $(110)$  and  $(21\bar{1})$  reflections. Thus, the burgers vector of the dislocations labelled a are  $\langle 1\bar{1}1 \rangle$ . The dislocations labelled "b" are in good contrast for  $(200)$ ,  $(020)$ ,  $(110)$ , and  $(01\bar{1})$  reflections and display weak contrast for  $(\bar{1}0\bar{1})$ ,  $(\bar{2}1\bar{1})$  and  $(\bar{1}10)$ . Therefore, the type b dislocation have burgers vectors of  $[11\bar{1}]$ .

TEM burgers vector analysis determined that  $\langle 111 \rangle$  slip was the active deformation mechanism in all of the deformed materials. This was true regardless of stoichiometry, boron level, or cooling rate. In the polycrystalline samples, these analyses were performed on both tensile and compression samples in ductile Fe-40Al, and on compression samples in brittle (in tension) Fe-50Al. In the single crystals, TEM specimens were taken parallel to the slip plane of the compression samples. Because  $\langle 111 \rangle$  slip was found in all of the materials, only representative analyses will be given here. These analyses will be from the two extremes in yield strength, Fe-40Al slow cooled and Fe-50Al oil quenched. Also, because of the ease of interpretation, the analyses presented will be from single crystal materials.

Figure 44 presents the  $\vec{g} \cdot \vec{b} = 0$  burgers vector analysis for the Fe-40Al slow cooled single crystal. It should be recalled that this material displays a very low critical resolved shear

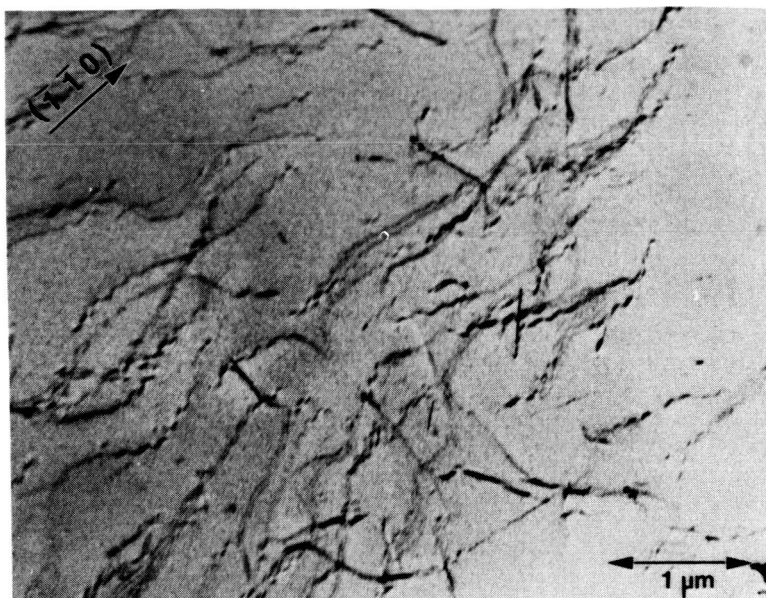


(a)



(b)

Figure 44. TEM burgers vector analysis for slow cooled Fe-40Al single crystal. a), b) are near  $(011)$ , c), d) near  $(001)$ , e) near  $(\bar{1}11)$ , f) near  $(111)$ .



(c)

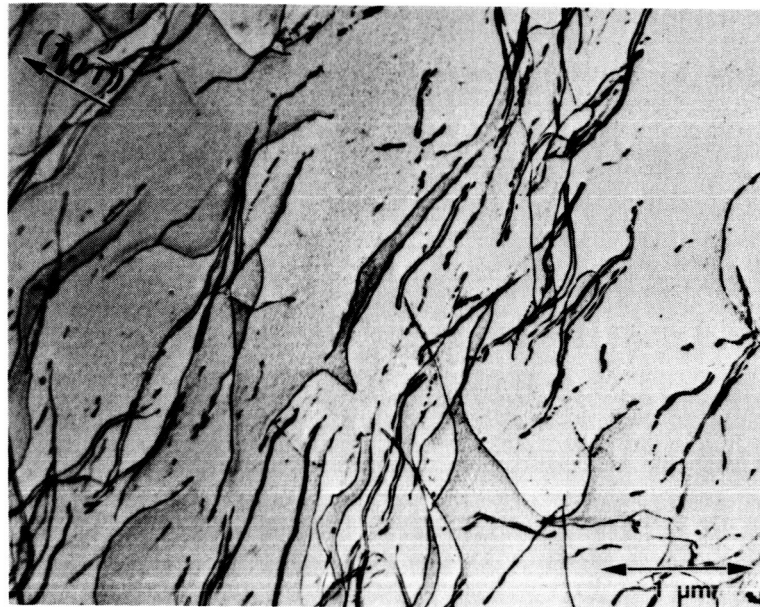


(d)

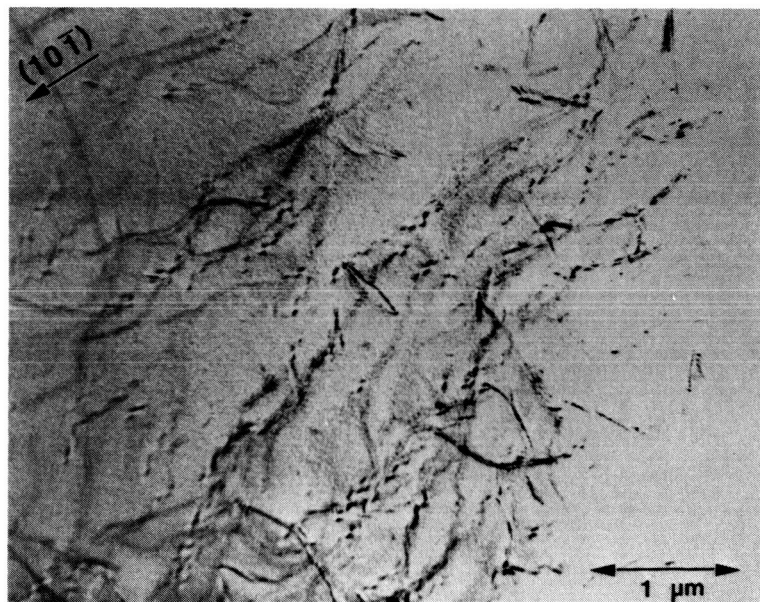
Figure 44 (cont.)



ORIGINAL PAGE IS  
OF POOR QUALITY



(e)



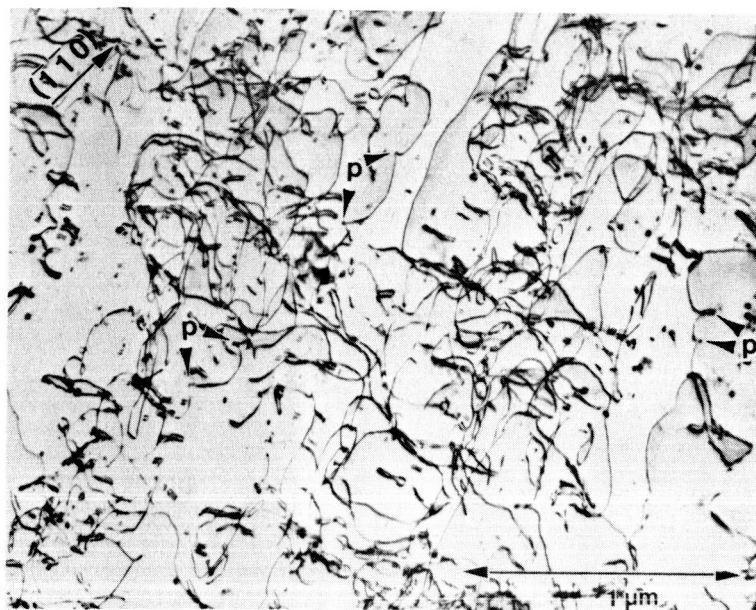
(f)

Figure 44 (cont.)

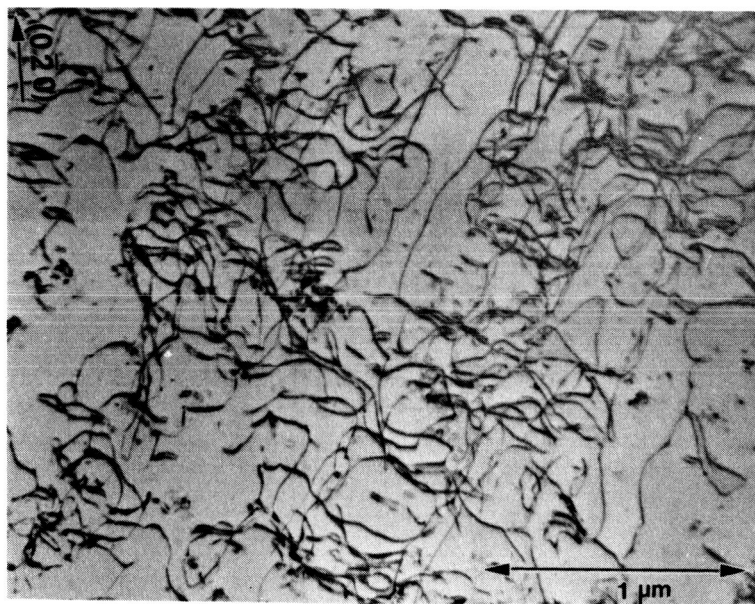
stress when compared with other conditions. As can be seen, these dislocations display an obvious orientation preference, yet are characterized by smooth bends and curves without straight segments and sharp jogs. Also, a number of dislocation pairs which make up superdislocations are evident. The majority of the dislocations are in good contrast using reflections of  $(0\bar{1}1)$ ,  $(200)$ ,  $(0\bar{2}0)$ , and  $(\bar{1}0\bar{1})$ . These same dislocations display weak contrast and double images using reflections of  $(\bar{1}\bar{1}0)$  and  $(10\bar{1})$ . Therefore, the slip direction in Fe-40Al slow cooled single crystals is  $[1\bar{1}1]$ . The plane of the foil (i.e. the observed slip plane) in this sample was  $(011)$  in which the  $[1\bar{1}1]$  direction lies. Thus, the analysis is consistent.

In contrast with the Fe-40Al slow cooled single crystals, the Fe-50Al oil quenched single crystals displayed very large critical resolved shear stresses. Figure 45 displays the contrast analysis used to determine the slip direction in this alloy. In these micrographs, no preferred orientation of the dislocations is readily apparent. However, a number of sharp jogs are evident, with the dislocations bowed out from them, indicating some pinning of dislocations may be occurring. Some of these kinks are shown labeled P in fig. 45a. Also, very few dislocation pairs are seen, indicating the APB energy is higher for Fe-50Al than for Fe-40Al. The dislocations are in good contrast in images taken with the reflections  $(\bar{1}\bar{1}0)$ ,  $(0\bar{2}0)$ ,  $(\bar{2}00)$ , and  $(0\bar{1}1)$ . Figures 45 d and f show images taken with  $(\bar{1}0\bar{1})$  and  $(1\bar{1}0)$  reflections respectively.

ORIGINAL PAGE IS  
OF POOR QUALITY



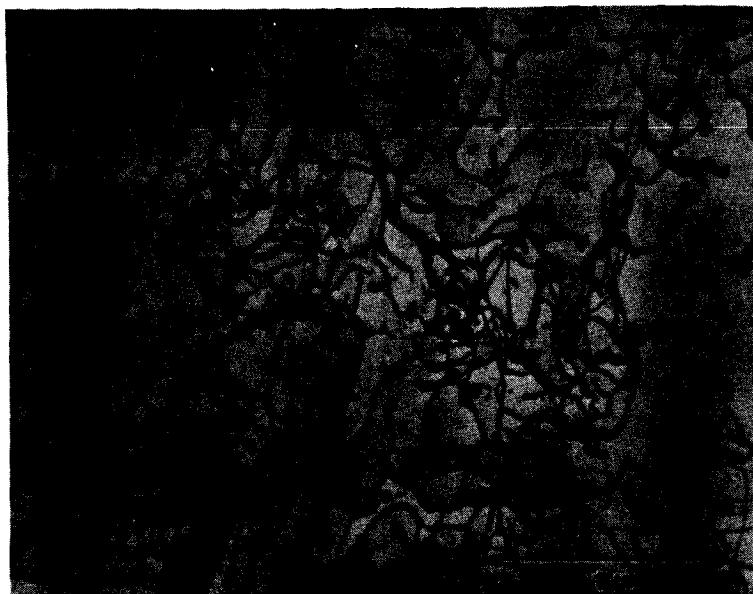
(a)



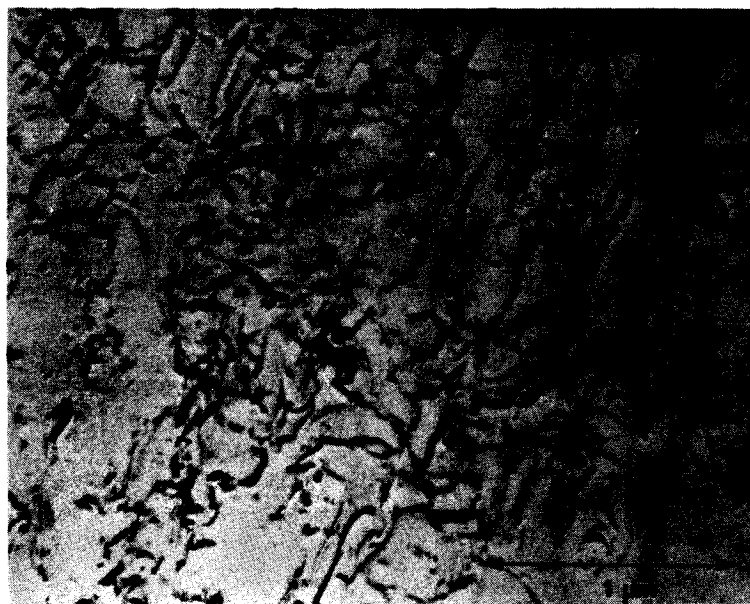
(b)

Figure 45. TEM burgers vector analysis for Fe-50Al oil quenched single crystal. a), b), c), d) are near (001), e) is  $(\bar{1}11)$ , f) is near (111).



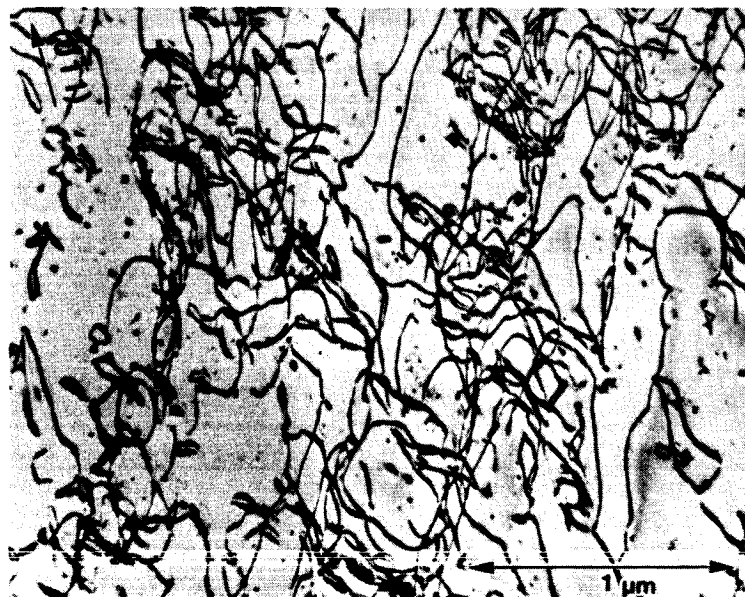


(c)

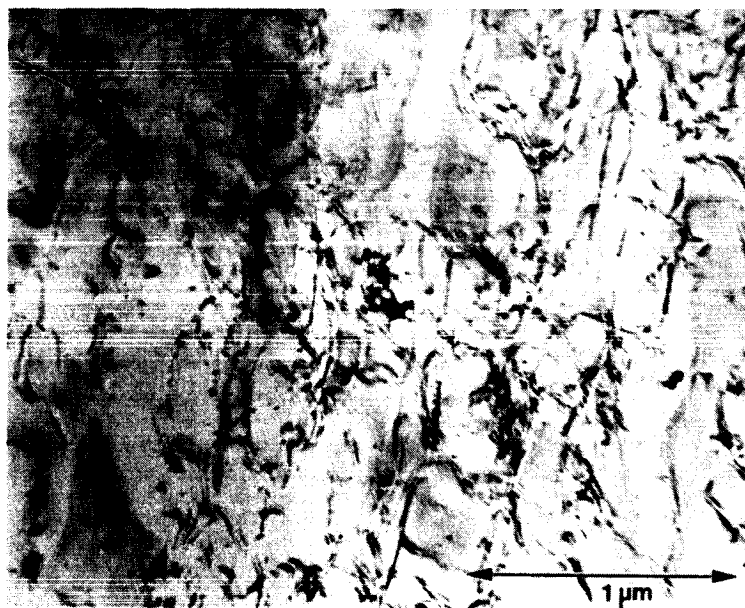


(d)

Figure 45 (cont.)



(e)



(f)

Figure 45 (cont.)

ORIGINAL PAGE IS  
OF POOR QUALITY

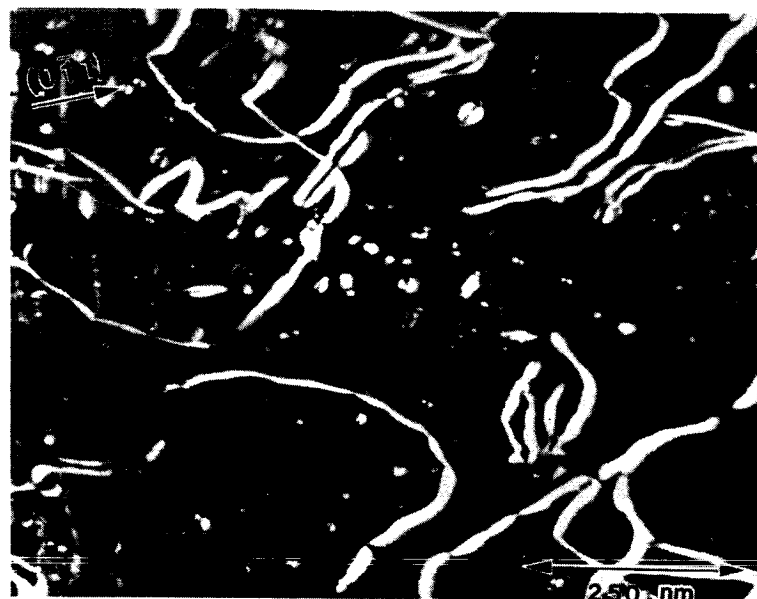
These images display very poor contrast and some double images, characteristic of materials with high elastic anisotropy. Therefore, it can be concluded that these dislocations have a slip direction of  $[11\bar{1}]$ . The plane from which the TEM specimen was cut was (011). The  $[11\bar{1}]$  direction lies in the (011) plane, which is consistent with the analysis.

#### Dislocation Loop Observations

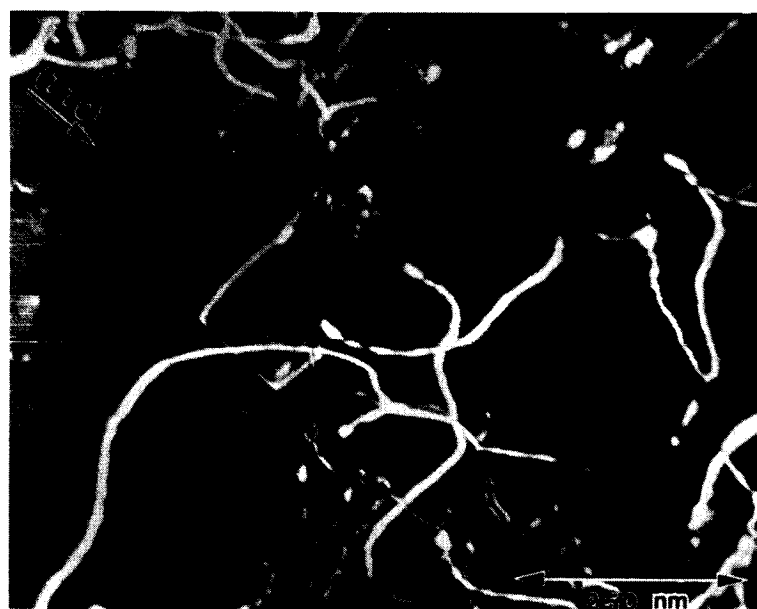
No significant differences in substructure were noticed between slow cooled and quenched polycrystalline samples. This may have been due to excessive deformation resulting in high dislocation densities which could have obscured substructural details. The single crystals however, displayed a substantial difference in substructure. Figures 46 and 47 show  $\vec{g} \cdot 3\vec{g}$  weak beam micrographs taken at high magnifications. The oil quenched samples display large numbers of very small loops throughout the substructure whereas in the slow cooled samples, very few loops were observed. This was true for both the stoichiometric Fe-50Al (fig. 46) and substoichiometric Fe-40Al (fig. 47). The loops are probably the result of quenched in vacancies forming vacancy loops. These loops may result in the pinning of the dislocations that have been observed in the quenched materials.

#### Precipitates

Optical microscopy has shown that the addition of boron

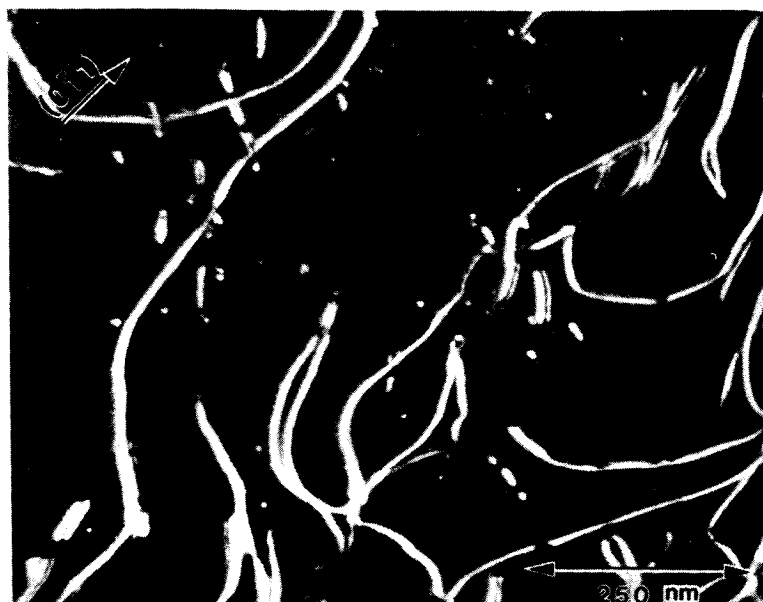


(a)



(b)

Figure 46.  $\vec{g} - 3\vec{g}$  weak beam micrographs of a) Fe-50Al oil quenched and b) Fe-50Al slow cooled single crystals.



(a)



(b)

Figure 47.  $\vec{g} - 3\vec{g}$  weak beam micrographs of a) Fe-40Al oil quenched and b) Fe-50Al slow cooled single crystals.

results in precipitation. Transmission electron microscopy has been used to examine these precipitates in more detail.

Thin foil electron microscopy found that the addition of boron to Fe-50Al results in thin, planar precipitates which resemble stacking faults. Examples of these are shown in fig. 48. It should be noted that this image was taken using a strong 2-beam condition of a regular lattice spot. Thus, this type of contrast cannot be due to antiphase boundaries. These types of precipitates were found in both the first and second series Fe-50Al extrusions which contained boron. Unfortunately, because of their very small size, it was impossible to perform chemical or diffraction analysis on them. However, Baker, et al. [65] have studied these same foils as well as another alloy, Fe-37Al-2.5Ni-0.25Mo, which displays the same type of defects, and have concluded the planar defects are precipitates lying on  $\{100\}$  and characterized by an  $(a/2)\langle 100 \rangle$  fault vector.

Other precipitates were analysed using extraction replicas from the first series extrusion, Fe-50Al-0.2B (fig. 49). It can be seen that this image corresponds well with the structure observed optically (fig. 8c) with rings of prior powder particle boundaries. Energy dispersive spectroscopy (EDS) showed that the prior particle boundaries were Al rich as can be seen in fig. 50. Wavelength dispersive spectroscopy (WDS) of the replicas in an SEM showed an oxygen peak to background ratio of approximately 2 to 1. Thus, as expected, the prior powder particle boundaries are  $\text{Al}_2\text{O}_3$ .

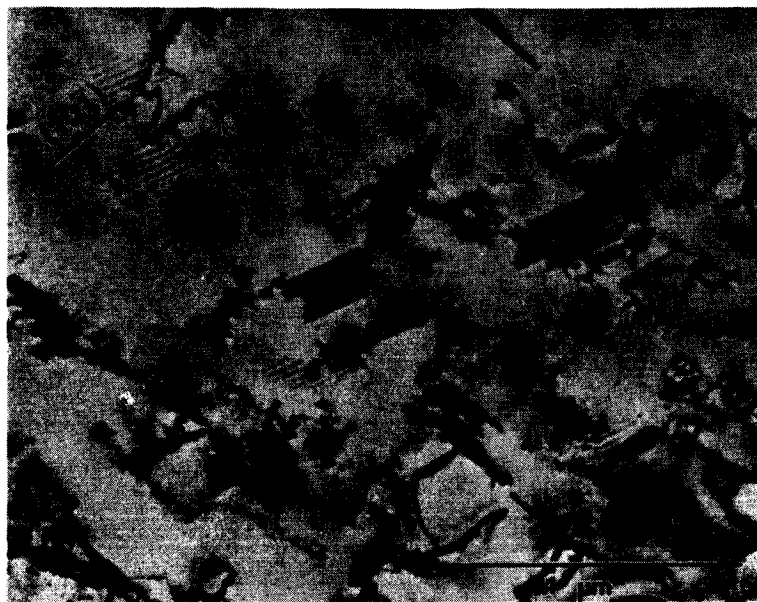


Figure 48. TEM bright field micrograph of the first series Fe-50Al-B alloy displaying planar precipitates.

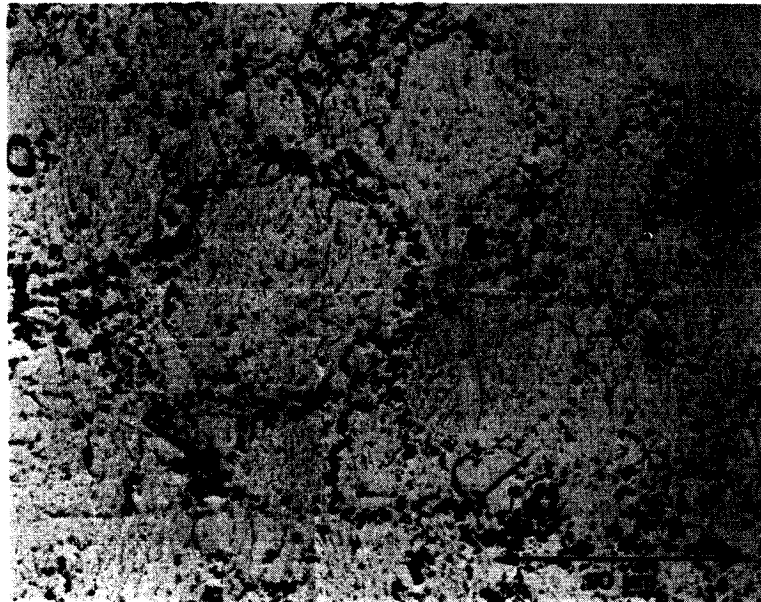


Figure 49. TEM micrograph of extraction replica from the first series Fe-50Al-B alloy.

ORIGINAL PAGE IS  
OF POOR QUALITY.



TN-5500 Case Western Reserve

WED 25-FEB-87 18:41

Cursor: 0.000keV = 0

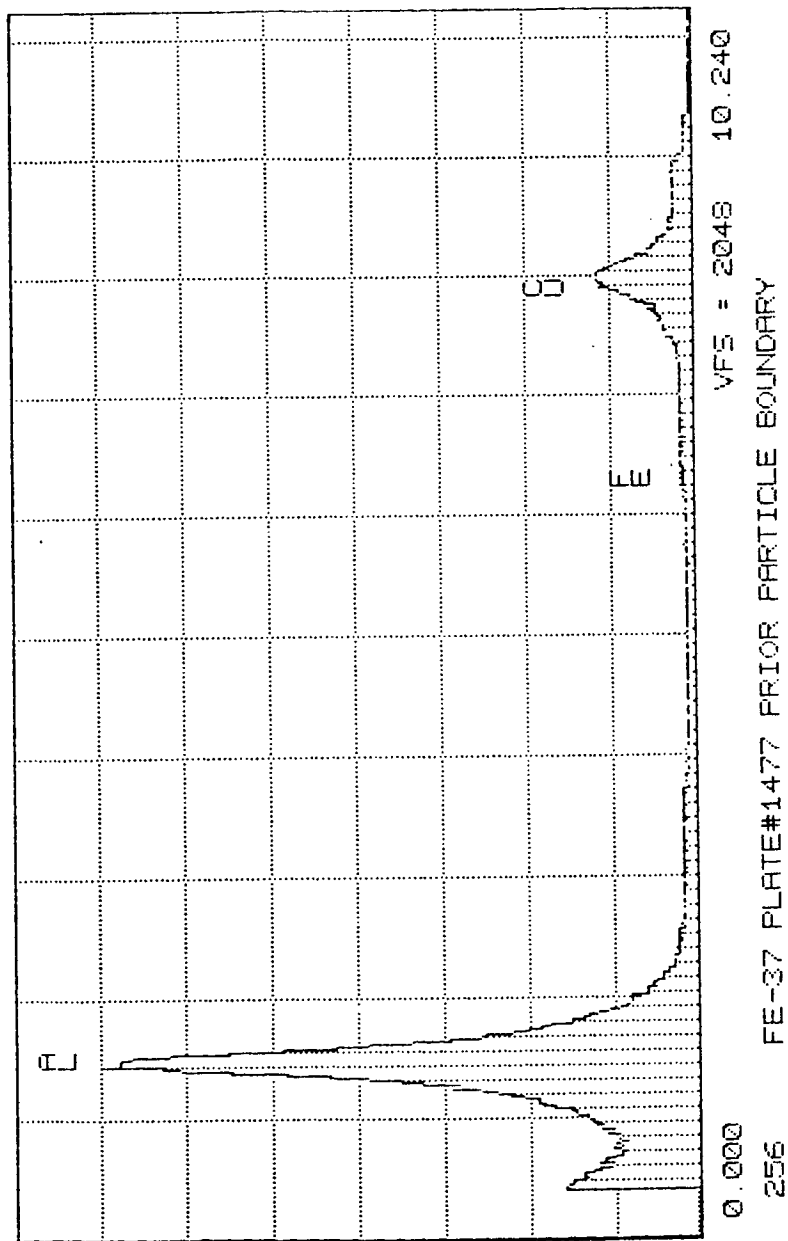


Figure 50. Energy dispersive X-ray spectrum from prior powder particle boundary in extraction replica shown in fig. 49.

Some large plate-like precipitates are also seen in fig. 49. These are shown in more detail in fig. 51. EDS indicates that the plate-like precipitates are iron-rich as indicated by the spectra displayed in fig. 52. The small Al peak is probably from surrounding  $\text{Al}_2\text{O}_3$  particles while the Cu peak results from the Cu grid which supports the replica. WDS of these particles shows boron peak to background ratios of approximately 4 to 1 with no significant oxygen peaks. Thus, these plate-like precipitates are probably some type of iron boride.

The fine mottled structure seen within the prior powder particle boundaries in fig. 49 is actually roughness in the carbon replica. This is a result of replicating fine pits in the etched sample. These pits are probably related etching effects of the planar precipitates observed in the thin foils and discussed above.

Figure 53 shows an extraction replica taken from the as-cast Fe-40Al-B. This replica corresponds well with the optical micrographs (fig. 12b) of this material. An energy dispersive spectrum for one of these precipitates is shown in fig. 54. As can be seen, these precipitates contain large amounts of Fe. No evidence of aluminum-rich precipitates was found in the cast materials. WDS also indicates that these precipitates are boron-rich, with peak to background ratios of almost 3 to 1 and no indication of oxygen. Thus, it is concluded that these precipitates in the cast material are also iron borides as in the

case of the powder processed alloys.

ORIGINAL PAGE IS  
OF POOR QUALITY



Figure 51. TEM micrograph of iron boride precipitate extracted from the first series Fe-50Al-B alloy.

TN-5500 Case Western Reserve

WED 25-FEB-87 18:32

Cursor: 0.000keV = 0

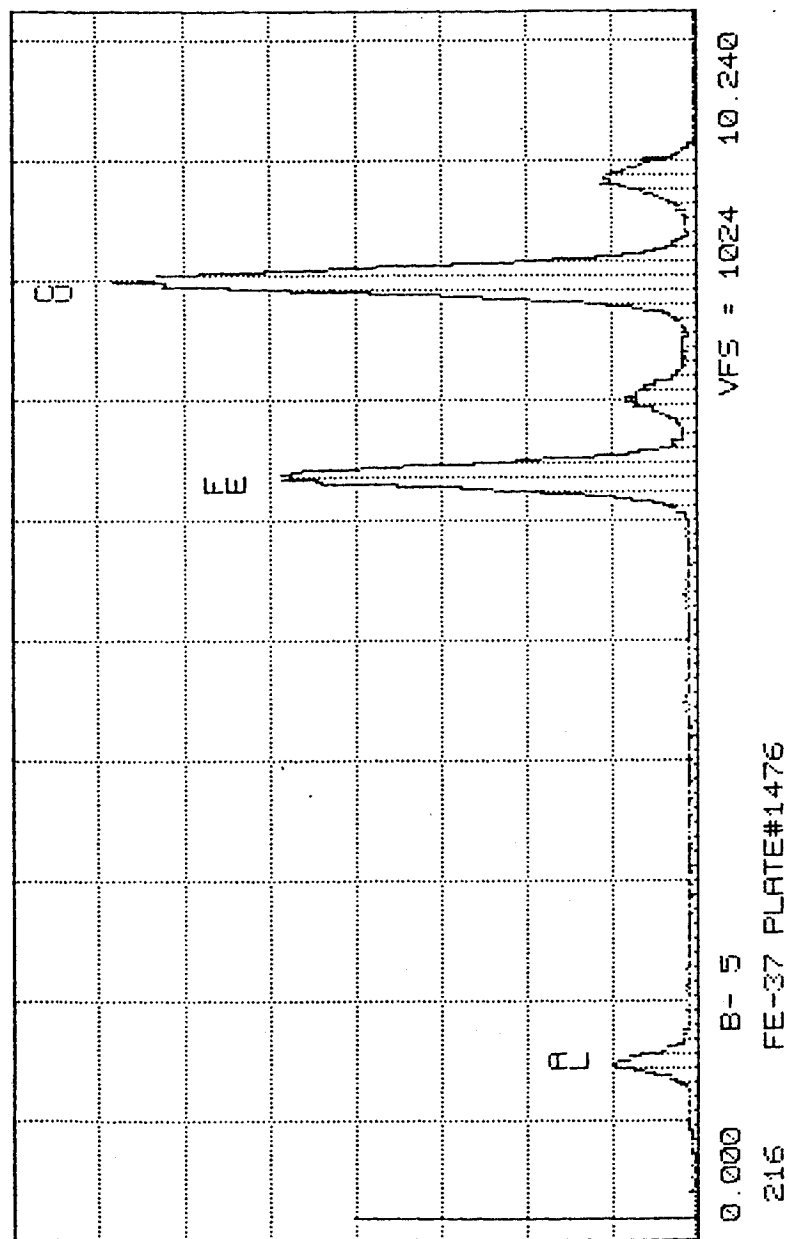


Figure 52. Energy dispersive X-ray spectrum from plate-like precipitate shown in fig. 51.

ORIGINAL PAGE IS  
OF POOR QUALITY

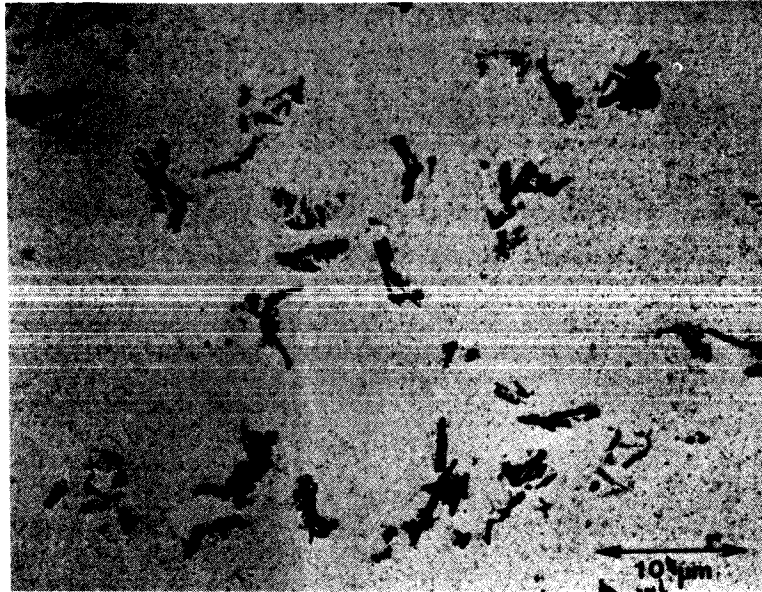


Figure 53. TEM micrograph of extraction replica from as-cast  
Fe-40Al-R

TN-5500 Case Western Reserve      WED 25-FEB-87 20:28  
 Cursor: 0.000keV = 0      ROI      (0) 0.000: 0.000

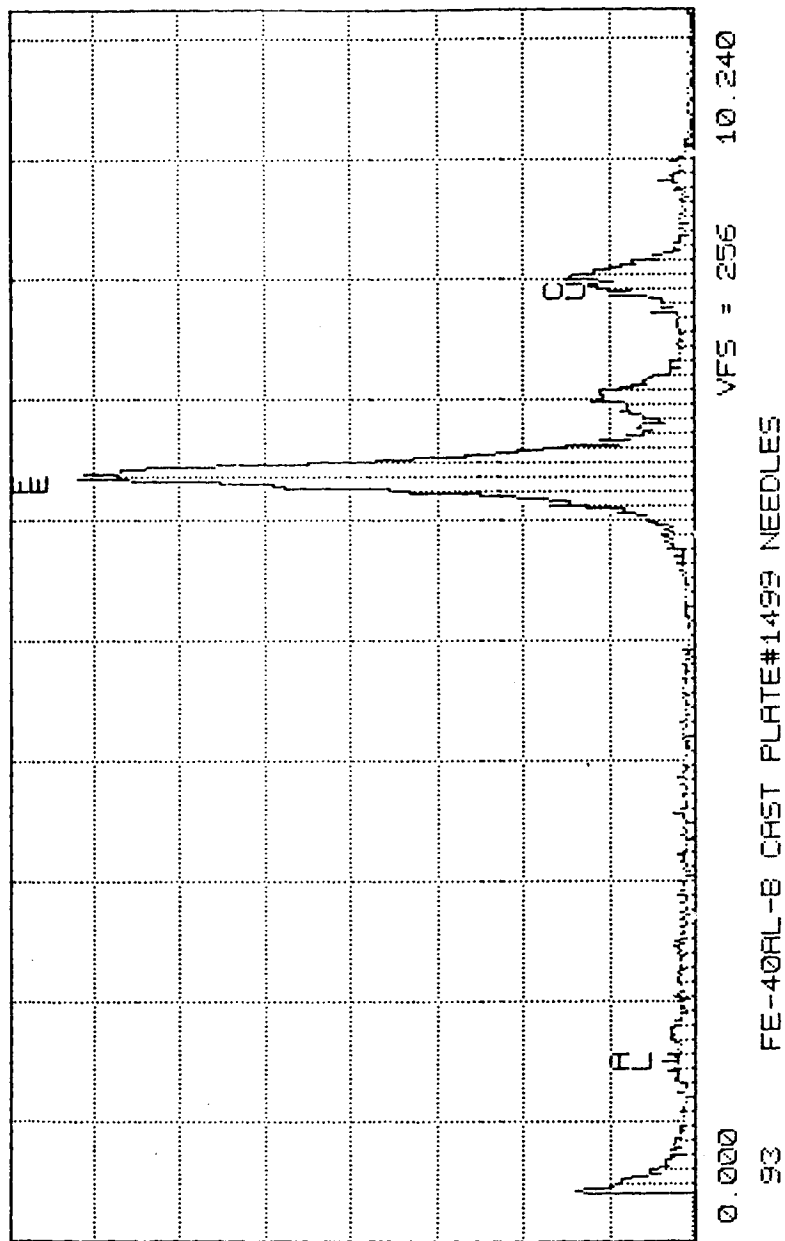


Figure 54. Energy dispersive X-ray spectrum from precipitate of the type shown in fig. 53.

## DISCUSSION

### Materials/Processing

While materials processing was not a major focus of this study, some observations are worth discussing. The nature of material consolidation used in this work, hot extrusion of powder, has distinct consequences on the microstructural development of these materials.

The original powder particle surfaces, stretched out into long stringers during extrusion, influence the grain growth behavior of FeAl. As has been presented, these prior powder particle boundaries, which have been identified as  $\text{Al}_2\text{O}_3$ , tend to limit the grain size in the as-extruded materials. In the second series of extrusions, increases in extrusion temperature from 1073 K to 1350 K resulted in only small increases in grain sizes, from about 10  $\mu\text{m}$  to about 15  $\mu\text{m}$ . In contrast to this, in the cast material which contained no prior powder particle boundaries, the resulting grain size after extrusion at 1150 K was about 100  $\mu\text{m}$ . It is reasonable to conclude then, that these prior powder particle boundaries are pinning grain boundaries and making grain growth due to the extrusion process difficult. However, it should be noted that the initial grain size in the cast material is much larger than that in the FeAl powder, and this may also influence the as-extruded grain size.



This limited grain growth is also reflected in the various heat treatments. In powder extruded samples, heat treatments from 1073 K to 1273 K resulted in very little grain growth. By contrast, in the cast and extruded material, heat treatment at 1273 K increased the grain size to around 500  $\mu\text{m}$ , from 100  $\mu\text{m}$ . This suggests that the inherent grain growth kinetics are not limiting the grain growth, and an external factor, the prior powder particle boundaries, is slowing the growth.

At higher temperatures, it appears that the ability of prior powder particle boundaries to limit grain growth diminishes. Figure 55 shows the grain growth,  $D_{\text{HT}}$  (grain size following heat treatment) divided by  $D_{\text{E}}$  (extruded grain size), as a function of heat treatment temperature. As can be seen, very little growth occurs below 1273 K. Above this temperature, significant grain growth begins, with very large increases in grain size occurring in some samples. A number of possibilities exist for this threshold temperature for grain growth. The first is that at this temperature the prior powder particle boundaries become less effective at pinning grain boundaries. Another possibility is that at this temperature, sufficient thermal activation occurs to overcome the pinning effects, and rapid grain growth is able to occur. Finally, it is possible that the oxide particles are becoming redistributed with the heat treatment process, allowing faster grain growth. This may result from coarsening of particles through an Oswald ripening type process.

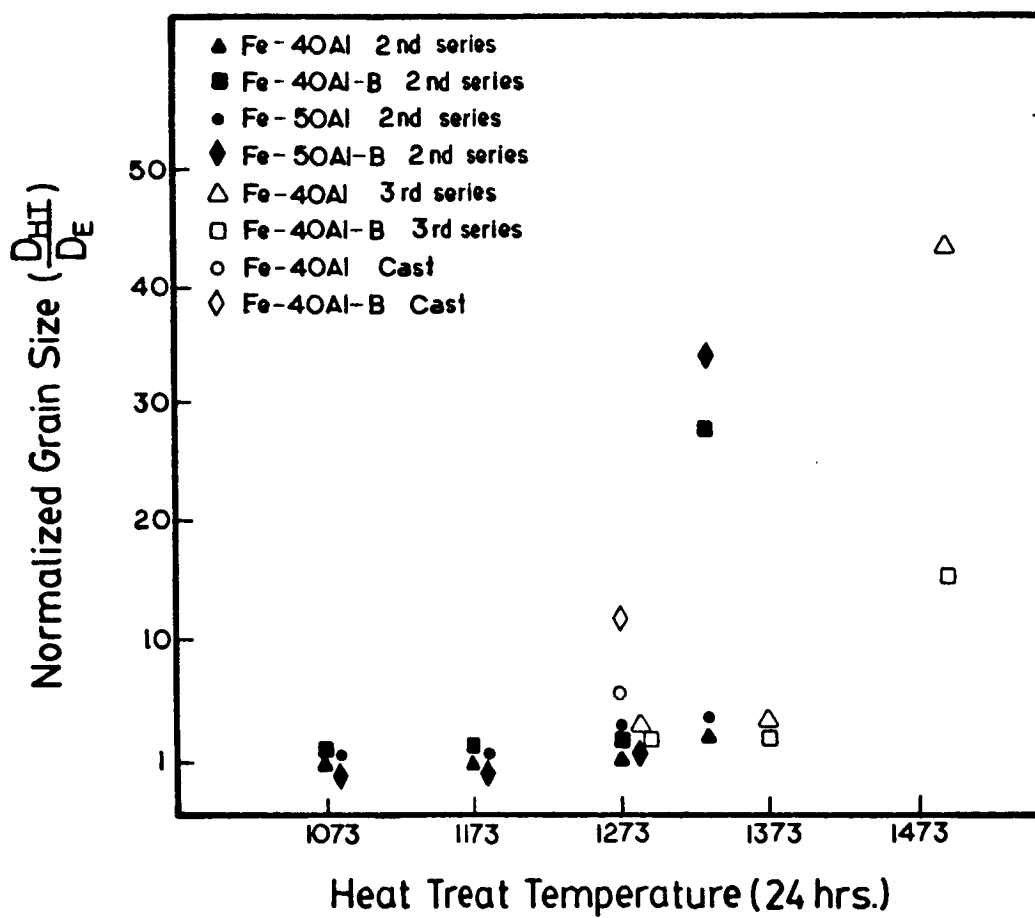


Figure 55. Plot of normalized grain size as a function of heat treatment temperature for a number of FeAl alloys.

The effect of boron on the grain growth behavior is not as clear. In the as-extruded condition, samples containing boron had slightly smaller grain sizes than their counterparts without B. Additionally, in the second series extrusions, increasing boron levels resulted in slight decreases in grain sizes. Thus, it is clearly evident that in the as-extruded conditions boron has limited the growth of grains to a slight extent.

The effects of heat treatments as related to boron additions are not as clear. While the same general results in terms of grain growth as a function of heat treatment temperature occur in alloys containing boron, the specifics vary somewhat. While the as-extruded samples containing boron had smaller grain sizes, once rapid grain growth begins, the boron containing alloys display larger grain sizes. This was typically related to abnormal grain growth and was observed in both powder processed and cast alloys. It is reasonable to expect that boron may influence the grain growth kinetics of FeAl as it may be segregated to grain boundaries. However, the details of this are not understood and therefore cannot be related to grain growth. It is interesting to note that while this grain growth occurs faster in boron containing alloys, in some of the larger grained samples, there appears to be significant pinning of grain boundaries as shown in fig. 12.

The presence of metallic impurities (second series extrusions) has not changed the general aspects of grain growth.

In the as-extruded condition, the grain sizes of contaminated versus non-contaminated do not vary significantly in samples with and without boron. The presence of these impurities has also not affected the temperature where dramatic grain growth begins.

#### Mechanical Behavior/Stoichiometry Effects

As has been shown in the results, Fe-50Al fails in a brittle intergranular manner in tension at room temperature, while Fe-40Al displays some yielding and plastic elongation before intergranular failure. By contrast, both Fe-40Al and Fe-50Al yield and display substantial ductility when tested in compression. These tensile and compressive behaviors are summarized in fig. 56. The major difference is that while both of these alloys fail in tension at approximately the same stress level, Fe-40Al yields at a much lower stress than Fe-50Al in compression.

The compressive ductility of Fe-50Al is evidence that the required number of slip systems can be activated for grain boundary compatibility in polycrystals (von Mises criteria) provided the stress can be raised high enough. The observation of  $\langle 111 \rangle \{110\}$  slip is consistent with this conclusion. However, in tension, fracture along grain boundaries occurs at a stress level far below the stress required for general yielding. In the case of Fe-40Al, since the stress required for general yielding is much lower, plastic deformation is observed before intergranular



failure. The critical issue therefore, is the competition between the stress for general yielding, and the stress for brittle intergranular failure, which explains the onset of significant tensile ductility in the off-stoichiometric Fe-40Al compared with stoichiometric Fe-50Al.

The dramatic decrease in compressive yield strength is consistent with the decrease in hardness found by Westbrook [36], but the reasons are not clear. This behavior is particularly interesting, since in other B2 aluminides, NiAl and CoAl, deviations on both sides of stoichiometry have been shown to result in defect hardening [36]. However, in contrast to FeAl where  $\langle 111 \rangle$  slip occurs at room temperature, NiAl and CoAl display  $\langle 100 \rangle$  slip at room temperature [66]. It should be remembered that  $\langle 100 \rangle$  slip in B2 results in no disordering of the structure and as a result,  $\langle 100 \rangle$  dislocations do not move in pairs or leave APB trails.

It has been shown that this large decrease in yield strength with stoichiometry is reflected in a correspondingly large decrease in critical resolved shear stress in single crystals. This is an important consequence because it shows that the changes in yield behavior are a result of changes in the slip behavior of  $\langle 111 \rangle \{110\}$  dislocations and are not associated with changes associated with polycrystallinity (i.e. changes in grain boundary structure with stoichiometry).

Because these changes in yield strength, and thus the ductile

or brittle behavior, are a direct result of changes in the critical resolved shear stress, it is important to discuss the factors which may affect  $\tau_{crss}$ .

Because the observation of the  $\langle 111 \rangle$  direction requires the movement of  $2 - 1/2 \langle 111 \rangle$  dislocations in superdislocation pairs and associated APB's, it is of interest to examine the effect of the APB energy on the critical resolved shear stress. Crawford and Ray [30] have measured the APB energy as a function of stoichiometry in B2 FeAl from 27 at%Al to 36 at%Al. In this composition range, the APB energy increased from 28 ergs/cm<sup>2</sup> at 27Al to 105 ergs/cm<sup>2</sup> at 36Al. Although no data are available on the APB energy at compositions above 36 at%Al, it is reasonable to assume the energy continues to increase. Based on calculations of changes in nearest neighbor positions, the APB energy can be shown to have the form:

$$\tau = \frac{4\sqrt{2} x^2 (v-w)}{a_0} \quad [4]$$

where:  $x$  = atomic fraction Al from 0.25 to 0.5

$a_0$  = lattice parameter

$v$  = nearest neighbor ordering energy

$w$  = next nearest neighbor ordering energy.

The development of this expression is presented in Appendix B.

Over the composition range of 29.5 to 50 at%Al, Taylor and Jones

[6] have shown that the lattice parameter varies from 0.290 nm to 0.292 nm. Thus, the lattice parameter will not effect this APB energy significantly. Machlin [67,68] has given the interaction energies as a function of interatomic separation as:

$$V_{ij} = \frac{-A^{\alpha\beta}}{(r_{ij})^4} + \frac{B^{\alpha\beta}}{(r_{ij})^8} \quad [5]$$

where  $A^{\alpha\beta}$  and  $B^{\alpha\beta}$  are constants and  $r_{ij}$  is the interatomic separation. As can be seen, the interactions are a strong function of separation. However, with the small variation in lattice parameter in these alloys, the interaction energies should at most vary by approximately 4%. Therefore, it is seen that the APB energy increases dramatically with aluminum contents and it is reasonable to extrapolate Crawford and Ray's data to higher aluminum levels. Figure 57 shows the data from Crawford and Ray as a solid line, and the extrapolated data as a dotted extension. As can be seen, the APB energy in the alloys studied ranges from about 150 ergs/cm<sup>2</sup> for Fe-40Al to about 250 ergs/cm<sup>2</sup> for Fe-50Al.

The APB energy influences dislocations in the following manner. Similar to partial dislocations with associated stacking faults, the individual dislocations of a superdislocation repel each other with a force due to their elastic interactions. This repulsive force is given by [69]:



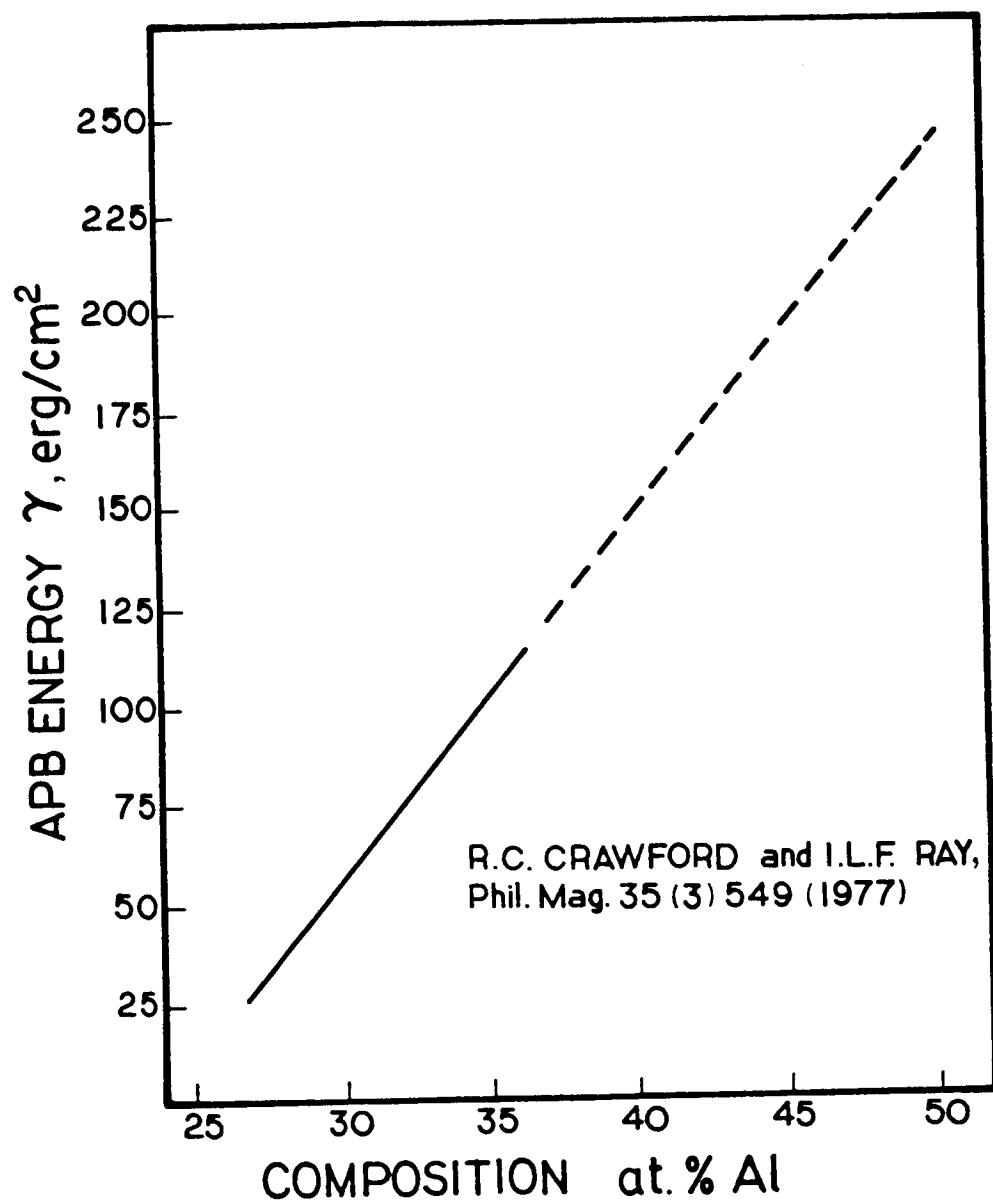


Figure 57. APB energy as a function of stoichiometry for B2 FeAl.

$$F_r = \frac{\mu b^2}{2\pi d} \quad [6]$$

where:  $\mu$  = shear modulus

$b$  = magnitude of  $1/2[111]$  dislocation

$d$  = distance between dislocations.

This repulsive force is balanced by the energy associated with the APB between the dislocations such that an equilibrium separation,  $d_o$ , is established [69]:

$$d_o = \frac{\mu b^2}{2\pi\gamma_{APB}} \quad [7]$$

Thus, like partial dislocations and stacking faults, the equilibrium separation of dislocations in an ordered alloy is inversely proportional to the APB energy. However, it is important to note that in ordered alloys, this separation of dislocations does not restrict cross slip as both individual dislocations have the same burgers vector, and can therefore cross slip without constricting together.

While the individual dislocations within a superdislocation move as a pair through the crystalline lattice, it should not be assumed that they make incremental steps through the lattice at the same time. For the dislocation to slip at the same instant to require that the thermal activation contribution to slip would act equally on both dislocations at the same time. This would require

the phonon wavelength to match the dislocation separation distance, which could only happen at specific temperatures. Therefore, above absolute zero, it is reasonable to assume that the individual dislocations make incremental steps independently. It is therefore necessary to examine how the forces related to repulsion and APB energy influence the incremental slip of individual dislocations. The total force acting on an individual dislocation is the sum of the repulsive and attractive forces and is given by:

$$F_T = F_A - F_R \quad [8]$$

where the attractive force is represented by the APB energy. Substituting equations 5 and 6 into this expression results in:

$$F_T = \frac{\mu b^2}{2\pi d_0} - \frac{\mu b^2}{2\pi d} \quad [9]$$

where  $d_0$  is the equilibrium separation distance, and  $d$  is the actual separation distance. The slope of the force versus distance is given by:

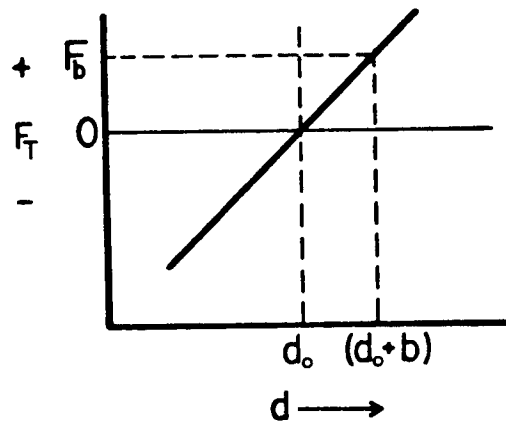
$$\frac{\partial F_T}{\partial d} = \frac{\mu b^2}{2\pi d^2} \quad [10]$$

This expression makes it clear that the higher the APB energy

(smaller  $d$ ), the more difficult it is to move the dislocation from its equilibrium position. That is, as the equilibrium separation decreases, the incremental change in the attractive or repulsive force increases for a given deviation from the equilibrium position. This process is illustrated schematically in fig. 58 where  $F_b$  represents the force resisting the movement of the dislocation from  $d_0$  to  $d_0 + b$ . Therefore, an increase in APB energy will make movement of the individual dislocations more difficult and will increase the strength.

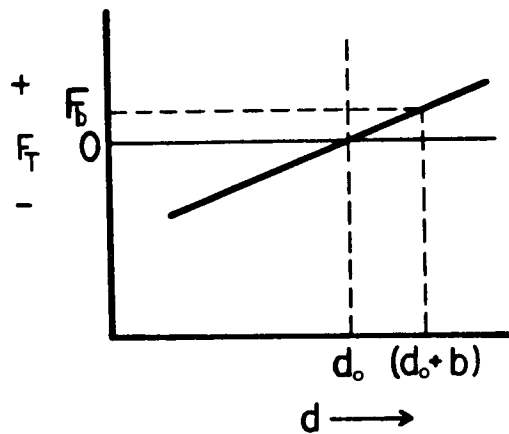
So far, this argument has ignored the periodic resistance to dislocation motion associated with the Peierls stress. If it is assumed that the Peierls stress is independent of composition, this periodic force will simply be superimposed on the force distance plots as shown in fig. 59. The result is that it is more difficult to move a dislocation from its equilibrium position in a high APB energy material.

The assumption that the Peierls stress remains constant with composition needs to be examined. As has been discussed, the APB energy is a strong function of alloy composition. This APB energy is an indication of the ordering strength of the material, with a low APB energy indicating a low ordering energy. This ordering energy should have an effect on the width of the dislocation  $W$ , which represents the distance over which the lattice is distorted due to the dislocations. At low APB energies, it should be easier for the dislocation to distort the lattice than at high APB



High APB energy  
small  $d_0$   
High Al content

(a)



Low APB energy  
large  $d_0$   
low Al content

(b)

Figure 58. Schematic representation of the force necessary to move a dislocation from its equilibrium position for two different APB energies.

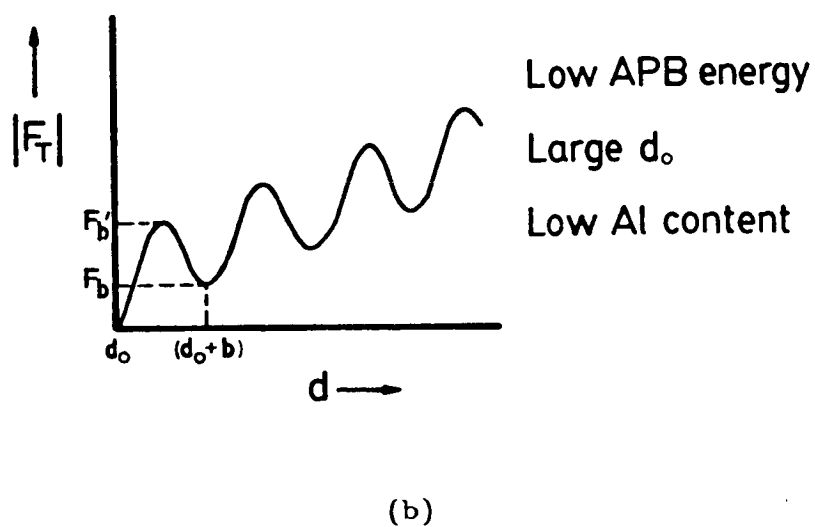
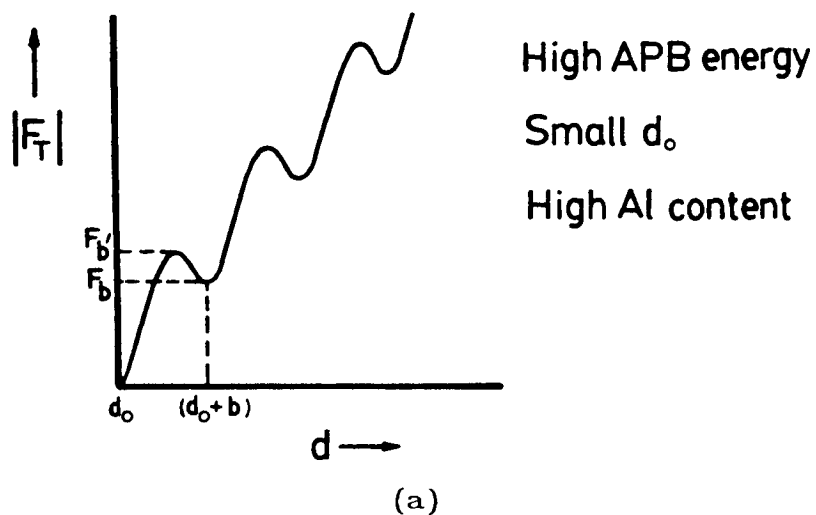


Figure 59. Schematic representation of the force required to move a dislocation from its equilibrium position including contributions from both the APB energy and the Peierls stress.

energies. This is because at high APB energies, distortion of the lattice leads to severe wrong neighbor interactions whereas at low APB energies, wrong neighbor interactions are not as severe. The Peierls stress depends on the dislocation width in the following manner [70]:

$$\tau_p \approx \mu e^{(-2\pi W/b)} \quad [11]$$

Therefore, the wider dislocation associated with lower APB energies will result in lower Peierls stresses. This suggests that in addition to the direct effect of APB energy on the slip behavior, there will also be an indirect effect. Both of these will contribute to the decrease in critical resolved shear stress with a decrease in Al content and are in agreement with the experimental results.

Another mechanism which may explain the decrease in critical resolved shear stress with decreasing APB energy is based on solute atoms interacting elastically with superdislocations. As an explanation for the composition dependence of the  $\langle 111 \rangle$  to  $\langle 100 \rangle$  transformation temperature in FeAl, Mendiratta, Kim and Lipsitt [44] have suggested that the strength of solute-superdislocation interactions depends upon the separation distance between the individual dislocations of the superdislocation. They argue that the smaller the distance, the greater the interaction, which gives rise to a thermally activated

transition at a lower temperature. Although they have not explained this mechanism in detail, it is presumed that the larger solute-superdislocation interaction results from the overlapping of elastic strain fields to increase the elastic maximum. The elastic strain field associated with a dislocation is proportional to  $1/r$  where  $r$  is the distance from the dislocation core. In the B2 FeAl alloys studied in this work, the equilibrium separation distance  $d_0$  is expected to range from around 5.0 nm in Fe-50Al to around 10.0 nm in Fe-40Al. With these separations, the increase in the elastic maximum of one dislocation due to overlap with the other dislocation will only be a few percent. This is because the elastic strain field from one dislocation will be very small at the dislocation core of the other dislocation. While these small changes may have a significant effect on the balance between  $\langle 111 \rangle$  and  $\langle 100 \rangle$  slip, it is doubtful that this mechanism effects the yield strength as a function of composition to any significant degree.

Hence, the mechanical behavior as a function of stoichiometry in B2 FeAl can be related directly to the APB energy. Fe-rich deviations from stoichiometry result in a decrease in the critical resolved shear stress, which in turn results in lower yield strengths. This in turn affects the balance between fracture and yielding and is reflected in increasing ductility with lower aluminum contents.



## Mechanical Behavior/Boron Effects

### Fe-50Al Alloys

In the first series of powder extrusions, the addition of boron has definitely improved the behavior of Fe-50Al. In this alloy, the change in fracture mode from brittle intergranular to transgranular cleavage under all conditions indicates that the grain boundary adhesion is improved with the addition of boron. This improvement is reflected in the mechanical behavior with the fracture stress increasing from around 80 ksi to around 140 ksi (fig. 17). This is in spite of the fact that the addition of boron has resulted in large voids in the material. The increase in grain boundary adhesion has also resulted in a decrease in the ductile to brittle transition temperature (fig. 17). This results from the competition between the brittle fracture stress and the yield stress which is illustrated schematically in fig. 60. In this figure, the stress required to initiate plastic flow, which typically decreases with temperature, is plotted along with the intergranular fracture stress for weak grain boundaries and the transgranular cleavage stress for strong grain boundaries as a function of temperature. If at a given temperature, the stress required to initiate intergranular or transgranular brittle fracture is less than that required to cause general yielding, the specimen will break in a brittle manner. If, on the other hand, the stress necessary to initiate yielding is lower than the

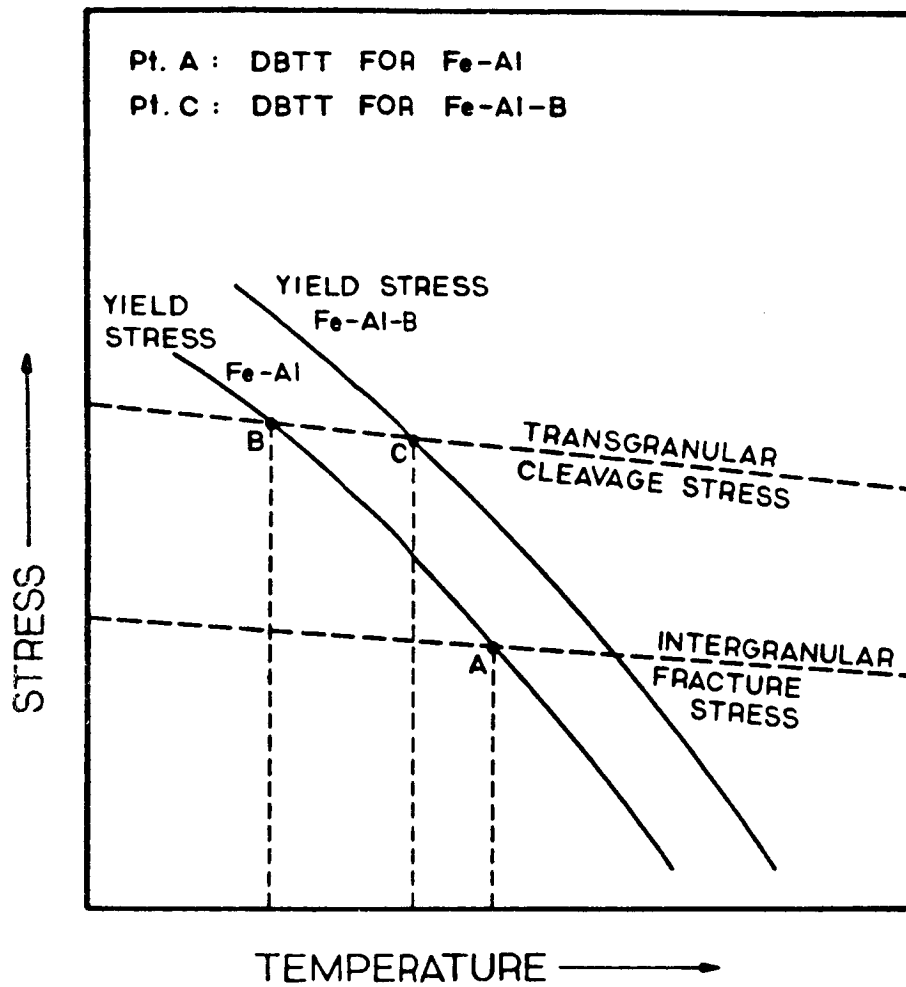


Figure 60. Schematic illustration of the competition between the yield stress and the brittle fracture stress as a function of temperature.

brittle fracture stress (as it is at higher temperatures), then the material yields and exhibits ductility. Hence, if the brittle fracture stress changes from intergranular to cleavage, the transition temperature will decrease as illustrated in fig. 60 from point A to point B, assuming the yield stress remains unchanged. That is, point A represents the transition temperature when grain boundaries are weak, and point B represents the transition temperature when grain boundary adhesion is improved. However, as the yield strength of the material increases (as has happened in Fe-Al-B probably due to a finer grain size), the curve for the stress required for plastic deformation will shift upwards. This results in an increase in the transition temperature (point C), and the advantage gained by strengthening the grain boundaries has been neutralized to a degree.

Even above the ductile to brittle transition temperature, the characteristic fracture surfaces of Fe-50Al (intergranular) and Fe-50Al-B (cleavage) are still observed. This indicates that although ductility is observed, the failure mechanisms are unchanged. What is occurring is that following yielding, work hardening increases the "effective flow stress" to a point where the applied stress equals the brittle fracture stress, at which point the material fails in the same manner.

The beneficial effects of B have not been reflected in the second series of Fe-50Al alloys. While the room temperature fracture strengths of the first and second series of Fe-50Al

alloys without boron compare favorably, the addition of boron has not improved the strength of the second series. Additionally, while the addition of boron resulted in a change in fracture mode in the first series, all of the second series extrusions displayed intergranular fracture, regardless of boron level. The reason for these differences is believed to be that although both of these series had nominal aluminum contents of 50 at%Al, the actual contents vary slightly. The first series extrusions containing boron had an actual stoichiometry of 48.7 at%Al and the second series 50.2 at%Al. Thus, the beneficial effects of boron are reflected only on the Fe-rich side of stoichiometry. This behavior is similar to that observed in  $\text{Ni}_3\text{Al}$  [50,51] where the beneficial effects of boron are only observed on the Ni-rich side of stoichiometry. In those studies, the segregation of boron to grain boundaries was found to be critically related to the alloy stoichiometry. Using Auger spectroscopy [50 51] the concentration of boron at grain boundaries was found to decrease from a maximum at 24 at%Al to a minimum at 25.25 at%Al. The corresponding tensile ductility decreased with this decreasing boron level. These studies also showed that as bulk Al concentration increased, the corresponding grain boundary concentration of Al increased. This may result in a reduction in the electronic interaction between Ni and B at the boundaries, thereby reducing the ductilization effect of B [50]. It is presumed that the dependence of composition on the boron effects observed near stoichiometry in this study is

similar to the observations in  $\text{Ni}_3\text{Al}$ . However, examination of these effects in detail in Fe-Al alloys would require an extensive Auger spectroscopic study which is beyond the scope of this work.

#### Fe-40Al Alloys

In Fe-40Al alloys, the question is not whether boron will cause ductilization or a decrease in the ductile to brittle transition, but rather will boron increase the ductility observed in Fe-40Al. However, the observed ductility appears to be influenced by the amount of metallic impurities within the base alloy. Therefore, the discussion of boron effects will be carried out in conjunction with the discussion of metallic impurities.

In the second series of extrusions, the Fe-40Al alloys contained significant amounts of impurities of Cr, Ta, Co, and Mn as designated in Table I. Without boron additions, these Fe-40Al alloys displayed about 2% ductile elongation. The addition of boron increased this to about 5% (fig. 18). It should be noted that the ductility observed in alloys containing boron was not dependent on the boron level in the range 0.05 to 0.20 wt%B. This indicates that the optimum boron level has been reached even at 0.05B, and subsequent additions have no effect. In terms of the observed fracture surfaces, boron has changed the fracture mode from predominantly intergranular to transgranular tearing. However, this change in fracture is not as distinct as in substoichiometric "Fe-50Al".

In the third extrusion series Fe-40Al alloys, which had much lower impurity levels, the observed ductility without boron was about 3% total deformation, slightly higher than that observed in the second series. The addition of boron did not increase this ductility to any significant amount. The fracture surfaces of these give an indication of the effects of boron and contamination. Without boron, the third extrusion series Fe-40Al displayed intergranular fracture which was much more distinct than that observed in the alloys containing impurities. Thus it appears that the metallic impurities, which were observed to cause precipitation at grain boundaries, have resulted in the fracture becoming more "dirty". The fracture surfaces of the third extrusion series with boron are rather complex and give insight into the reason why no significant improvement in ductility is observed in this alloy. As has been shown in fig. 31, these fractures initiated at a pore or inclusion, with an area of pure cleavage around the initiation site, and a gradual change to a mix of intergranular and cleavage as the distance from the initiation site increases. What appears to be occurring in this alloy is that during the powder mixing and extrusion process, the elementally blended boron is not being distributed uniformly. This results in boron rich inclusions which serve to initiate the fracture prematurely. Around these inclusions, some boron has diffused into the surrounding material which has increased the grain boundary adhesion. Thus, the fracture surface displays

cleavage around these inclusions. Further from the fracture initiation, the amount of boron which has diffused into the material is less, and as a result the fracture begins to display intergranular failure, presumably due to lower grain boundary adhesion. This fracture behavior suggests that boron additions have the possibility to enhance the mechanical properties of Fe-40Al to a large degree. In the area around the inclusions, the change in fracture mode to pure cleavage in the impurity free Fe-40Al is much more dramatic than the change in fracture associated with boron in the contaminated Fe-40Al. However, because of the method of boron mixing used, any improvements in mechanical behavior due to improved grain boundary strength is negated by the detrimental effects of inclusions. It may be possible to overcome these effects of inclusions by using pre-alloyed boron additions. In this manner the inclusions would be eliminated, and the benefits of increased grain boundary adhesion realized.

It has been shown that boron increases the grain boundary adhesion of sub-stoichiometric B<sub>2</sub> FeAl alloys as indicated by changes in fracture mode, and as a result improves the mechanical properties to a degree. However, at this point it is not known why the boron improves this adhesion. Two possibilities for this exist. The first is that boron strengthens inherently weak grain boundaries while the second is that boron acts as a scavenger of harmful impurities such as P and S. The only way to determine

which of these is occurring is by a detailed Auger spectroscopy study. This would allow determination of whether or not impurities are present in FeAl prone to intergranular fracture. However, this is beyond the scope of the present work.

The observation that the fracture mode changes from intergranular to cleavage with increasing grain size regardless of boron or stoichiometry (figs. 28,29) is rather interesting and has not been examined before. The critical grain size for this transition is around 100  $\mu\text{m}$ . One possible reason for this behavior is that the intergranular and cleavage fracture stresses are a function of grain size. Stroh [71,72] has predicted that the cleavage fracture stress is related to the grain size in the following way:

$$\sigma_c = \sigma_i + K_f d^{-1/2} . \quad [12]$$

This was developed by an argument similar to that used in development of the Hall-Petch relationship [73,74], but, in this equation  $K_f$  is the critical value of local tensile stresses required to fracture the second grain. While this expression does not fit experimental data exactly because it ignores other microstructural features, it is well accepted that increases in grain size decrease the cleavage fracture stress [75]. The effect of grain size on the intergranular fracture stress is not as



clear. The mechanism involved in the nucleation and propagation of intergranular cracks are not well understood. Evenson et al. [76] have examined the intergranular fracture stress in age hardened Al-Mg-Si alloys. They have found the intergranular fracture stress is also a function of grain size, but the relationship is significantly different from the cleavage stress. An expression for the intergranular fracture stress as a function of grain size was developed as [76]:

$$\sigma_{IG} = \frac{4\mu\gamma}{K_y} d^{-1/2} \quad [13]$$

where:  $\mu$  = shear modulus

$\gamma$  = work per unit area for crack growth

$K_y$  = Hall-Petch slope.

Although both the cleavage fracture stress and the intergranular fracture stress may be a function of  $d^{-1/2}$ , they do not follow the exact same form. Thus at finer grain sizes, the intergranular fracture stress may be lower while at larger grain sizes, the cleavage fracture stress may be lower. This is shown schematically in fig. 61. The reason that a change in fracture mode as a function of grain size is being observed in FeAl may be because the cleavage and intergranular fracture stresses are relatively close together in the grain sizes studied.

This result has an important implication concerning the

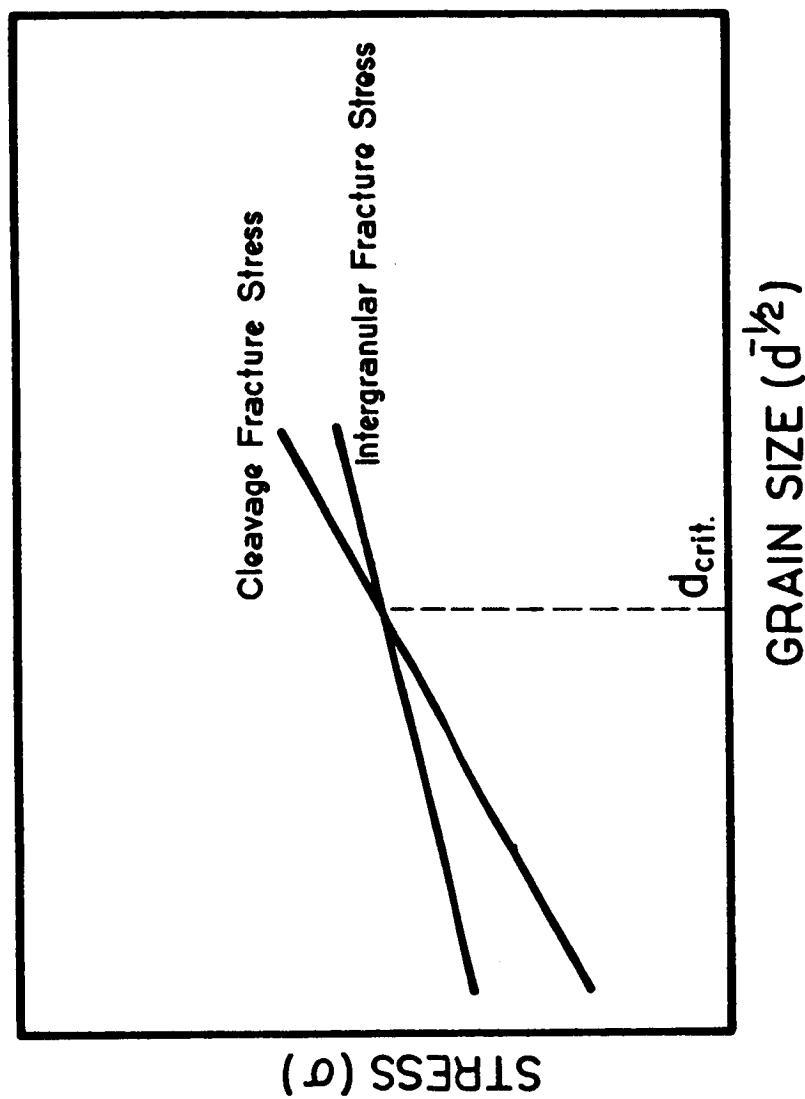


Figure 61. Schematic illustration of the competition between the intergranular and cleavage fracture stresses responsible for a change in fracture mode with grain size.

addition of boron to FeAl alloys in order to improve the grain boundary adhesion. If the grain size increases, the fracture will change to cleavage and any beneficial effect of boron will not be reflected. This is what is observed in the cast and extruded material where grain sizes are very large. No significant differences exist in the mechanical behavior of cast Fe-40Al and cast Fe-40Al-B. Both of these materials display total cleavage fracture in all of the conditions tested (fig. 32).

Both of the cast and extruded alloys displayed greater ductility than any of the powder processed alloys ( $\approx 6.5\%$  for cast versus  $\approx 5.0\%$  for powder processed). A number of factors may be responsible for this. First, because the cast materials have large grain sizes, yielding occurs at a lower stress and more plastic strain may be required to work harden the material to the cleavage fracture stress (for the given grain size). A second reason may be that the cast materials have a much lower number of inclusions. As has been discussed, the powder processed alloys have a significant amount of inclusions in the form of oxides from prior powder particle boundaries. These oxides may act as fracture initiation sites and as such, limit ductility. The cast material, by contrast, has very few oxide inclusions (fig. 13) and hence fracture may not be initiated until greater strains.

To summarize the boron effects, it has been shown that boron improves the grain boundary adhesion of FeAl as indicated by fracture mode modifications. While this increased adhesion does

not have the dramatic effect observed in  $\text{Ni}_3\text{Al}$ , it does improve the ductility and fracture properties to a significant degree. This boron effect has been shown to be sensitive to stoichiometry with beneficial effects observed only on the Fe-rich side of stoichiometry. Because of the grain size dependence of fracture in FeAl, improvements in properties due to the addition of boron are observed only at fine grain sizes.

#### Mechanical Behavior/Cooling Rate Effects

The experimental results clearly indicate that the cooling rate following heat treatment has a dramatic effect on the mechanical behavior of these alloys. These results will be discussed in terms of polycrystals, then in terms of single crystal behavior and the results correlated.

In the second series extrusions, Fe-40Al alloys, increasing the cooling rate transforms the tensile stress-strain behavior from ductile to brittle. At slow cooling rates, yielding and significant ductility similar to that observed in the as-extruded condition, takes place. As the cooling rate is increased by air quenching, the yield strength goes up, and the ductility decreases, while at the highest cooling rates, oil and water quenching, the yield strength has continued to increase and almost totally brittle behavior is exhibited (fig. 19). Associated with this increased strength and resulting decrease in ductility, the fracture surfaces also change in the Fe-40Al materials with

metallic impurities. In the Fe-40Al without boron, the intergranular fracture becomes more distinct or "cleaner" (fig. 27a). In the Fe-40Al-B, the fracture becomes pure cleavage in the quenched state (fig. 27b), compared with the transgranular tearing observed in slow cooled specimens (fig. 26b). This can be attributed to suppression of grain boundary precipitation related to the metallic impurities. In the Fe-40Al, without this grain boundary precipitation to "dirty-up" the fracture, the observed fractures more closely match those in Fe-40Al without metallic impurities (pure intergranular). In the Fe-40Al with boron, suppression of these grain boundary precipitates allows the boron to act more strongly on the grain boundaries, and the fracture becomes pure cleavage, like that in Fe-40Al-B without impurities.

The large increases in yield strength, however are not related to the quenching in of these metallic impurities. This can be concluded because the third series Fe-40Al extrusions, which were essentially free of metallic impurities, also displayed large increases in yield strength with increasing cooling rate. In terms of fracture mode, no changes were observed between samples slow cooled and oil quenched of these "cleaner" materials with as well as without boron. This has two important implications. First, quenching from as high as 1373 K was not able to inhibit boron segregation to grain boundaries. This is contrary to results in  $\text{Ni}_3\text{Al}$  which found quenching increased intergranular fracture by reducing the amount of beneficial boron

segregated at grain boundaries [60]. Secondly, it indicates that the changes in fracture modes with cooling rate observed in the contaminated materials is directly attributable to the impurities.

Although it was not possible to machine tensile bars from Fe-50Al samples subjected to high cooling rates, the results of the limited compression tests indicated that the same effects are occurring. As with the Fe-40Al materials, large increases in yield strength were observed with increasing cooling rate. The yield strength was found to double, from around 70 ksi in slow cooled specimens, to around 145 ksi in oil and water quenched specimens.

These large increases in yield strength are also observed in the single crystal specimens. The results of the single crystal cooling rates studied are important as they indicate that these effects are related to a change in the slip behavior, and are not associated with polycrystalline complications. As has been shown, the observed slip system is  $\langle 111 \rangle \{110\}$  in all conditions of stoichiometry and cooling rate. This shows that the yield strength increases are the result of a fundamental change in the critical resolved shear stress, and not related to changes in crystal structure or slip system.

The increase in strength with cooling rate can be attributed to effects related to the quenching in of large numbers of thermal vacancies. As has been discussed in the introduction, a number of studies [12-14,16,17] looked at the vacancies in B2 FeAl alloys

and have shown that large numbers of thermal vacancies, on the order of  $10^{-2}$  mole fraction, can be retained at room temperature by quenching. It is expected then that these quenched in vacancies are responsible for the strengthening effects.

Two possible mechanisms for this strengthening due to vacancies are possible. The first is that the vacancies themselves are acting to pin dislocations. The introduction of a vacancy into a crystalline lattice results in a large elastic strain field around the vacancy. This elastic strain field is able to interact with the elastic strain field of a dislocation and effectively pin the dislocation. The result is that the force necessary to move the dislocation through the lattice increases as the dislocation must overcome the pinning effects of the vacancy.

The other possibility is that the excess vacancies collect to form vacancy loops which in turn act to pin the vacancies. In the quenched single crystals, considerable numbers of loops have been observed compared with the slow cooled specimens (figs. 43,44). However, it is unknown whether the observed loops, vacancies in solution, or a combination of both are responsible for the strengthening effects. It should be noted however, that considerable pinning of dislocations was observed in the quenched single crystals as displayed in fig. 42a. This indicates that regardless of the exact mechanism, pinning of some type is occurring in these quenched materials.

It should be noted that this is not the first time that

increases in yield strength have been observed in ordered alloys. In Fe-Co-2%V and Fe<sub>3</sub>Al, increases in quench temperature have resulted in increased room temperature strength [77]. These increases have been attributed to changes in the long range order parameter near the order disorder temperature. However, the as-quenched strength increases of Fe-Co-2%V are much greater than the strength increases observed at temperature. This indicates that factors other than just long range order effects may be associated with the increases in strength.

In  $\beta$ -brass, an increase in strength due to increased quench temperature has also been reported [78]. In this study, the strengthening has been attributed to quenched in vacancies formed by quenching through the order-disorder transformation.

Hence, it appears that the cooling rate has a very significant effect on the mechanical behavior of FeAl alloys. Increasing cooling rates increase the amounts of vacancies retained from high temperature and in turn, results in increased yield strengths and corresponding decreases in ductility.

#### Yield Behavior/Grain Size Effects

The effect of grain size on the yield strength has been mentioned briefly. In this section, the relationship between these two will be briefly examined in more detail.

Figure 62 shows the Hall-Petch [73,74] plots of yield strength versus grain size for Fe-40Al in the form:



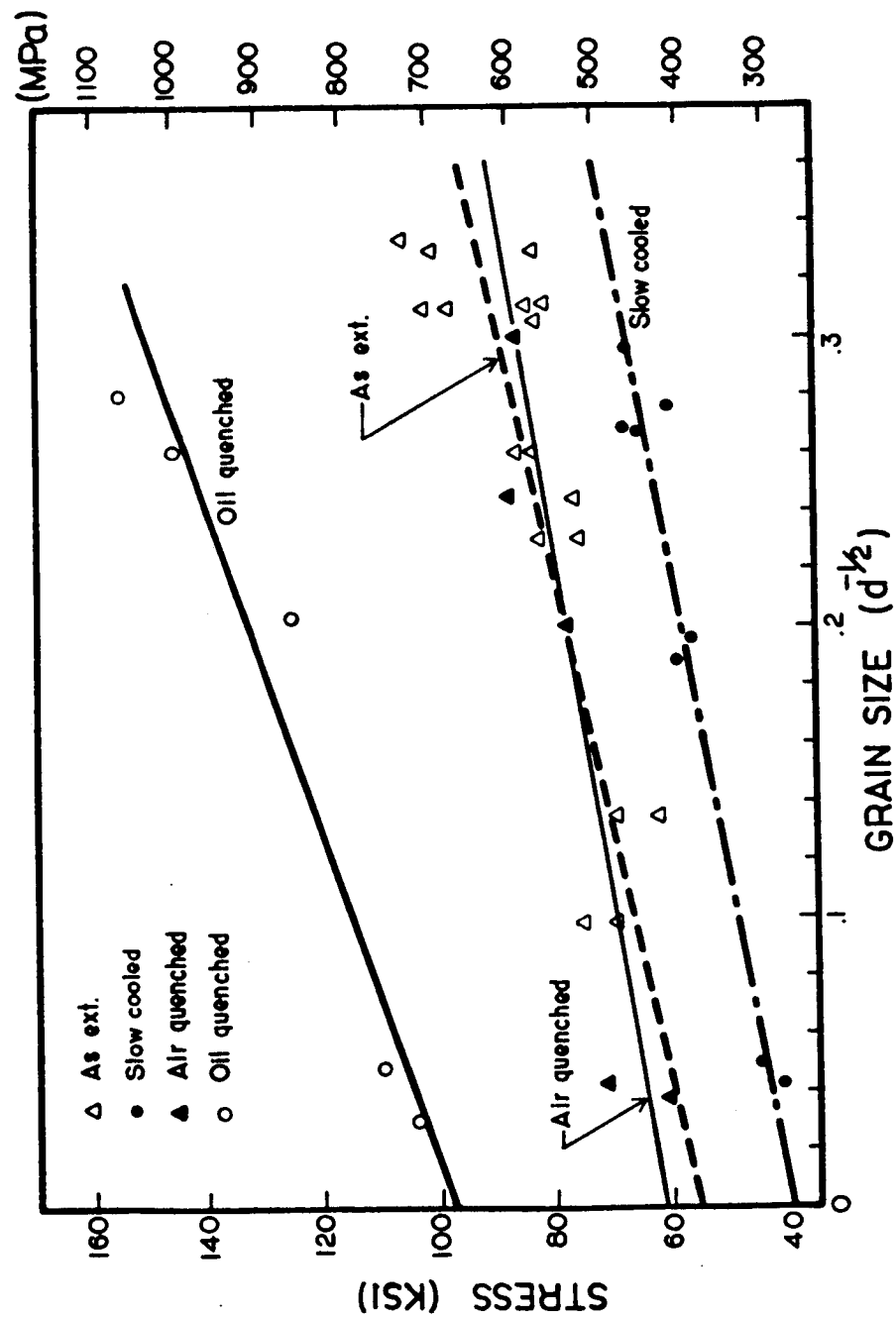


Figure 62. Hall-Petch plots of yield strength versus grain size for Fe-40Al alloys.

$$\sigma_{ys} = \sigma_o + K_y d^{-1/2} \quad [14]$$

where:  $\sigma_{ys}$  = observed yield strength

$\sigma_o$  = overall lattice resistance to dislocation slip

$K_y$  = constant related to hardening due to grain boundaries

$d$  = grain size .

Although there is a significant amount of scatter in the data, it is clear that the cooling rate effects are realized across a wide range of grain sizes. The scatter may be attributed to a number of different factors including: 1) the difficulty of measuring large grain sizes accurately, 2) variations in cooling rates due to different size specimens, 3) variations in compositions between materials, i.e.: different powder lots, castings, 4) a small number of grains in large grained materials may result in an arbitrary orientation and unconstrained deformation, 5) variations in grain size may affect the ability to quench in vacancies. The best fit lines from least squares analysis have been drawn through these data points. The resulting equations for the four conditions plotted are:

$$\text{Fe-40Al as ext.: } \sigma_{ys} = 56 \pm 6 \text{ ksi} + 108 \pm 24 d^{-1/2} \text{ ksi, } r = 0.73$$

$$\text{Fe-40Al oil: } \sigma_{ys} = 98 \pm 7 \text{ ksi} + 179 \pm 34 d^{-1/2} \text{ ksi, } r = 0.95$$

$$\text{Fe-40Al air: } \sigma_{ys} = 63 \pm 5 \text{ ksi} + 83 \pm 24 d^{-1/2} \text{ ksi, } r = 0.95$$

$$\text{Fe-40Al S.C.: } \sigma_{ys} = 40 \pm 2 \text{ ksi} + 91 \pm 10.5 d^{-1/2} \text{ ksi, } r = 0.96.$$

Except for the oil quenched sample, the variation with the Hall-Petch slope is not very great. The differences in the oil quenched samples are probably due to the scatter discussed above. If this slope does not change to a large degree, it indicates that cooling rate does not effect the ability of grain boundaries to inhibit slip. The critical feature of these equations is the y-intercept term. It is evident that the cooling rate affects this term to a large degree.

It is possible to relate this y-intercept with the critical resolved shear stress found in single crystals. This is done by dividing the lattice resistance term  $\sigma_0$ , by an average orientation term. For slip on {110} in bcc metals, this orientation term has been determined to be 2.75 [79]. For the oil quenched Fe-40Al, this results in a resolved shear stress of 35.6 ksi, while for the slow cooled Fe-40Al, the result is 14.5 ksi. These values compare very well with the critical resolved shear stress obtained experimentally from single crystals with  $\tau_{crss} = 44.1$  ksi for oil quenched samples and  $\tau_{crss} = 14.1$  ksi for slow cooled samples.

Conrad [80] has shown that the lattice resistance term of the Hall-Petch relationship can be separated into two components such that:

$$\sigma_{ys} = \sigma_s + \sigma_l + K_y d^{-1/2} \quad [15]$$

where  $\sigma_s$  is related to short range effects ( $< 1.0 \mu\text{m}$ ) such as the Peierls stress, and  $\sigma_l$  is related to longer range effects (10.0 - 100.0 nm) such as dislocation stress field effects. In this work, these constants can be related to the effects observed. In the slow cooled materials, the effects of dislocation stress field have been minimized, and  $\sigma_o$  is made up of primarily  $\sigma_s$  - Peierls stress effects. In the oil quenched materials, the introduction of vacancies and loops increase the contributions of  $\sigma_l$  while  $\sigma_s$  remains essentially constant, and as a result  $\sigma_o$  increases. Changes in stoichiometry, on the other hand, result in changes in  $\sigma_s$  while  $\sigma_l$  remains constant, and the lattice resistance  $\sigma_o$  changes accordingly.

Hence, it appears that in addition to the grain size dependence of fracture behavior discussed earlier, the grain size also effects the yield behavior. This behavior shows a Hall-Petch relationship with the yield stress a function of  $d^{-1/2}$ . The cooling rate effects are reflected over a wide range of grain sizes and can be related to the lattice resistance term of the Hall-Petch equation. Consistent with this, the critical resolved shear stresses from single crystal specimens are in good agreement with the Hall-Petch intercept values from polycrystalline samples.

## CONCLUSIONS

[1] B2 FeAl undergoes a transition from brittle to ductile behavior as the aluminum content is decreased from stoichiometry. This transition occurs as a result of a large decrease in the stress required for general yielding as the aluminum content decreases. Thus, the balance in the competition between yielding and fracture is changed, and significant yielding occurs before the onset of fracture. This large decrease in yield strength occurs despite the fact that  $\langle 111 \rangle \{110\}$  slip remains the active slip system as the stoichiometry of the alloys is changed. The changes in yield strength can be directly attributed to changes in the critical resolved shear stress for  $\langle 111 \rangle \{110\}$  slip as a function of composition. Decreases in  $\tau_{\text{CRSS}}$  can be related to the effects of the decreases in the APB energy with decreasing aluminum content.

[2] The addition of boron to B2 FeAl has the ability to improve the mechanical properties. However, improvements are observed only on the iron-rich side of stoichiometry. In slightly iron-rich alloys near stoichiometry, the addition of boron results in increased brittle fracture strengths and associated changes in fracture mode from intergranular to cleavage. Related to this, the ductile to brittle transition temperature decreases with boron additions as the balance between yielding and fracture is shifted.

However, these improvements are not reflected in Al-rich alloys near stoichiometry. In Fe-40Al, where some ductility ( $\approx 3\%$ ) is present without boron, the addition of boron results in improvements in ductility ( $\approx 6\%$ ) and modification of the fracture to transgranular failure. No significant changes in properties were observed by varying the boron level from 0.05 wt% to 0.20 wt%. This suggests that the optimum effects of boron can be reached at 0.05B and additional amounts of boron have no benefits. Improvements in mechanical behavior of these FeAl alloys due to boron additions have been attributed to increases in the grain boundary adhesion as reflected by changes in fracture mode.

[3] It has been shown that increases in grain size results in a transition from intergranular fracture to cleavage. This may result from differences in the grain size dependencies of the intergranular and cleavage fracture stresses. Because of this transition, the beneficial effects of boron are only reflected in materials with fine grain sizes.

[4] The cooling rate following heat treatment has a dramatic effect on the mechanical properties of B2 FeAl. Increases in cooling rate result in large increases in the observed yield strength. Correspondingly, the ductility diminishes with faster cooling. These large increases in strength, which have been observed in both polycrystals and single crystals, have been

attributed to quenching in of large numbers of thermal vacancies. These vacancies, which occur in much larger quantities than normal metals, result in pinning of dislocations. The exact pinning mechanism may result either from the vacancies themselves, vacancy loops formed by vacancy collapse, or by a combination of both.

[5] The effect of grain size on the yield strength of Fe-40Al has been shown to follow a Hall-Petch relationship. The cooling rate effects are reflected over a large range of grain sizes and are attributed to a change in the Hall-Petch intercept,  $\sigma_0$ , with no significant effects due to the Hall-Petch slope,  $K_y$ . The Hall-Petch intercepts corrected for random orientations, agree well with the value for critical resolved shear stress from single crystals. The effects of stoichiometry on the yield strength of FeAl can be related to short range effects of the intercept while cooling rate effects can be attributed to long range contributions to the Hall-Petch intercept.

### SUGGESTIONS FOR FUTURE WORK

[1] As has been described, the APB energy has a dramatic effect on the critical resolved shear stress of B2 FeAl. This may be in part due to the APB energy effect on the dislocation width, which in turn affects the Peierls stress. To examine this in more detail, the dislocation core structures could be examined using high resolution electron microscopy. Thus, a detailed understanding of the dislocation cores could be obtained as a function of APB energy and alloy stoichiometry.

[2] The addition of boron to B2 FeAl has been shown to improve the mechanical behavior by increasing the grain boundary cohesion. The reasons for this improvement however, are not well understood. Auger electron spectroscopy is the ideal method for examining these problems. Using AES, it would be possible to determine if the intergranular failure of B2 FeAl alloys is a result of microcontamination or due to inherently brittle grain boundaries. From this information, it would be possible to determine in what manner boron strengthens grain boundaries. Additionally, AES would allow the study of the boron segregation as a function of alloy stoichiometry in an effort to determine why boron related improvements to the mechanical behavior are observed only on the iron-rich side of stoichiometry.



[3] Because of their change in fracture mode as a function of grain size, these alloys offer a unique material for the study of brittle fracture. By examining the intergranular and cleavage fracture stresses as a function of grain size, it may be possible to gain a better understanding of these processes.

[4] The effects of cooling rate on the yield strength of these alloys have been presented. A more detailed study of quenching from a number of cooling rates, along with measurements of the vacancy concentrations may result in a more complete understanding of the effectiveness of vacancies and/or vacancy loops in pinning dislocations.

## REFERENCES

- [1] N. S. Stoloff, MRS symposia proceedings, 39,  
High-Temperature Ordered Intermetallic Alloys, 3 (1985).
- [2] J. R. Stephens, *ibid* p. 381.
- [3] C. T. Liu, C. L. White, and J. A. Horton, *Acta Met.*, 33 (2),  
213 (1985).
- [4] H. Lipisitt, *Aviation Week*, Jan. 26, 81 (1976).
- [5] R. T. Fortnum and D. E. Mikkola, *Mat. Sci. and Eng.*, in  
press.
- [6] A. Taylor and R. M. Jones, *J. Phys. Chem. Solids*, 6, 16  
(1958).
- [7] A. J. Bradley and A. H. Jay, *Proc. Roy. Soc.* A136, 210  
(1932).
- [8] J. P. Neumann, Y. A. Chang and C. M. Lee, *Acta Met.*, 24, 701  
(1976).
- [9] J. P. Neumann, *Acta Met.*, 28, 1165 (1980).
- [10] J. P. Neumann, Y. A. Chang and H. Ipser, *Scripta Met.*, 10,  
917 (1976).
- [11] R. O. Simmons and R. W. Balluffe, *Phys. Rev.*, 125, 862  
(1962).
- [12] K. Ho and R. A. Dodd, *Scripta Met.*, 12, 1055 (1978).
- [13] D. Paris, P. Lesbates and J. Levy, *Scripta Met.*, 9, 1373  
(1975).
- [14] D. Paris and P. Lesbates, *J. Nucl. Mater.*, 69, 628 (1978).
- [15] K. M. Ralls, T. M. Courtney and J. Wulff, "Introduction to  
Materials Science and Engineering", J. Wiley and Sons, New  
York, 189 (1976).
- [16] A. Fourdeux and P. Lesbates, *Phil. Mag. A.*, 45, (1) 81  
(1982).
- [17] N. Junqua, J. C. Desoyer and P. Moine, *Phys. Stat. Sol.*,  
18a, 387 (1973).

- [18] N. A. Zeigler, Trans. AIME, 100, 297 (1932).
- [19] M. J. Marcinkowski, M. E. Taylor and F. X. Kayser, J. Mat. Sci., 10, 406 (1975).
- [20] J. J. Leamy, Ph. D. Thesis, Iowa State University (1966).
- [21] M. G. Mendiratta, K. K. Ehlers, D. K. Chatterjee and H. A. Lipsitt, Met. Trans. A, 18A, 283 (1987).
- [22] W. R. Kerr, Met. Trans. A, 17A, 2298 (1987).
- [23] A. Lawley, E. A. Vidoz and R. W. Cahn, Acta Met., 9, 287 (1961).
- [24] H. J. Leamy and F. X. Kayser, Phys. Stat. Sol., 34, 765 (1969).
- [25] M. J. Marcinkowski and N. Brown, Acta Met., 9, 764 (1961).
- [26] M. J. Marcinkowski and N. Brown, J. Appl. Phys., 33, (2) 537 (1962).
- [27] H. J. Leamy, F. X. Kayser and M. J. Marcinkowski, Phil. Mag., 20, 763 (1969).
- [28] H. J. Leamy, F. X. Kayser and M. J. Marcinkowski, Phil. Mag., 20, 779 (1969).
- [29] R. C. Crawford, I. L. F. Ray and D. J. H. Cockayne, J. of Microscopy, 98, 196 (1973).
- [30] R. C. Crawford and I. L. F. Ray, Phil. Mag., 35, 549 (1977).
- [31] G. Sainfort, P. Mouturat, Mme. P. Pepin, J. Petit, G. Cabane, and M. Salesse, Men. Sc. Rev. Met., 40, 125 (1963).
- [32] M. G. Mendiratta, S. K. Ehlers and D. K. Chatterjee, Proceedings of the Third Conference on Rapid Solidification, R. Mehrabian, ed., 240 (1982).
- [33] I. Baker and D. J. Gaydos, MRS symposia proceedings, 81, High Temperature Ordered Intermetallic Alloys, (1987).
- [34] I. Baker, private communications.
- [35] D. J. Gaydos and M. A. Crimp, MRS symposia proceedings, 39, High Temperature Ordered Intermetallic Alloys, 429 (1985).
- [36] J. H. Westbrook, J. Electrochem. Soc., 103, 54 (1956).

- [37] R. C. Crawford, *Phil. Mag.*, 33, (3) 529 (1976).
- [38] T. Yamagata and H. Yoshida, *Mat. Sci. and Eng.*, 12, 95 (1973).
- [39] T. Yamagata, *Trans. JIM*, 18, 715 (1977).
- [40] A. K. Head, M. H. Loretto and P. Humble, *Phys. Stat. Sol.*, 20, 505 (1967).
- [41] A. K. Head, M. H. Loretto, and P. Humble, *Phys. Stat. Sol.*, 20 521 (1967).
- [42] Y. Umakoshi and M Yamaguchi, *Phil. Mag. A*, 41, (4) 573 (1980).
- [43] Y. Umakoshi and M. Yamaguchi, *Phil. Mag. A*, 44, (3) 711 (1981).
- [44] M. G. Mendiratta, H. Kim and H. A. Lipsitt, *Met. Trans. A*, 15A, 395 (1984).
- [45] I. L. F. Ray, R. C. Crawford and D. J. H. Cockayne, *Phil. Mag.*, 21 1027 (1970).
- [46] R. C. Crawford, *Phil. Mag.*, 35, 567 (1977).
- [47] A. E. Vidoz and L. M. Brown, *Phil. Mag.*, 7, 1167 (1962).
- [48] C. T. Chou and Sir Peter Hirsch, *Proc. R. Soc. Lond.*, A387, 91 (1983).
- [49] K. Aoki and O. Izumi, *Nippon Kinzoku Gakkaishi*, 43, 1190 (1979).
- [50] C. T. Liu and C. L. White and J. A. Horton, *Acta Met.*, 33, (2) 213 (1985).
- [51] C. T. Liu and C. L. White, *MRS symposia proceedings*, 39, High Temperature Ordered Intermetallic Alloys, 365 (1985).
- [52] T. Takasugi and O. Izumi, *Acta Met.*, 31, (8) 1187 (1983).
- [53] C. L. White and D. F. Stein, *Met. Trans. A*, 9A, 13 (1978).
- [54] J. Ogura, S. Hanada, T. Masumoto and O. Izumi, *Met. Trans. A*, 16A, 441 (1985).

- [55] C. T. Liu, C. L. White, C. C. Koch and E. H. Lee, Proc. Symp. High Temp. Mat. Chem II, Z. A. Munir and D. Cubicciotti eds., The Electrochemical Soc., 32 (1983).
- [56] C. L. White, R. A. Padgett, C. T. Liu and S. M. Yalisove, Scripta Met., 18, 1417 (1984).
- [57] J. R. Rice, Effect of Hydrogen on Behavior of Materials, A. W. Thompson and I. M. Bernstein, eds., AIME, 455 (1976).
- [58] P. S. Khadkikar, K. Vedula and B. S. Shabel, Met. Trans. A, 18A, 425 (1987).
- [59] E. M. Shulson, J. P. Weihs, I. Baker, H. J. Frost and J. A. Horton, Acta Met., 34, (7) 1395 (1986).
- [60] A. Choudhury, C. L. White and C. R. Brooks, Scripta Met., 20, 1061 (1986).
- [61] Y. Ogino and T. Yamasaki, Scripta Met., 15, 821 (1981).
- [62] R. A. Varin and K. Tangri, Mat. Sci. and Eng., 72, 177 (1985).
- [63] E. R. Slaughter and S. K. Das, 2nd Int. Conf. on Rapid Solidification Processing, Claitors Pub., 354 (1980).
- [64] C. S. Barratt, "Structure of Metals", McGraw-Hill, New York, 39 (1943).
- [65] I. Baker and D. J. Gaydosch, Phys. Stat. Sol. A, 96, 185 (1986).
- [66] A. Ball and R. E. Smallman, Acta Met., 14, 1517 (1966).
- [67] E. S. Machlin, Acta Met., 22, 1433 (1974).
- [68] E. S. Machlin, Acta Met., 24, 534 (1976).
- [69] D. Hull, "Introduction to Dislocations", 2nd edition, Pergamon Press, New York (1975).
- [70] R. W. Hertzberg, "Deformation and Fracture Mechanics of Engineering Materials", J. Wiley and Sons, New York (1976).
- [71] A. N. Stroh, Proc. R. Soc., A223, 404 (1954).
- [72] A. N. Stroh, Adv. Phys. Soc., 6, 418 (1957).
- [73] E. O. Hall, Proc. Phys. Soc., 64B, 747 (1951).

- [74] N. J. Petch, J. Iron Steel Inst., 173, 25 (1953).
- [75] J. F. Knott, "Fundamentals of Fracture Mechanics", Butterworths Pub., Boston, (1973).
- [76] J. D. Evensen, N. Ryum and J. D. Embury, Mat. Sci. and Eng., 18, 221 (1975).
- [77] N. S. Stoloff and R. G. Davies, Acta Met., 12, 473 (1964).
- [78] N. Brown, Acta Met., 7, 210 (1959).
- [79] P. O. Kettunen, Phil. Mag., 16, 253 (1967).
- [80] H. Conrad, J. Iron and Steel Inst., 198, 364 (1961).

## APPENDIX A

The following sheets are copies of the original extrusion sheets for the materials used in this study. They contain information concerning peak pressure, extrusion ratio, extrusion temperature and other extrusion parameters. They have been provided by Dr. J. D. Whittenberger who carried out these extrusions at NASA Lewis Research Center.

HOT EXTRUSION DATA SHEET  
(PFS-HotExtDS)

1A

Engineer's Name: Titran  
Eng's ID: RHT:FeAl-50 (FeAl-25)  
Charge Number: YCG2296  
Date Submitted: 84/02/13  
Date Completed: 84/08/03

General Type of Material: Intermetallic

Nominal Composition: Fe-32.57Al (wt pct); Fe-50Al (at pct)

Type of Billet: Loose powder canned in mild steel with 0.03 inch ss liner.  
Size of Billet (inches) Diameter: 2. Length: 5.63

Proposed Extrusion Conditions  
Temperature (F): 1790  
Type of Die: Round  
Punch Speed (inch/min): Maximum  
Reduction Ratio: 16:1  
Special Conditions: presoak 2h

Safety Checks  
Leak Test: X Date: 84/02/01  
Heat Test (2h 1500F): X Date: 84/02/26

Actual Extrusion Conditions  
Date: 84/08/03 Ext. ID: L-2084  
Crew: W/E/A/Gr  
Temperature: 1790 Reduction Ratio: 16:1  
Type of Die Round: X Sh Bar: Other: Angle: 90  
Special Conditions:

Valve Selection 1/8: 7/16: Preset Punch Speed:  
(X to specify) 3.5: X Valve Opening: 0.25

Side Ram: X Pressure (psi): 3100 Max Tonnage: 340  
Main Ram: Pressure (psi): Max Tonnage:  
Comb Ram: Pressure (psi): Max Tonnage:

Lubricant Container: Dylon Graphite Paper: X  
Die: Formkote

Dummy Thickness: 2. Carbon Thickness: 1.5  
Container Mat: NuDie V Cont Temp (F): 600 Times Used: 199  
Stem Material: VAR 218 Stem ID: CH#6 Times Used: 199

Time at Temperature (h): 2 Transfer Time (s): 13.

Post Test Analysis of Extrusion  
Successful: X Unsuccessful:  
Comment:

Shooter: Butt left in Die: 0.25 Sticker:  
Break thru Pressure (ksi): 177.2 Punch Speed: 4.1 "/s  
Running Pressure (ksi): 145.3 Time to Ext: 1.3 s  
Condition of Extrusion: good

Length of Ext: 51.5" Nominal Cross Section: 0.535" dia  
Condition of Die:

General Comments:



1.8

HOT EXTRUSION DATA SHEET  
(PFS-HotExtDS)

Engineer's Name: Titran Date Submitted: 84/02/14  
 Eng's ID: RHT-FeAlB Charge Number: YCG2296 Date Completed: 84/02/17

General Type of Material: Intermetallic <sup>.24</sup> <sup>12</sup>

Nominal Composition: Fe-30.8Al-0.1b (wt pct); Fe-48Al-0.3B (at pct)

Type of Billet: Loose powder canned in mild steel with 0.03 inch ss-liner.  
 Size of Billet (inches) Diameter: 2. Length: 5.63

Proposed Extrusion Conditions Temperature (F): 1790 Reduction Ratio: 16:1  
 Type of Die: Round  
 Punch Speed (inch/min): Maximum  
 Special Conditions: presoak 2h; slow cool

Safety Checks Leak Test: X Date: 84/02/01  
 Heat Test (2h 1500F): X Date: 84/02/14

Actual Extrusion Conditions Date: 84/02/17 Ext. ID: L-2046  
 Crew: W/E/A/Giordano/Clifford  
 Temperature: 1790 Reduction Ratio: 16:1  
 Type of Die Round: X Sh Bar: Other: Angle: 90  
 Special Conditions: Slow cool in lime not possible

Valve Selection 1/8: 7/16: Preset Punch Speed:  
 (X to specify) 3.5: X Valve Opening: 0.25

Side Ram: X Pressure (psi): 3100 Max Tonnage: 340  
 Main Ram: Pressure (psi): Max Tonnage:  
 Comb Ram: Pressure (psi): Max Tonnage:

Lubricant Container: Dylon Graphite Paper: X  
 Die: Formkote

Dummy Thickness: 2. Carbon Thickness: 1.5  
 Container Mat: Nu Die V Cont Temp (F): 600 Times Used: 161  
 Stem Material: VAR 218 Stem ID: CH#6 Times Used: 161

Time at Temperature (h): 2. Transfer Time (s): 12.2

Post Test Analysis of Extrusion Successful: X Unsuccessful:  
 Comment:

Shooter: Butt left in Die: .25" Sticker:  
 Break thru Pressure (ksi): 168.5 Punch Speed: 4.3 "/s  
 Running Pressure (ksi): 150.1 Time to Ext: 1.25 s  
 Condition of Extrusion: good

Length of Ext: 55.25" Nominal Cross Section: 0.535" dia  
 Condition of Die:

General Comments: Furnace overtemperated 50 F

ORIGINAL PAGE IS  
OF POOR QUALITY

HOT EXTRUSION DATA SHEET  
(PFS-HotExtDS)

Second Series First Extrusion  
Fe-40Al

Engineer's Name: Gaydosch  
Eng's ID: E-1A (2)

Charge Number: YCG-5694

Date Submitted: 85/04/26  
Date Completed: 27May/85

General Type of Material: Intermetallic

Nominal Composition: Fe-40Al

Type of Billet: Loose powder  
Size of Billet (inches)

Diameter: 3"

Length: 5"

Proposed Extrusion  
Conditions

Temperature (F): 1790  
Type of Die: Round  
Punch Speed (inch/min): Max  
Special Conditions:

Reduction Ratio: 8:1

Safety Checks

Leak Test: X  
Heat Test (2h 1500F): X

Date: 4-28-85  
Date: 4-30-85

Actual Extrusion  
Conditions

Date: 27May/85  
Crew: W/E/K/A

Ext. ID: L-2215

Temperature: 1790

Reduction Ratio: 8:1

Type of Die Round: X Sh Bar: Other: Angle: 90  
Special Conditions:

Valve Selection 1/8: 7/16: Preset Punch Speed:  
(X to specify) 3/8: X Valve Opening: .25

Side Ram: Pressure (psi): Max Tonnage:  
Main Ram: X Pressure (psi): 3500 Max Tonnage: 680  
Comb Ram: Pressure (psi): Max Tonnage:

Lubricant Container: Dylon Graphite Paper: X  
Die: Formkote

Dummy Thickness: 2.0 Carbon Thickness: 1.25  
Container Mat: Na Die V Cont Temp (F): 600 Times Used: 452  
Stem Material: VAR 218 Stem ID: NASA#1 Times Used: 472

Time at Temperature (h): 2.4 Transfer Time (s): 7.5s

Post Test Analysis  
of Extrusion

Successful: X Unsuccessful:  
Comment:

Shooter: Butt left in Die: - Stickers:  
Break thru Pressure (ksi): 95 Punch Speed: 2.5"/s  
Running Pressure (ksi): 88.2 Time to Ext: 2s  
Condition of Extrusion: Good

Length of Ext: 32" Nominal Cross Section: 1.095"  
Condition of Die:

General Comments:

HOT EXTRUSION DATA SHEET  
(PFS-HotExtDS)

Second Series First Extrusion  
Fe-40Al-0.05B

Engineer's Name: Gaydosh  
Eng's ID: B-2A (3)

Charge Number: YCG-5694

Date Submitted: 85/04/26  
Date Completed: 2 May/85

General Type of Material: Intermetallic

Nominal Composition: Fe-40Al-.21B

Type of Billet: Loose powder

Size of Billet (inches)

Diameter: 3"

Length: 5"

Proposed Extrusion  
Conditions

Temperature (F): 1790

Reduction Ratio: 8:1

Type of Die: Round

Punch Speed (inch/min): Max

Special Conditions:

Safety Checks

Leak Test: X

Date: 4-29-85

Heat Test (2% 1500F): X

Date: 4-30-85

Actual Extrusion  
Conditions

Date: 2/May/85

Ext. ID: L-2216

Crew: W/E/L/A

Temperature: 1790

Reduction Ratio: 8:1

Type of Die: Round: X

Sh Bar:

Other:

Angle: 90

Special Conditions:

Valve Selection

1/8:

7/16:

Preset Punch Speed:

(X to specify)

3/8: X

Valve Opening: .25

Side Ram:

Pressure (psi):

Max Tonnage:

Main Ram: X

Pressure (psi): 3500

Max Tonnage: 600

Comb Ram:

Pressure (psi):

Max Tonnage:

Lubricant

Container: Dylon

Graphite Paper: X

Die: Formate

Dummy Thickness: 2.0

Carbon Thickness: 1.25

Container Mat: No Die V Cont Temp (F): 600

Times Used: 455

Stem Material: VAR C16

Stem ID: NASA#1

Times Used: 473

Time at Temperature (h): 2.6

Transfer Time (s): 0.3

Post Test Analysis  
of Extrusion

Successful: X Unsuccessful:  
Comment:

Shooter:

Butt left in Die: -

Sticker:

Break thru Pressure (ksi): 101.8

Punch Speed: 0.5"/s

Running Pressure (ksi): 92.3

Time to Ext: 2

Condition of Extrusion:

Length of Ext: 32.5"

Nominal Cross Section: 1.059"

Condition of Die:

General Comments:

ORIGINAL PAGE IS  
OF POOR QUALITY

ORIGINAL PAGE IS  
OF POOR QUALITY

Second Series first ext.  
Fe-40Al-0.1B

HOT EXTRUSION DATA SHEET  
(PFS-HotExtDS)

Engineer's Name: Gaydosch Date Submitted: 85/04/26  
Eng's ID: B-3A (4) Charge Number: YCG-5694 Date Completed: 2/11/85

General Type of Material: Intermetallic

Nominal Composition: Fe-40Al-.41B

Type of Billet: Loose powder

Size of Billet (inches) Diameter: 3" Length: 5"

Proposed Extrusion Conditions Temperature (F): 1790 Reduction Ratio: 8:1  
Type of Die: Round  
Punch Speed (inch/min): Max  
Special Conditions:

Safety Checks Leak Test: X Date: 4-29-85  
Heat Test (Ch 1500F): X Date: 4-30-85

Actual Extrusion Conditions Date: 2/11/85 Ext. ID: L-221Z  
Crew: W/E/K/A  
Temperature: ~~1790~~ 1790 Reduction Ratio: 8:1  
Type of Die: Round: X Sh Per: Other: Angle: 90  
Special Conditions:

Valve Selection 1/8: 7/16: Preset Punch Speed:  
(X to specify) 3/8: X Valve Opening: .25

Side Ram: Pressure (psi): Max Tonnage:  
Main Ram: X Pressure (psi): 3500 Max Tonnage: 480  
Comb Ram: Pressure (psi): Max Tonnage:

Lubricant Container: Dylon Graphite Paper: X  
Die: Forakote

Dummy Thickness: 2.0 Carbon Thickness: 1.25  
Container Mat: No Die V Cont Temp (F): 600 Times Used: 454  
Stop Material: VAR 218 Stem ID: NASA#1 Times Used: 474

Time at Temperature (h): 2.8 Transfer Time (h): 7.8

Post Test Analysis Successful: X Unsuccessful:  
on Extrusion Comment:

Shooter: Butt left in Die: - Stickon:  
Break thru Pressure (psi): 110.2 Punch Speed: 2.4  
Running Pressure (psi): 97.7 Time to Exit: 2.1s  
Condition of Extrusion: Good

Length of Ext: 32.5" Nominal Cross Section: 1.105"  
Condition of Die:

General Comments:

HOT EXTRUSION DATA SHEET  
(FFS-HotExtDS)

Second Series First ext.

Fe-40Al-0.2B

Engineer's Name: Gaydosh  
Eng's ID: E-4A (S)

Charge Number: YCG-5694

Date Submitted: 85/04/26  
Date Completed: 27May/85

General Type of Material: Intermetallic

Nominal Composition: Fe-40Al-.82B

Type of Billet: Loose powder  
Size of Billet (inches)

Diameter: 3"

Length: 5"

Proposed Extrusion  
Conditions

Temperature (F): 1790

Type of Die: Round

Punch Speed (inch/min): Max

Special Conditions:

Reduction Ratio: 8:1

Safety Check

Leak Test: X

Heat Test (2h 1500F): X

Date: 4-29-85

Date: 4-30-85

Actual Extrusion  
Conditions

Date: 2/May/85

Crew: W/E/K/A

Temperature: 1790

Type of Die Round: X Sh Bar:

Special Conditions:

Ext. ID: L-2218

Reduction Ratio: 8:1

Other: Angle: 90

Valve Selection: 1/8: 7/16: Preset Punch Speed:  
(X to specify) 3.5: X Valve Opening: .25

Side Ram: Pressure (psi): Max Tonnage:

Main Ram: X Pressure (psi): 3500 Max Tonnage: 600

Comb Ram: Pressure (psi): Max Tonnage:

Lubricant Container: Dylon  
Die: Formkote

Graphite Paper: X

Dummy Thickness: 2.0 Carbon Thickness: 1.25

Container Mat: Nu Die V Cont Temp (F): 600 Times Used: 455

Stem Material: VAR 218 Stem ID: NASA#1 Times Used: 470

Time at Temperature (h): 3.0

Transfer Time (s): 8.5

Post Test Analysis  
of Extrusion

Successful: X Unsuccessful:  
Comment:

Shooter: Butt left in Die: -

Break thru Pressure (ksi): 96.6

Running Pressure (ksi): 95

Condition of Extrusion: Good

Sticker:

Punch Speed: 2.4

Time to Ext: 2.08

Length of Ext: 32.5"

Nominal Cross Section: 1.100"

Condition of Die:

General Comments:

Second Series 150 ext  
Fc-50A1

HOT EXTRUSION DATA SHEET  
(FFS-HotExtDS)

Engineer's Name: Gaydosh Date Submitted: 85/01/31  
J's ID: Crimp-1A (1A) Charge Number: YCG-0652 Date Completed: 85/02/13

General Type of Material: Intermetallic

Nominal Composition: Fe-50Al

Type of Billet: Loose powder  
Size of Billet (inches) Diameter: 3 Length: 5.5

Proposed Extrusion Conditions Temperature (F): 1790 Reduction Ratio: 8:1  
Type of Die: Round  
Punch Speed (inch/min): Max  
Special Conditions:

Safety Checks Leak Test: X Date: 1-25-85  
Heat Test (2h 1500F): X Date: 1-31-85

Actual Extrusion Conditions Date: 85/01/13 Ext. ID: L-2205  
Crew: W/E/C/K  
Temperature: 1790 Reduction Ratio: 8:1  
Type of Die Round: X Sh Bar: Other: Angle: 90  
Special Conditions:

Valve Selection 1/8: 7/16: Preset Punch Speed:  
(X to specify) 3.5: X Valve Opening: .25

Side Ram: Pressure (psi): Max Tonnage:  
Main Ram: X Pressure (psi): 3500 Max Tonnage: 480  
Comb Ram: Pressure (psi): Max Tonnage:

Lubricant Container: Dylon Graphite Paper: X  
Die: Formkote

Dummy Thickness: 2 Carbon Thickness: 1.25  
Container Mat: NuDie V Cont Temp (F): 600 Times Used: 442  
Stem Material: Var 218 Stem ID: NASA #1 Times Used: 462

Time at Temperature (h): 2.7 Transfer Time (s): 8.3

Post Test Analysis Successful: X Unsuccessful:  
of Extrusion Comment:

Shooter: Butt left in Die: -- Sticker:  
Break thru Pressure (ksi): 105.9 Punch Speed: 2.75 "/s  
Running Pressure (ksi): 86.7 Time to Ext: 2.0  
Condition of Extrusion: Good

Length of Ext: 35 Nominal Cross Section: 1.042 " dia  
Condition of Die:

General Comments:

Second Series First ext.

Fe-50Al-0.05B

HOT EXTRUSION DATA SHEET  
(FFS-HotExtDS)

Engineer's Name: Gaydosh  
J's ID: Crimp-2A (2A)

Charge Number: YCG-0652

Date Submitted: 85/01/31  
Date Completed: 85/02/13

General Type of Material: Intermetallic

Nominal Composition: Fe-50Al-.19B

Type of Billet: Loose powder

Size of Billet (inches)

Diameter: 3

Length: 5.5

Proposed Extrusion  
Conditions

Temperature (F): 1790

Type of Die: Round

Punch Speed (inch/min): Max

Special Conditions:

Reduction Ratio: 8:1

Safety Checks

Leak Test: X

Heat Test (2h 1500F): X

Date: 1-25-85

Date: 1-31-85

Actual Extrusion  
Conditions

Date: 85/01/13

Crew: W/E/C/K

Temperature: 1790

Type of Die: Round: X

Special Conditions:

Ext. ID: L-2206

Reduction Ratio: 8:1

Sh Bar: Other: Angle: 90

Valve Selection 1/8: 7/16: Preset Punch Speed:  
(X to specify) 3.5: X Valve Opening: .25

Side Ram: Pressure (psi): Max Tonnage:  
Main Ram: X Pressure (psi): 3500 Max Tonnage: 680  
Comb Ram: Pressure (psi): Max Tonnage:

Lubricant Container: Dylon Graphite Paper: X  
Die: Formkote

Dummy Thickness: 2 Carbon Thickness: 1.25  
Container Mat: NuDie V Cont Temp (F): 600 Times Used: 443  
Stem Material: Var 218 Stem ID: NASA #1 Times Used: 463

Time at Temperature (h): 2.8 Transfer Time (s): 7

Post Test Analysis  
of Extrusion

Successful: X Unsuccessful:  
Comment:

Shooter: Butt left in Die: -- Sticker:  
Break thru Pressure (ksi): 108.6 Punch Speed: 2.75 "/s  
Running Pressure (ksi): 103.1 Time to Ext: 2  
Condition of Extrusion: Good

Length of Ext: 31.5 Nominal Cross Section: 1.097 " dia  
Condition of Die:

General Comments:

Second series test

Fe-50Al-0.1B

HOT EXTRUSION DATA SHEET  
(PFS-HotExtDS)

Engineer's Name: Gaydosh Date Submitted: 85/01/31  
's ID: Crimp-3A (3A) Charge Number: YCG-0652 Date Completed: 85/02/13

General Type of Material: Intermetallic

Nominal Composition: Fe-50Al-.38B

Type of Billet: Loose powder  
Size of Billet (inches) Diameter: 3 Length: 5.5

Proposed Extrusion Temperature (F): 1790 Reduction Ratio: 8:1  
Conditions Type of Die: Round  
Punch Speed (inch/min): Max  
Special Conditions:

Safety Checks Leak Test: X Date: 1-25-85  
Heat Test (2h 1500F): X Date: 1-31-85

Actual Extrusion Date: 85/01/13 Ext. ID: L-2207  
Conditions Crew: W/E/C/K  
Temperature: 1790 Reduction Ratio: 8:1  
Type of Die Round: X Sh Bar: Other: Angle: 90  
Special Conditions:

Valve Selection 1/8: 7/16: Preset Punch Speed:  
(X to specify) 3.5: X Valve Opening: .25

Side Ram: Pressure (psi): Max Tonnage:  
Main Ram: X Pressure (psi): 3500 Max Tonnage: 680  
Comb Ram: Pressure (psi): Max Tonnage:

Lubricant Container: Dylon Graphite Paper: X  
Die: Formkote

Dummy Thickness: 2 Carbon Thickness: 1.25  
Container Mat: NuDie V Cont Temp (F): 600 Times Used: 444  
Stem Material: Var 218 Stem ID: NASA #1 Times Used: 464

Time at Temperature (h): 3 Transfer Time (s): 9

Post Test Analysis Successful: X Unsuccessful:  
of Extrusion Comment:

Shooter: Butt left in Die: -- Sticker:  
Break thru Pressure (ksi): 108.6 Punch Speed: 2.75 "/s  
Running Pressure (ksi): 103.1 Time to Ext: 2.0  
Condition of Extrusion: Good

Length of Ext: 32.75 Nominal Cross Section: 1.096 " dia  
Condition of Die:

General Comments:

C-3



Second series first ext.  
Fe-50Al-0.2B

HOT EXTRUSION DATA SHEET  
(FFS-HotExtDS)

Engineer's Name: Gaydosh  
J's ID: Crimp-4A (4A) Charge Number: YCG-0652

Date Submitted: 85/01/31  
Date Completed: 85/02/13

General Type of Material: Intermetallic

Nominal Composition: Fe-50Al-.77B

Type of Billet: Loose powder

Size of Billet (inches) Diameter: 3 Length: 5.5

Proposed Extrusion  
Conditions

Temperature (F): 1790  
Type of Die: Round  
Punch Speed (inch/min): Max  
Special Conditions:

Reduction Ratio: 8:1

Safety Checks

Leak Test: X Date: 1-25-85  
Heat Test (2h 1500F): X Date: 1-31-85

Actual Extrusion  
Conditions

Date: 85/01/13 Ext. ID: L-2208  
Crew: W/E/C/K  
Temperature: 1790 Reduction Ratio: 8:1  
Type of Die: Round: X Sh Bar: Other: Angle: 90  
Special Conditions:

Valve Selection 1/8: 7/16: Preset Punch Speed:  
(X to specify) 3.5: X Valve Opening: .25

Side Ram: Pressure (psi): Max Tonnage:  
Main Ram: X Pressure (psi): 3500 Max Tonnage: 680  
Comb Ram: Pressure (psi): Max Tonnage:

Lubricant Container: Dylon Graphite Paper: X  
Die: Formkote

Dummy Thickness: 2 Carbon Thickness: 1.25  
Container Mat: NuDie V Cont Temp (F): 600 Times Used: 445  
Stem Material: Var 218 Stem ID: NASA #1 Times Used: 465

Time at Temperature (h): 3.1 Transfer Time (s): 8.9

Post Test Analysis  
of Extrusion

Successful: X Unsuccessful:  
Comment:

Shooter: Butt left in Die: -- Sticker:  
Break thru Pressure (ksi): 108.6 Punch Speed: 2.4 "/s  
Running Pressure (ksi): 105.9 Time to Ext: 2.25  
Condition of Extrusion: Good

Length of Ext: 32 Nominal Cross Section: 1.097 " dia  
Condition of Die:

General Comments:

Second series low T 2nd ext  
Fe-40Al

HOT EXTRUSION DATA SHEET  
(FFS-HotExtDS)

Engineer's Name: Gaydosh Date Submitted: 05/06/04  
Eng's ID: Crimp BL (1A) Charge Number: YCG-5694 Date Completed: 07/06/05

General Type of Material: Intermetallic

Nominal Composition: Fe-40Al

Type of Billet: Canned solid

Size of Billet (inches) Diameter: 2 Length: 5

Proposed Extrusion Conditions Temperature (F): 1472 Reduction Ratio: 6:1  
Type of Die: Round  
Punch Speed (inch/min): Max  
Special Conditions:

Safety Checks Leak Test: NA Date:  
Heat Test (2h 1500F): NA Date:

Actual Extrusion Conditions Date: 07/06/05 Ext. ID: L-2238  
Crew:  
Temperature: 1472 Reduction Ratio: 6:1  
Type of Die Round: X Sh Bar: Other: Angle: 120  
Special Conditions:

Valve Selection 1/8: 7/16: Preset Punch Speed:  
(X to specify) 3.5: X Valve Opening: .25

Side Ram: X Pressure (psi): 3100 Max Tonnage: 340  
Main Ram: Pressure (psi): Max Tonnage:  
Comb Ram: Pressure (psi): Max Tonnage:

Lubricant Container: Dylon Graphite Paper: Y  
Die: Formikote

Dummy Thickness: 2.0" Carbon Thickness: 1.5"  
Container Mat: NuDie V Cont Temp (F): 600 Times Used: 47  
Stem Material: ? Stem ID: New Times Used: 47

Time at Temperature (h): 2.4 Transfer Time (s): 10.3

Post Test Analysis Successful: X Unsuccessful:  
of Extrusion Comment:

Shooter: Butt left in Die: .25 Sticker:  
Break thru Pressure (ksi): 168.5 Punch Speed:  
Running Pressure (ksi): 145.9 Time to Ext: 1.3s  
Condition of Extrusion:

Length of Ext: 20.75" Nominal Cross Section: 0.670"  
Condition of Die:

General Comments:

second series low T 2nd ext  
Fe-40Al-0.5B

HOT EXTRUSION DATA SHEET  
(PFS-HotExtDS)

Engineer's Name: Gaydosh Date Submitted: 05/06/84  
Eng's ID: Crimp CL (2A) Charge Number: YCG-5694 Date Completed: 07/06/84

General Type of Material: Intermetallic

Nominal Composition: Fe-40Al-.21B

Type of Billet: Canned solid  
Size of Billet (inches) Diameter: 2 Length: 5

Proposed Extrusion Conditions Temperature (F): 1472 Reduction Ratio: 6:1  
Type of Die: Round  
Punch Speed (inch/min): Max  
Special Conditions:

Safety Checks Leak Test: NA Date:  
Heat Test (2h 1500F): NA Date:

Actual Extrusion Conditions Date: 07/06/85 Ext. ID: L-2239  
Crew:  
Temperature: 1472 Reduction Ratio: 6:1  
Type of Die Round: X Sh Bar: Other: Angle: 120  
Special Conditions:

Valve Selection 1/8: 7/16: Preset Punch Speed:  
(X to specify) 3/8: X Valve Opening: .25

Side Ram: X Pressure (psi): 3100 Max Tonnage: 340  
Main Ram: Pressure (psi): Max Tonnage:  
Comb Ram: Pressure (psi): Max Tonnage:

Lubricant Container: Dylon Graphite Paper: Y  
Die: Forakote

Dummy Thickness: 2.0" Carbon Thickness: 1.5"  
Container Mat: NuDie V Cont Temp (F): 600 Times Used: 48  
Stem Material: ? Stem ID: New Times Used: 48

Time at Temperature (h): 2.5 Transfer time (s): 13.2

Post Test Analysis Successful: X Unsuccessful:  
of Extrusion Comment:

Shooter: Butt left in Die: .25 Sticker:  
Break thru Pressure (ksi): 176.0 Punch Speed:  
Running Pressure (ksi): 141. Time to Ext: 1.8s  
Condition of Extrusion:

Length of Ext: 20.75" Nominal Cross Section: 0.877"  
Condition of Die:

General Comments:

Second Series lowT Zndext  
Fe-40Al-0.18

HOT EXTRUSION DATA SHEET  
(FES-HotExtDS)

Engineer's Name: Gaydosch Date Submitted: 85/06/04  
Eng's ID: Crimp DL (3A) Charge Number: YCG-5694 Date Completed: 07/06/85

General Type of Material: Intermetallic

Nominal Composition: Fe-40Al-.42R

Type of Bullet: Canned solid

Size of Bullet (inches) Diameter: 2 Length: 5

Proposed Extrusion Conditions Temperature (F): 1472 Reduction Ratio: 6:1  
Type of Die: Round  
Punch Speed (inch/min): Max  
Special Conditions:

Safety Checks Leak Test: NA Date:  
Heat Test (2h 1500F): NA Date:

Actual Extrusion Conditions Date: 07/06/85 Ext. ID: L-2240  
Crew:  
Temperature: 1472 Reduction Ratio: 6:1  
Type of Die Round: X Sh Bar: Other: Angle: 120  
Special Conditions:  
Valve Selection 1/8: 7/16: Preset Punch Speed:  
(X to specify) 1.5: X Valve Opening: .25  
Side Ram: X Pressure (psi): 3100 Max Tonnage: 340  
Main Ram: Pressure (psi): Max Tonnage:  
Comb Ram: Pressure (psi): Max Tonnage:  
Lubricant Container: Dylon Graphite Paper: Y  
Die: Formite  
Dummy Thickness: 2.0" Carbon Thickness: 1.5"  
Container Mat: Nubie V Cont Temp (F): 600 Times Used: 45  
Stem Material: ? Stem ID: New Times Used: 45  
Time at Temperature (h): 2.7 Transfer Time (s): 11.2

Post Test Analysis Successful: X Unsuccessful:  
of Extrusion Comment:  
Shooter: Butt left in Die: .25 Sticker:  
Break thru Pressure (ksi): 175.9 Punch Speed:  
Running Pressure (ksi): 137.9 Time to Ext: 1.5s  
Condition of Extrusion:  
Length of Ext: 20.5" Nominal Cross Section: 0.849"  
Condition of Die:  
General Comments:

Second Series lowT Zndext  
Fe-40Al-0.2B

HOT EXTRUSION DATA SHEET  
(PFS-HotExtDS)

Engineer's Name: Gaydosch  
Eng. ID: Crisp EL (4A) Charge Number: YCG-5694

Date Submitted: 8/7/84  
Date Completed: 07/06/85

General Type of Material: Intermetallic

Nominal Composition: Fe-40Al-.84B

Type of Billet: Canned solid

Size of Billet (inches)

Diameter: 2

Length: 5

Proposed Extrusion  
Conditions

Temperature (F): 1472

Type of Die: Round

Punch Speed (inch/min): Max

Special Conditions:

Reduction Ratio: 5:1

Safety Checks

Leak Test: NA

Heat Test (2h 1500F): NA

Date:

Date:

Actual Extrusion  
Conditions

Date: 07/06/85

Ext. ID: L-2241

Crew:

Temperature: 1472

Reduction Ratio: 6:1

Type of Die Round: X Sh Bar: Other: Angle: 120

Special Conditions:

Valve Selection 1/8: 7/16: Preset Punch Speed:  
(X to specify) 3.5: X Valve Opening: .25

Side Ram: X Pressure (psi): 3100 Max Tonnage: 340  
Main Ram: Pressure (psi): Max Tonnage:  
Comb Ram: Pressure (psi): Max Tonnage:

Lubricant Container: Dylon  
Die: Formkote

Graphite Paper: Y

Dummy Thickness: 2.0" Carbon Thickness: 1.5"

Container Mat: NuDie V Cont Temp (F): 600 Times Used: 50

Stem Material: ? Stem ID: Now Times Used: 50

Time at Temperature (h): 2.8

Transfer Time (s): 6.7

Post Test Analysis  
of Extrusion

Successful: X Unsuccessful:  
Comment:

Shooter: Butt left in Die: 0.5

Break thru Pressure (ksi): 177.7

Running Pressure (ksi): 137.9

Condition of Extrusion:

Sticker:

Punch Speed:

Time to Ext: 1.3

Length of Ext: 17.5"

Nominal Cross Section: 0.874"

Condition of Die:

General Comments: Odd load-time curve. Sharp load drop  
during running portion.

ORIGINAL PAGE IS  
OF POOR QUALITY

Second Series lowT Endtest  
Fe-50Al

HOT EXTRUSION DATA SHEET  
(PFS-HotExtDS)

Engineer's Name: Gaydosch Date Submitted: 05/06/04  
Eng's ID: Crimp FL (5A) Charge Number: YCG-5694 Date Completed: 07/06/85

General Type of Material: Intermetallic

Nominal Composition: Fe-50Al

Type of Billet: Canned solid

Size of Billet (inches) Diameter: 2 Length: 5

Proposed Extrusion Conditions Temperature (F): 1472 Reduction Ratio: 6:1  
Type of Die: Round  
Punch Speed (inch/min): Max  
Special Conditions:

Safety Checks Leak Test: NA Date:  
Heat Test (2h 1500F): NA Date:

Actual Extrusion Conditions Date: 07/06/85 Ext. ID: L-2242  
Crew:  
Temperature: 1472 Reduction Ratio: 6:1  
Type of Die: Round: X Sh. Bar: Other: Angle: 120  
Special Conditions:

Valve Selection 1/8: 7/16: Preset Punch Speed:  
(X to specify) 3/8: X Valve Opening: .25

Side Ram: X Pressure (psi): 3100 Max Tonnage: 340  
Main Ram: Pressure (psi): Max Tonnage:  
Comb Ram: Pressure (psi): Max Tonnage:

Lubricant Container: Dylon Graphite Paper: Y  
Die: Formkote

Dummy Thickness: 2.0" Carbon Thickness: 1.5"  
Container Mat: NuDie V Cont Temp (F): 600 Times Used: 51  
Stem Material: ? Stem ID: Now Times Used: 51

Time at Temperature (h): 3.1 Transfer Time (s): 6.6

Post Test Analysis of Extrusion Successful: X Unsuccessful:  
Comment:

Shooters: Butt left in Die: 1. Sticker:  
Break thru Pressure (ksi): 168.5 Punch Speed:  
Running Pressure (ksi): 122.6 Time to Ext: 1.3s  
Condition of Extrusion:

Length of Ext: 16.75" Nominal Cross Section: 0.868"  
Condition of Die:

General Comments: Loud crack during extrusion, large load drop during running portion of load-time curve.

Second series low T Index  
Fe-50Al-0.05B

HOT EXTRUSION DATA SHEET  
(FES-HotExtDS)

Engineer's Name: Gaydosch  
Eng's ID: Crimp GL (6A) Charge Number: YCG-5694

Date Submitted: 05/06/04  
Date Completed: 07/06/05

General Type of Material: Intermetallic

Nominal Composition: Fe-50Al-.21B

Type of Billet: Canned solid  
Size of Billet (inches) Diameter: 2 Length: 5

Proposed Extrusion Conditions Temperature (F): 1472 Reduction Ratio: 6:1  
Type of Die: Round  
Punch Speed (inch/min): Max  
Special Conditions:

Safety Checks Leak Test: N/A Date:  
Heat Test (2h 1500F): NA Date:

Actual Extrusion Conditions Date: 07/06/05 Ext. ID: L-2243  
Crew:  
Temperature: 1472 Reduction Ratio: 6:1  
Type of Die: Round: X Sh Bar: Other: Angle: 120  
Special Conditions:  
Valve Selection 1/8: 7/16: Preset Punch Speed:  
(X to specify) 3/8: X Valve Opening: .25  
Side Ram: X Pressure (psi): 3100 Max Tonnage: 340  
Main Ram: Pressure (psi): Max Tonnage:  
Comb Ram: Pressure (psi): Max Tonnage:  
Lubricant Container: Dylon Graphite Paper: Y  
Die: Ferralote  
Dummy Thickness: 2.0" Carbon Thickness: 1.5"  
Container Mat: NoDie V Cont Temp (F): 600 Times Used: 52  
Stem Material: T Stem ID: Nev Times Used: 52  
Time at Temperature (h): 3.3 Transfer Time (s): 12.3

Post Test Analysis of Extrusion Successful: X Unsuccessful:  
Comments:  
Shooter: Butt left in Die: .25 Sticker:  
Break thru Pressure (ksi): 183.9 Punch Speed:  
Running Pressure (ksi): 168.5 Time to Ext: 2.5  
Condition of Extrusion:  
Length of Ext: 21.5" Nominal Cross Section: 0.673"  
Condition of Die:  
General Comments:

ORIGINAL PAGE IS  
OF POOR QUALITY

Second Series low T 2nd ext

Fe-50Al-0.18

HOT EXTRUSION DATA SHEET  
(PFS-HotExIDS)

Engineer's Name: Gaydosch Date Submitted: 80/08/10+  
Eng's ID: Crimp HL (7A) Change Number: YCG-5694 Date Completed: 07/08/80

General Type of Material: Intermetallic

Nominal Composition: Fe-50Al-.42B

Type of Billet: Canned solid  
Size of Billet (inches) Diameter: 2 Length: 5  
Proposed Extrusion Conditions Temperature (F): 1472 Reduction Ratio: 8:1  
Type of Die: Round  
Punch Speed (inch/min): Max  
Special Conditions:

Safety Checks Leak Test: NA Date:  
Heat Test (2H 1500F): NA Date:

Actual Extrusion Conditions Date: 07/06/85 Ext. ID: L-2244  
Crew:  
Temperature: 1472 Reduction Ratio: 8:1  
Type of Die Round: X Sh Bar: Other: Angle: 120  
Special Conditions:

Valve Selection 1/8: 7/16: Preset Punch Speed:  
(X to specify) 3.5: X Valve Opening: .25

Side Ram: X Pressure (psi): 3100 Max Tonnage: 340  
Main Ram: Pressure (psi): Max Tonnage:  
Comb Ram: Pressure (psi): Max Tonnage:

Lubricant Container: Dylon Graphite Paper: Y  
Die: Formlote

Dummy Thickness: 2.0" Carbon Thickness: 1.5"  
Container Mat: NoDie V Cont Temp (F): 600 Times Used: 50  
Stem Material: C Stem ID: New Times Used: 50

Time at Temperature (h): 3.5 Transfer Time (s): 15.

Post Test Analysis Successful: X Unsuccessful:  
of Extrusion Comment:

Shooter: Butt left in Die: .25 Sticker:  
Break thru Pressure (ksi): 176.3 Punch Speed:  
Running Pressure (ksi): 147.0 Time to Ext: 1.5s  
Condition of Extrusion:

Length of Ext: 20.5" Nominal Cross Section: 0.872"  
Condition of Die:

General Comments:



Second Series lowT Index

Fe-50Al-0.2B

HOT EXTRUSION DATA SHEET  
(FFS-HotExtDS)

Eng. Order's Name: Gaydosh  
Eng's ID: Crimp IL (BA) Charge Number: YCG-5694

Date Submitted: 88/06/04  
Date Completed: 07/06/89

General Type of Material: Intermetallic

Nominal Composition: Fe-50Al-.84B

Type of Billet: Canned solid  
Size of Billet (inches)

Diameter: 2

Length: 5

Proposed Extrusion  
Conditions

Temperature (F): 1472  
Type of Die: Round  
Punch Speed (inch/min): Max  
Special Conditions:

Reduction Ratio: 6:1

Safety Checks

Leak Test: NA  
Heat Test (2h 1500F): NA

Date:  
Date:

Actual Extrusion  
Conditions

Date: 07/06/85

Ext. ID: L-2245

Crew:

Temperature: 1472

Reduction Ratio: 6:1

Type of Die: Round: X Sh Bar: Other: Angle: 120

Special Conditions:

Valve Selection 1/8: 7/16: Preset Punch Speed:  
(X to specify) 3.5: X Valve Opening: .25

Side Ram: X Pressure (psi): 3100 Max Tonnage: 340  
Main Ram: Pressure (psi): Max Tonnage:  
Comb Ram: Pressure (psi): Max Tonnage:

Lubricant Container: Dylon Graphite Paper: Y  
Die: Forakote

Dummy Thickness: 2.0" Carbon Thickness: 1.5"

Container Mat: NuDie V Cont Temp (F): 600 Times Used: 54

Stem Material: ? Stem ID: New Times Used: 54

Time at Temperature (h): 3.6 Transfer Time (s): 17.1

Post Test Analysis  
of Extrusion

Successful: X Unsuccessful:  
Comment:

Shooter: Butt left in Die: .25 Sticker:  
Break thru Pressure (ksi): 180.8 Punch Speed:  
Running Pressure (ksi): 147.1 Time to Ext: 1.5s  
Condition of Extrusion:

Length of Ext: 20.5" Nominal Cross Section: .0.876"  
Condition of Die:

General Comments:

ORIGINAL PAGE 13  
OF POOR QUALITY

Second Series High T 2nd ext  
Fe-40Al

HOT EXTRUSION DATA SHEET  
(PFS-HotExtDS)

Eng. neer's Name: Daydosh  
Eng's ID: Crimp B (1)

Charge Number: YCG-5694

Date Submitted: 85/06/04  
Date Completed: 05/06/05

General Type of Material: Intermetallic

Nominal Composition: Fe-40Al

Type of Billet: Canned solid  
Size of Billet (inches)

Diameter: 2

Length: 5

Proposed Extrusion  
Conditions

Temperature (F): 1970

Reduction Ratio: 6:1

Type of Die: Round

Punch Speed (inch/min): Max

Special Conditions:

Safety Checks

Leak Test: NA

Date:

Heat Test (2h 1500F): NA

Date:

Actual Extrusion  
Conditions

Date: 05/06/95

Ext. ID: L-2227

Crew:

Temperature: 1970

Reduction Ratio: 6:1

Type of Die: Round: X Sh. Bar: Other: Angle: 120

Special Conditions:

Valve Selection 1/8: 7/16: Preset Punch Speed:  
(X to specify) 3.5: X Valve Opening: .25

Side Ram: X Pressure (psi): 3100 Max Tonnage: 340

Main Ram: Pressure (psi): Max Tonnage:

Comb Ram: Pressure (psi): Max Tonnage:

Lubricant Container: Dylon  
Die: Formkote

Graphite Paper: Y

Dummy Thickness: 2.0" Carbon Thickness: 1.5"

Container Mat: NuDie V Cont Temp (F): 600 Times Used: 36

Stem Material: ? Stem ID: New Times Used: 36

Time at Temperature (h): 2.9

Transfer Time (s): 8.25

Post Test Analysis  
of Extrusion

Successful: X Unsuccessful:

Comment:

Shooter: Butt left in Die: .25

Sticker:

Break thru Pressure (ksi): 99.3

Punch Speed: 5.9"/s

Running Pressure (ksi): 61.3

Time to Ext: 0.8s

Condition of Extrusion:

Length of Ext: 22.25"

Nominal Cross Section: 0.871"

Condition of Die:

General Comments:

second Series High T 2nd ext  
Fe-40Al - 0.05B

HOT EXTRUSION DATA SHEET  
(FFS-HotExIDS)

Engineer's Name: Gaydosch  
Eng's ID: Crimp C (2)

Charge Number: YCG-5694

Date Submitted: 05/06/04  
Date Completed: 05/06/04

General Type of Material: Intermetallic

Nominal Composition: Fe-40Al-.21B

Type of Billet: Canned solid

Size of Billet (inches)

Diameter: 2

Length: 5

Proposed Extrusion  
Conditions

Temperature (F): 1970

Reduction Ratio: 6:1

Type of Die: Round

Punch Speed (inch/min): Max

Special Conditions:

Safety Checks

Leak Test: NA

Date:

Heat Test (2h 1500F): NA

Date:

Actual Extrusion  
Conditions

Date: 05/06/05

Ext. ID: L-2020

Crew:

Temperature: 1970

Reduction Ratio: 6:1

Type of Die: Round: X Sh Bar: Other:

Angle: 120

Special Conditions:

Valve Selection 1/8: 7/16: Pressed Punch Speed:  
(X to specify) 3.5: X Valve Opening: .25

Side Ram: X Pressure (psi): 3100

Max Tonnage: 340

Main Ram: Pressure (psi):

Max Tonnage:

Comb Ram: Pressure (psi):

Max Tonnage:

Lubricant Container: Dylon  
Die: Formkote

Graphite Paper: Y

Dummy Thickness: 2.0"

Carbon Thickness: 1.5"

Container Mat: NuDie V Cont Temp (F): 600 Times Used: 37

Stem Material: ?

Stem ID: New

Times Used: 37

Time at Temperature (h): 3.3

Transfer Time (s): 8.3

Post Test Analysis  
of Extrusion

Successful: X Unsuccessful:  
Comment:

Shooter: Butt left in Die: .25

Sticker:

Break thru Pressure (ksi): 116.5

Punch Speed: 5.3"/s

Running Pressure (ksi): 73.5

Time to Ext: 0.9s

Condition of Extrusion:

Length of Ext: 22.25"

Nominal Cross Section: 0.808"

Condition of Die:

General Comments:

Second Series High T Zndext  
Fe-40Al-0.10B

HOT EXTRUSION DATA SHEET  
(FFS-HotExtDS)

Engineer's Name: Gaydosh Date Submitted: 05/06/84  
Eng's ID: Crimp D (3) Charge Number: YCG-5694 Date Completed: 05/06/85

General Type of Material: Intermetallic

Nominal Composition: Fe-40Al-.42B

Type of Billet: Canned solid  
Size of Billet (inches) Diameter: 2 Length: 5

Proposed Extrusion Conditions Temperature (F): 1970 Reduction Ratio: 4:1  
Type of Die: Round  
Punch Speed (inch/min): Max  
Special Conditions:

Safety Checks Leak Test: NA Date:  
Heat Test (2h 1500F): NA Date:

Actual Extrusion Conditions Date: 05/06/85 Ext. ID: L-2229  
Crow:  
Temperature: 1970 Reduction Ratio: 6:1  
Type of Die: Round: X Sh Bar: Other: Angle: 120  
Special Conditions:

Valve Selection 1/5: 7/16: Preset Punch Speed:  
(X to specify) 3.5: X Valve Opening: .25

Side Ram: X Pressure (psi): 3100 Max Tonnage: 340  
Main Ram: Pressure (psi): Max Tonnage:  
Comb Ram: Pressure (psi): Max Tonnage:

Lubricant Container: Nylon Graphite Paper: Y  
Die: Formable

Dummy Thickness: 2.0" Carbon Thickness: 1.5"  
Container Mat: Nudic V Cont Temp (F): 600 Times Used: 18  
Stem Material: ? Stem ID: New Times Used: 30

Time at Temperature (hr): 3.5 Transfer Time (s): 11.5

Post Test Analysis of Extrusion Successful: X Unsuccessful:  
Comment:

Shooter: Butt left in Die: .25 Sticker:  
Break thru Pressure (ksi): 116.5 Punch Speed: 5.37/s  
Running Pressure (ksi): 79.7 Time to Ext: 0.9s  
Condition of Extrusion:

Length of Ext: 23." Nominal Cross Section: 0.967"  
Condition of Die:

General Comments:

Second Series High T 2nd ext.  
Fe-40Al-0.2B

HOT EXTRUSION DATA SHEET  
(HPS-HotExtDS)

Engineer's Name: Gaydosch Date Submitted: 05/06/95  
Eng's ID: Crimp E (4) Charge Number: YCG-5694 Date Completed: 05/06/95

General Type of Material: Intermetallic

Nominal Composition: Fe-40Al-.82B

Type of Billet: Canned solid  
Size of Billet (inches) Diameter: 2 Length: 5

Proposed Extrusion Conditions Temperature (F): 1970 Reduction Ratio: 6:1  
Type of Die: Round  
Punch Speed (inch/min): Max  
Special Conditions:

Safety Checks Leak Test: NA Date:  
Heat Test (2h 1500F): NA Date:

Actual Extrusion Conditions Date: 05/06/95 Ext. ID: L-2230  
Crew:  
Temperature: 1970 Reduction Ratio: 6:1  
Type of Die: Round: X Sh. Bar: Other: Angle: 120  
Special Conditions:

Valve Selection 1/8: 7/16: Preset Punch Speed:  
(X to specify) 3/8: X Valve Opening: .25

Side Ram: X Pressure (psi): 3100 Max Tonnage: 340  
Main Ram: Pressure (psi): Max Tonnage:  
Comb Ram: Pressure (psi): Max Tonnage:

Lubricant Container: Dylon Graphite Paper: Y  
Die: Formdite

Dummy Thickness: 2.0" Carbon Thickness: 1.5"  
Container Mat: Nudie V Cont Temp (F): 600 Times Used: 39  
Stem Material: ? Stem ID: New Times Used: 39

Time at Temperature (h): 3.75 Transfer Time (s): 9.5

Post Test Analysis of Extrusion Successful: X Unsuccessful:  
Comment:

Shooter: Butt left in Die: .25 Sticker:  
Break thru Pressure (ksi): 113.4 Punch Speed: 5.3"/s  
Running Pressure (ksi): 73.5 Time to Ext: 0.9s  
Condition of Extrusion:

Length of Ext: 22." Nominal Cross Section: 0.892"  
Condition of Die:

General Comments:

Second series high T 2nd ext  
Fe-50Al

HOT EXTRUSION DATA SHEET  
(FFS-HotExtDS)

Engineer's Name: Gaydos  
Eng's ID: Crimp F (5)

Charge Number: YCG-5624

Date Submitted: 05/06/84  
Date Completed: 05/08/85

General Type of Material: Intermetallic

Nominal Composition: Fe-50Al

Type of Billet: Canned solid  
Size of Billet (inches)

Diameter: 2

Length: 6

Proposed Extrusion  
Conditions

Temperature (F): 1970  
Type of Die: Round  
Punch Speed (inch/min): N/A  
Special Conditions:

Reduction Ratio: 6:1

Safety Checks

Leak Test: N/A  
Heat Test (2H 1500F): N/A

Date:  
Date:

Actual Extrusion  
Conditions

Date: 05/06/85

Ext. ID: L-2231

Crack:

Temperature: 1970

Reduction Ratio: 6:1

Type of Die: Round: X Sh Bar: Other: Angle: 120  
Special Conditions:

Valve Selection 1/8: 7/16: Preset Punch Speed:  
(X to specify) 3/8: X Valve Opening: .25

Side Ram: X Pressure (psi): 3100 Max Tonnage: 340  
Main Ram: Pressure (psi): Max Tonnage:  
Comb Ram: Pressure (psi): Max Tonnage:

Lubricant Container: Dylon Graphite Paper: Y  
Die: Formkote

Dummy Thickness: 2.0" Carbon Thickness: 1.5"  
Container Mat: NuDie V Cont Temp (F): 600 Times Used: 40  
Steel Material: ? Stem ID: New Times Used: 40

Time at Temperature (h): 4.25 Transfer Time (s): 11.5

Post Test Analysis  
of Extrusion

Successful: X Unsuccessful:  
Comment:

Shooter: Butt left in Die: .25 Sticker:  
Break thru Pressure (ksi): 110.3 Punch Speed: 5.3"/s  
Running Pressure (ksi): 73.9 Time to Ext: 0.9s  
Condition of Extrusion:

Length of Ext: 21.5" Nominal Cross Section: 0.871"  
Condition of Die:

General Comments:

second series High T end ext  
Fe-50Al-a1B

HOT EXTRUSION DATA SHEET  
(FFS-HotExtDS)

Engineer's Name: Gaydos  
Eng's ID: Crimp H (7)

Charge Number: YCG-5694

Date Submitted: 05/06/04  
Date Completed: 05/06/05

General Type of Material: Intermetallic

Nominal Composition: Fe-50Al-.42B

Type of Billet: Canned solid  
Size of Billet (inches)

Diameter: 2

Length: 5

Proposed Extrusion  
Conditions

Temperature (F): 1970  
Type of Die: Round  
Punch Speed (inch/min): Max  
Special Conditions:

Reduction Ratio: 6:1

Safety Checks

Leak Test: NA  
Heat Test (2H 1500F): NA

Date:  
Date:

Actual Extrusion  
Conditions

Date: 05/06/05

Ext. ID: L-2233

Crew:

Temperature: 1970

Reduction Ratio: 6:1

Type of Die: Round: X Sh Bar: Other: Angle: 120

Special Conditions:

Valve Selection 1/8: 7/16: Preset Punch Speed:  
(X to specify) 3.5: X Valve Opening: .25

Side Ram: X Pressure (psi): 3100 Max Tonnage: 340  
Main Ram: Pressure (psi): Max Tonnage:  
Comb Ram: Pressure (psi): Max Tonnage:

Lubricant Container: Dylon Graphite Paper: Y  
Die: Formkote

Dummy Thickness: 2.0" Carbon Thickness: 1.5"  
Container Mat: NuDie V Cont Temp (F): 600 Times Used: 42  
Stem Material: ? Stem ID: New Times Used: 42

Time at Temperature (h): 5.25 Transfer Time (s): 10.

Post Test Analysis  
of Extrusion

Successful: X Unsuccessful:  
Comment:

Shooter: Butt left in Die: .25 Sticker:  
Break thru Pressure (ksi): 107.3 Punch Speed: 5.3"/s  
Running Pressure (ksi): 75.5 Time to Ext: 0.9s  
Condition of Extrusion:

Length of Ext: 23" Nominal Cross Section: 0.865"  
Condition of Die:

General Comments:

Second Series High T Index  
Fe-50Al-0.20B

HOT EXTRUSION DATA SHEET  
(PFS-HotExtDS)

Engineer's Name: Gaydosch Date Submitted: 05/06/04  
Eng's ID: Crimp I (8) Charge Number: YCG-5694 Date Completed: 05/08/05

General Type of Material: Intermetallic

Nominal Composition: Fe-50Al-.82B

Type of Billet: Canned solid  
Size of Billet (inches) Diameter: 2 Length: 5

Proposed Extrusion Conditions Temperature (F): 1970 Reduction Ratio: 3:1  
Type of Die: Round  
Punch Speed (inch/min): Max  
Special Conditions:

Safety Checks Leak Test: NA Date:  
Heat Test (2h 1500F): NA Date:

Actual Extrusion Conditions Date: 05/06/05 Ext. ID: L-2234  
Crew:  
Temperature: 1970 Reduction Ratio: 6:1  
Type of Die Round: X Sh Bar: Other: Angle: 120  
Special Conditions:

Valve Selection 1/0: 7/16: Preset Punch Speed:  
(X to specify) 3/5: X Valve Opening: .25

Side Ram: X Pressure (psi): 3100 Max Tonnage: 340  
Main Ram: Pressure (psi): Max Tonnage:  
Comb Ram: Pressure (psi): Max Tonnage:

Lubricant Container: Dylon Graphite Paper: Y  
Die: Formkote

Dummy Thickness: 2.0" Carbon Thickness: 1.5"  
Container Mat: NuDie V Cont Temp (F): 600 Times Used: 40  
Stem Material: C Stem ID: New Times Used: 40

Time at Temperature (h): 5.5 Transfer Time (s): 3.

Post Test Analysis Successful: X Unsuccessful:  
of Extrusion Comment:

Shooter: Butt left in Die: .25 Sticker:  
Break thru Pressure (ksi): 116.5 Punch Speed: 4.0"/s  
Running Pressure (ksi): 67.4 Time to Ext: 1s  
Condition of Extrusion:

Length of Ext: 22.5" Nominal Cross Section: 0.846"  
Condition of Die:

General Comments:

ORIGINAL PAGE IS  
OF POOR QUALITY



HOT EXTRUSION DATA SHEET  
(PFS-HotExtDS)

3.A  
Fe-40Al

Engineer's Name: Gaydosh  
Eng's ID: 11

Charge Number: YAG2272

Date Submitted: 86/11/07  
Date Completed: 86/11/21

General Type of Material: Intermetallic

Nominal Composition: Fe-40Al A-18%?

Type of Billet: Loose Powder  
Size of Billet (inches)

Diameter: 2.0

Length: 5.5

Proposed Extrusion  
Conditions

Temperature (F): 1790

Reduction Ratio: 16:1

Type of Die: Round

Punch Speed (inch/min): Maximum

Special Conditions:

Safety Checks

Leak Test: X

Date: 86/11/05

Heat Test (2h 1500F): X

Date: 86/11/06

Actual Extrusion  
Conditions

Date: 86/11/21

Ext. ID: L-2327

Crew:

Temperature: 1790

Reduction Ratio: 16:1

Type of Die Round: X Sh Bar: Other:

Angle: 90

Special Conditions:

Valve Selection 1/8: 7/16: Preset Punch Speed:  
(X to specify) 3.5: X Valve Opening: 0.25

Side Ram: X Pressure (psi): 3100 Max Tonnage: 340

Main Ram: Pressure (psi): Max Tonnage:

Comb Ram: Pressure (psi): Max Tonnage:

Lubricant Container: Formkote  
Die: Dylon

Graphite Paper: X

Dummy Thickness: 2. Carbon Thickness: 1.5

Container Mat: NuDie V Cont Temp (F): 600 Times Used: 127

Stem Material: ? Stem ID: new Times Used: 127

Time at Temperature (h): 2.5 Transfer Time (s): 9

Post Test Analysis  
of Extrusion

Successful: X Unsuccessful:  
Comment:

Shooter: Butt left in Die:

Sticker:

Break thru Pressure (ksi): 184

Punch Speed: 3.8 "/s

Running Pressure (ksi): 153

Time to Ext: 1.4 s

Condition of Extrusion:

Length of Ext: 57

Nominal Cross Section: 0.525

Condition of Die:

General Comments:

HOT EXTRUSION DATA SHEET  
(PFS-HotExtDS)

3.8  
Fe-40Al-0.1B

Engineer's Name: Gaydosh  
Eng's ID: 12

Charge Number: YAG2272

Date Submitted: 86/11/07  
Date Completed: 86/11/21

General Type of Material: Intermetallic

Nominal Composition: Fe-40Al-0.41B *A-18%?+B*

Type of Billet: Loose Powder

Size of Billet (inches)      Diameter: 2.0      Length: 5.5

Proposed Extrusion  
Conditions

Temperature (F): 1790  
Type of Die: Round  
Punch Speed (inch/min): Maximum  
Special Conditions:

Reduction Ratio: 16:1

Safety Checks

Leak Test: X      Date: 86/11/05  
Heat Test (2h 1500F): X      Date: 86/11/06

Actual Extrusion  
Conditions

Date: 86/11/21      Ext. ID: L-2328  
Crew:  
Temperature: 1790      Reduction Ratio: 16:1  
Type of Die Round: X    Sh Bar:    Other:    Angle: 90  
Special Conditions:

Valve Selection    1/8:    7/16:    Preset Punch Speed:  
(X to specify)    3.5: X    Valve Opening: 0.25

Side Ram: X    Pressure (psi): 3100    Max Tonnage: 340  
Main Ram:    Pressure (psi):    Max Tonnage:  
Comb Ram:    Pressure (psi):    Max Tonnage:

Lubricant    Container: Formkote    Graphite Paper: X  
Die: Dylon

Dummy Thickness: 2.      Carbon Thickness: 1.5  
Container Mat: NuDie V'    Cont Temp (F): 600    Times Used: 128  
Stem Material: ?      Stem ID: New      Times Used: 128

Time at Temperature (h):      Transfer Time (s):

Post Test Analysis  
of Extrusion

Successful: X    Unsuccessful:  
Comment:

Shooter:      Butt left in Die:      Sticker:  
Break thru Pressure (ksi):      Punch Speed:  
Running Pressure (ksi):      Time to Ext:  
Condition of Extrusion:

Length of Ext:      Nominal Cross Section:  
Condition of Die:

General Comments: RAN OUT OF CHART PAPER

Fe-40Al cast

HOT EXTRUSION DATA SHEET  
(PFS-HotExtDS)

Engineer's Name: Gaydosh  
Eng's ID: D

Charge Number: YAG2272

Date Submitted: 86/11/07  
Date Completed: 86/11/21

General Type of Material: Intermetallic

Nominal Composition: Fe-40Al

Type of Billet: Loose Powder

*CAST*

Size of Billet (inches)

Diameter: 2.0

Length: 5.5

Proposed Extrusion  
Conditions

Temperature (F): 1790

Reduction Ratio: 16:1

Type of Die: Round

Punch Speed (inch/min): Maximum

Special Conditions:

Safety Checks

Leak Test: X

Date: 86/11/05

Heat Test (2h 1500F): X

Date: 86/11/06

Actual Extrusion  
Conditions

Date: 86/11/21

Ext. ID: L-2330

Crew:

Temperature: 1790

Reduction Ratio: 16:1

Type of Die Round: X Sh Bar: Other: Angle: 90

Special Conditions:

Valve Selection 1/8: 7/16: Preset Punch Speed:  
(X to specify) 3.5: X Valve Opening: 0.25

Side Ram: X Pressure (psi): 3100 Max Tonnage: 340

Main Ram: Pressure (psi): Max Tonnage:

Comb Ram: Pressure (psi): Max Tonnage:

Lubricant Container: FORMKOTE  
Die: DYLON

Graphite Paper: x

Dummy Thickness: 2. Carbon Thickness: 1.5

Container Mat: NuDie V' Cont Temp (F): 600 Times Used: 130

Stem Material: ? Stem ID: New Times Used: 130

Time at Temperature (h): 3.5

Transfer Time (s): 8.5

Post Test Analysis  
of Extrusion

Successful: X Unsuccessful:  
Comment:

Shooter: Butt left in Die:

Break thru Pressure (ksi): 184

Running Pressure (ksi): 168

Condition of Extrusion:

Sticker:

Punch Speed: 2.1 "/s

Time to Ext: 2.5 s

Length of Ext: 63.5

Nominal Cross Section: 0.525

Condition of Die:

General Comments:

Fe-40Al-B Cast

HOT EXTRUSION DATA SHEET  
(PFS-HotExtDS)

Engineer's Name: Gaydosh Date Submitted: 86/11/07  
Eng's ID: C Charge Number: YAG2272 Date Completed: 86/11/21

General Type of Material: Intermetallic

Nominal Composition: Fe-40Al-0.8B

*CAST*

Type of Billet: Cast

Size of Billet (inches)

Diameter: 2.0

Length: 5.5

Proposed Extrusion  
Conditions

Temperature (F): 1790

Reduction Ratio: 16:1

Type of Die: Round

Punch Speed (inch/min): Maximum

Special Conditions:

Safety Checks

Leak Test: X

Date: 86/11/05

Heat Test (2h 1500F): X

Date: 86/11/06

Actual Extrusion  
Conditions

Date: 86/11/21

Ext. ID: L-2329

Crew:

Temperature: 1790

Reduction Ratio: 16:1

Type of Die: Round: X Sh Bar:

Other:

Angle: 90

Special Conditions:

Valve Selection

1/8:

7/16:

Preset Punch Speed:

(X to specify)

3.5: X

Valve Opening: 0.25

Side Ram: X Pressure (psi): 3100

Max Tonnage: 340

Main Ram: Pressure (psi):

Max Tonnage:

Comb Ram: Pressure (psi):

Max Tonnage:

Lubricant Container: Formkote

Graphite Paper: X

Die: Dylon

Dummy Thickness: 2.

Carbon Thickness: 1.5

Container Mat: NuDie V' Cont Temp (F): 600

Times Used: 129

Stem Material: ?

Stem ID: New

Times Used: 129

Time at Temperature (h):

Transfer Time (s): 7.5

Post Test Analysis  
of Extrusion

Successful: X Unsuccessful:

Comment:

Shooter: Butt left in Die:

Sticker:

Break thru Pressure (ksi): 187

Punch Speed: 1.5 "/s

Running Pressure (ksi): 181

Time to Ext: 3.6 s

Condition of Extrusion:

Length of Ext: 66

Nominal Cross Section: 0.525

Condition of Die:

General Comments:

## APPENDIX B

The specific case of the calculation of the APB energy for Fe-50Al will be presented first, then the more general solution for aluminum concentration from 25 at%Al to 50 at%Al will be developed. The general method described below has been used to determine the form of the APB energy at 25 at%Al by Marcinkowski and Brown [26]. However, the general expression has not been developed before.

Figure A1 shows 2 layers of ( $\bar{1}10$ ) planes of a stoichiometric (50 at%Al) B2 alloy. The Fe and Al are designated as shown, and the subscripts A designate atoms above the slip plane and subscripts B designate atoms below the slip plane. In the area defined  $2a_0 \times \sqrt{2}a_0$ , the number and type of nearest neighbor and next nearest neighbor bonds are:

$$NN - Fe-Al \rightarrow 8$$

$$NNN - Fe-Fe \rightarrow 4$$

$$NNN - Al-Al \rightarrow 4.$$

Figure A1 b shows these same planes of atoms after the passage of a  $\frac{1}{2}[111]$  dislocation. The bonds across this plane then change to:

$$NN - Fe-Fe \rightarrow 4$$

$$NN - Al-Al \rightarrow 4$$

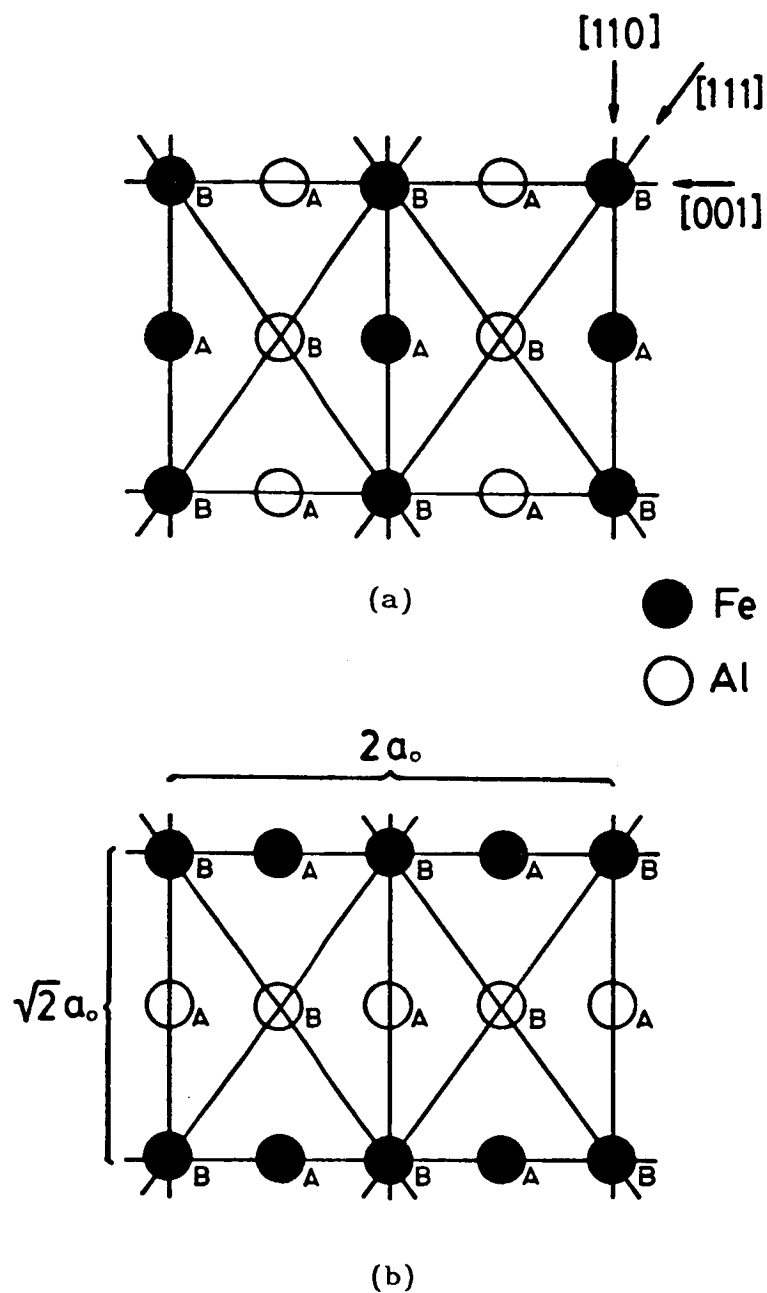


Figure A1. Representation of 2 layers of (110) plane a) before and b) after passage of a  $\frac{1}{2}\langle 111 \rangle$  dislocation. Atoms labelled A lie above the slip plane while those labelled B lie below.

$$\text{NNN} - \text{Fe-Al} \rightarrow 8.$$

The changes in the bonds are then given by:

$$\Delta \text{NN} = 4(\text{Fe-Fe}) + 4(\text{Al-Al}) - 8(\text{Fe-Al}) \quad [1a]$$

$$\Delta \text{NNN} = 8(\text{Fe-Al}) - 4(\text{Fe-Fe}) - 4(\text{Al-Al}). \quad [2a]$$

The ordering energy for nearest neighbors is:

$$V = V_{AA} + V_{BB} - 2V_{AB} \quad [3a]$$

where the  $V_{xx}$ 's are the interaction potentials for nearest neighbors. Therefore, the passage of a  $\frac{1}{2}[111]$  dislocation results in a  $4V$  energy increase. Likewise, the ordering energy for next nearest neighbors is:

$$W = W_{AA} + W_{BB} - 2W_{AB} \quad [4a]$$

where the  $W_{xx}$ 's are the next nearest neighbor interaction potentials. The passage of a  $\frac{1}{2}[111]$  dislocation therefore results in a  $-4W$  decrease in energy. The antiphase boundary energy is then the sum of the energy changes associated with a disordering dislocation per unit area. Therefore, the APB energy for a perfect stoichiometric B2 alloy on a  $\{110\}$  plane is:

$$\gamma_{\text{APB}} = \frac{4}{2\sqrt{2} a_0^2} (V - W). \quad [5a]$$

Theoretically, the ordering energies for third, fourth, etc., nearest neighbors should be included, but the contributions for these will be minimal.

The more general case will now be presented. If the atomic fraction of aluminum atoms is given as  $x$  over the range 0.25 to 0.50, and the excess Fe atoms are assumed to occupy Al sites, the type and number of nearest neighbor bonds before slip are:

$$\text{NN} - \text{Fe-Fe} \rightarrow 8(1 - 2x)$$

$$\text{NN} - \text{Fe-Al} \rightarrow 8(2x)$$

$$\text{NN} - \text{Al-Al} \rightarrow 0.$$

Likewise after slip, the nearest neighbor bonds are:

$$\text{NN} - \text{Fe-Fe} \rightarrow 4 + 4(1 - 2x)^2$$

$$\text{NN} - \text{Fe-Fe} \rightarrow 4(4x - 8x^2)$$

$$\text{NN} - \text{Al-Al} \rightarrow 4(4x^2).$$

The changes in nearest neighbor bonds are then:

$$\Delta \text{NN} = \text{Fe-Fe}[16x^2] + \text{Al-Al}[16x^2] - \text{Fe-Al}[32x^2]. \quad [6a]$$



Thus, passage of a  $\frac{1}{2}[111]$  dislocation results in a  $16x^2V$  energy increase.

Using the same approach for next nearest neighbors, the resulting energy decrease is  $-16x^2W$ . Therefore, the general expression of the APB energy is:

$$\begin{aligned}\gamma_{\text{APB}} &= \frac{16x^2}{2\sqrt{2} a_0} (V - W) \\ &= \frac{4\sqrt{2} x^2}{a_0} (V - W) \quad [7a]\end{aligned}$$

over the composition range of 0.25 to 0.50 Al.

# Report Documentation Page

1. Report No. <b>NASA CR-180810</b>		2. Government Accession No.		3. Recipient's Catalog No.	
4. Title and Subtitle <b>Ductility and Fracture in B2 FeAl Alloys</b>				5. Report Date <b>August 1987</b>	
				6. Performing Organization Code	
7. Author(s) <b>Martin A. Crimp</b>				8. Performing Organization Report No. <b>None</b>	
				10. Work Unit No. <b>505-63-01</b>	
9. Performing Organization Name and Address <b>Case Western Reserve University Dept. of Materials Science and Engineering Cleveland, Ohio 44106</b>				11. Contract or Grant No. <b>NAG3-563</b>	
				13. Type of Report and Period Covered <b>Contractor Report Final</b>	
12. Sponsoring Agency Name and Address <b>National Aeronautics and Space Administration Lewis Research Center Cleveland, Ohio 44135</b>				14. Sponsoring Agency Code	
15. Supplementary Notes <b>Project Manager, Michael V. Nathal, Materials Division, NASA Lewis Research Center. This report was a dissertation submitted in partial fulfillment of the requirements for the degree of Doctor of Philosophy to Case Western Reserve University, Cleveland, Ohio in May 1987.</b>					
16. Abstract <p>The mechanical behavior of B2 FeAl alloys has been studied. Stoichiometric Fe-50Al exhibits totally brittle behavior while iron-rich Fe-40Al yields and displays about 3 percent total strain. This change in behavior results from large decreases in the yield strength with iron-rich deviations from stoichiometry while the fracture stress remains essentially constant. Single crystal studies show that these yield strength decreases are directly related to decreases in the critical resolved shear stress for <math>\langle 111 \rangle \{110\}</math> slip. This behavior is rationalized in terms of the decrease in antiphase boundary energy with decreasing aluminum content. The addition of boron results in improvements in the mechanical behavior of alloys on the iron-rich side of stoichiometry. These improvements are increased brittle fracture stresses of near-stoichiometric alloys, and enhanced ductility of up to 6 percent in Fe-40Al. These effects have been attributed to increased grain boundary adhesion as reflected by changes in fracture mode from intergranular to transgranular failure. Increasing the cooling rate following heat treatment has been found to dramatically increase the yield strength of these alloys. This results in a change from ductile to brittle behavior in Fe-40Al. These increases in yield strength, which are observed in both polycrystals and single crystals, results from the quenching in of large numbers of thermal vacancies. Hall-Petch plots show that the cooling rate effects are a direct result of changes in the Hall-Petch intercept/lattice resistance term. Values of the critical resolved shear stress measured on single crystals compare favorably with the results of Hall-Petch intercepts from polycrystalline samples.</p>					
17. Key Words (Suggested by Author(s)) <b>Mechanical behavior Intermetallics Iron aluminide</b>			18. Distribution Statement <b>Unclassified - unlimited STAR Category 26</b>		
19. Security Classif. (of this report) <b>Unclassified</b>		20. Security Classif. (of this page) <b>Unclassified</b>		21. No of pages <b>220</b>	
				22. Price* <b>A10</b>	